Broadband optical wireless communications for the teleoperation of mining equipment

by

Alberto Rui Frutuoso Barroso

A thesis submitted in partial fulfilment
of the requirements for the degree of
Master of Science (MSc) in Natural Resources Engineering

The Faculty of Graduate Studies
Laurentian University
Sudbury, Ontario, Canada

THESIS DEFENCE COMMITTEE/COMITÉ DE SOUTENANCE DE THÈSE
Laurentian Université/Université Laurentienne
Faculty of Graduate Studies/Faculté des études supérieures

Title of Thesis
Titre de la thèse: BROADBAND OPTICAL WIRELESS COMMUNICATIONS FOR THE TELEOPERATION OF MINING EQUIPMENT

Name of Candidate
Nom du candidat: Frutuoso Barroso, Alberto

Degree
Diplôme: Master of Science

Department/Program
Département/Programme: Natural Resources Engineering

Date of Defence
Date de la soutenance December 15, 2016

APPROVED/APPROUVÉ

Thesis Examiners/Examinateurs de thèse:

Dr. Greg Baiden
(Supervisor/Directeur(trice) de thèse)

Dr. Osman Abou-Rabia
(Committee member/Membre du comité)

Dr. Brahim Chebbi
(Committee member/Membre du comité)

Dr. Meysar Zeinali
(Committee member/Membre du comité)

Dr. Tim Joseph
(External Examiner/Examinateur externe)

Dr. Clarence Virtue
(Internal Examiner/Examinateur interne)

Approved for the Faculty of Graduate Studies
Approuvé pour la Faculté des études supérieures
Dr. David Lesbarrères
Monsieur David Lesbarrères
Dean, Faculty of Graduate Studies
Doyen, Faculté des études supérieures

ACCESSIBILITY CLAUSE AND PERMISSION TO USE

Abstract

The current level of technological advancement of our civilization serving more than seven billion human population requires new sources of biotic and abiotic natural resources. The depletion and scarcity of high-grade mineral deposits in dry land are forcing the Natural Resources industry to look for alternate sources in underwater environments and outer space, requiring the creation of reliable broadband omnidirectional wireless communication systems that allows the teleoperation of exploration and production equipment. Within these objectives, Optical Wireless Communications (OWC) are starting to be used as an alternative or complement to standard radio systems, due to important advantages that optical wavelengths have to transmit data: potential for Terabit/s bit rates, broadband operation in underwater environments, energy efficiency and better protection against interference and eavesdropping. This research focus in two crucial design aspects required to implement broadband OWC systems for the teleoperation of mining equipment: high bandwidth wide beam photon emission and low noise omnidirectional Free-Space Optical (FSO) receivers. Novel OWC omnidirectional receivers using guided wavelength-shifting photon concentration are experimented in over 100 meters range vehicle teleoperation.

Acknowledgments

I would like to express my deepest gratitude to my supervisor, Dr. Greg Baiden who gave me the opportunity to study and research Optical Wireless Communications and always provided me with continuous support, assistance and motivation.

It is my pleasure to thank my advisory committee members at LU Barthi school of Engineering, Dr. Osman Abou-Rabia, Dr. Brahim Chebbi and Dr. Meysar Zeinali.

I am also very thankful to Dr. Julia Johnson at LU Computer Science department, Penguin ASI Mechanical Engineering department and electronic shop, especially Wesley Groom, Anna Kretzschmar, Luc Lacasse, Dan Oconnell and Scott Parks, for the help they gave me in the construction of multiple prototypes with which I experimented during this research.

Finally, I thank my family and friends for the encouragement they gave me to enroll in this MASc.

Contents

List of Tables

List of Figures

List of Acronyms

ACO-OFDM: Asymmetrical Clipped Optical OFDM

ADC: Analog to Digital Conversion

AGC: Automatic Gain Control

AOP: Apparent Optical Properties

APD: Avalanche Photodiode

AWGN: Additive White Gaussian Noise

BER: Bit Error Rate

BPSK: Binary Phase-Shift Keying

BRICS: Brazil, Russia, India, China and South Africa

CAGR: Compound Annual Growth Rate

CCC: Communications Computers Consumer

CPC: Compound Parabolic Concentrator

DCO-OFDM: Direct-Current biased Optical OFDM

DD: Direct Detection

DFA: Doped Fiber Amplifier

E-O-E: Electrical-Optical-Electrical

ELF: Extremely Low Frequency

EMI: Electromagnetic interference

ESR: Equivalent Series Resistance

FET: Field-Effect Transistor

FFT: Fast Fourier Transform

FOV: Field of View

FPGA: Field Programmable Gate Array

FSO: Free-Space Optical

IFFT: Inverse Fast Fourier Transform

IOP: Inherent Optical Properties

IoT: Internet of Things

IrDA: Infrared Data Association

IREDES: International Rock Excavation Data Exchange Standard

ITS: Intelligent Transportation Systems

LED: Light-Emitting Diode

LHC: Large Hadron Collider

Li-Fi: Light Fidelity

LIDAR: Light Detection And Ranging

LIGO: LASER Interferometer Gravitational-Wave Observatory

LLCD: Lunar Laser Communication Demonstration

LLGT: Lunar Laser Ground Terminal

LLST: Lunar Laser-comm Space Terminal

LMDS: Local Multipoint Distribution Service

LOS: Line-of-Sight

LQG: Loop Quantum Gravity

LTE: Long-Term Evolution

LU: Laurentian University

M2M: Machine-to-Machine

MCP-PMT: Micro-Channel Plate PMT

MIMO: Multiple-Input and Multiple-Output

MISO: Multiple-Input and Single-Output

NEP: Noise-Equivalent Power NLOS Non-Line-of-Sight

OFDM: Orthogonal Frequency Division Multiplexing

OFSO: Omnidirectional Free-Space Optical

OOK: On-Off Keying

OPA: Optical Parametric Amplification

OSHA: Occupational Safety & Health Administration

OWC: Optical Wireless Communications

P2MP: Point-to-Multipoint Communication

PAM: Pulse-Amplitude Modulation

PAR: Photosynthetically Active Radiation

PET: Positron Emission Tomography

PiN: Positive Intrinsic Negative

PMT: Photomultiplier tubes

PSK: Phase Shift Keying

PSNR: Peak-Signal-to-Noise-Ratio

QAM: Quadrature Amplitude Modulation

QED: Quantum electrodynamics

RF: Radio Frequency

RFI: Radio Frequency Interference

SISO: Single-Input and Single-Output

SNR: Signal-to-Noise Ratio

SRS: Stimulated Raman Scattering

TDM: Time Division Multiplexing

UHF: Ultra High Frequency

ULF: Ultra-Low Frequencies

V2I: Vehicle-to-Infrastructure

V2V: Vehicle-to-Vehicle

VHF: Very High Frequency

VLC: Visible light communication

VLCC: Visible Light Communications Consortium

VLF: Very Low Frequencies

WDM: Wavelength-Division Multiplexing

Wi-Fi: Wireless Fidelity

WiMAX: Worldwide Interoperability for Microwave Access

WLS: Wave-Length Shifting

WUCN: Wireless Underground Communication Network

Chapter 1

Introduction

"According to Edholms law, the demand for point-to-point bandwidth in wireless short-range communications has doubled every 18 months over the last 25 years. It can be predicted that data rates of around 510 Gb/s will be required in ten years." [3]

The Telstar-1 satellite was the first communications device put into Earth's orbit [15] that demonstrated the potential to connect multiple remote users using wireless communications. Since that date (1962) the usage of wireless communications has had an exponential growth in which the world saw military technologies like cell radios, Internet and GPS being implemented in civil applications causing a depletion of the electromagnetic spectrum.

The electromagnetic spectrum is currently licensed from 3 Hz (ELF) to 170 GHz (D band), some bands cannot be used in civil applications, and the frequencies licensed for civil use (IEEE 802.11a/g, GSM, WiMAX, LTE, etc.) are experiencing interference and low warranty of service.

Trying to mitigate this problem, the telecommunications industry initiated a process to expand wireless communications to Tera Hertz [1] [3] and optical bands [14].

1.1 Motivation

In the last 20 years, global mineral markets had trouble to supply raw materials during peaks of industrial demand causing surges in the price of commodities. The origin of natural resources has come from land-based assets (surface oil and gas wells, open pit or underground mining, agriculture, farming) with the exceptions of offshore oil platforms and offshore aquaculture production sites. However, a more intense exploration and extraction of natural resources in underwater environments need to be implemented, because the majority of land-based assets are depleting fast due to the exponential increase in human population, and the appearance of more emerging economies [7]. High demand commodities like tantalum [5], potash, phosphorous, oil and lithium are predicted to deplete from dry-earth in some decades, and rare earth metals used in modern electrical motors (e.g., neodymium) require new mining sources [4]. Developing countries like Brazil, Russia, India, China and South Africa (BRICS) have dynamic economies that are modernizing infrastructures, and industrial sectors are creating strong domestic markets and causing instabilities in the price of the main commodities [11].

The current number of natural resources production sources is insufficient to feed growth cycles of the world economy, and this supply-demand problem needs to be addressed today by identifying future extraction sources, and by developing technology to allow a sustained exploration and production of natural resources in underwater environments comprising 71% of Earth's surface or the Jupiter moon Europa.

The concepts of celestial bodies mining require more time to mature it's economically and technological aspects [10], while the extraction of natural resources in underwater zones of Earth has begun to reach the mining industry mainstream [2]. In most cases, mining underwater will require access to extreme depths where only custom-built machines can operate.

It is also clear that a significant level of Teleoperation or Teleautonomy will be required to maneuver and maintain the production equipment with the ultimate aim to remove all persons from hazardous areas [8] and work without tethers in challenging environments.

1.2 Problem statement

Current wireless communications technologies do not offer efficient network solutions for the teleoperation of mining equipment in tunnels and underwater environments. Underwater Teleoperation of multiple equipment requires bit rates that the current underwater radio frequency (RF) modems [13] and underwater acoustical modems [6] cannot provide, but light in the visible light region can be transmitted in water with low attenuation and high bit rate transport capabilities. Some companies are already developing underwater free space optical (FSO) communications systems using lasers [9] or LEDs, that lack a wide field of view (FOV), cannot be used in zones with intense illumination, and do not implement a multiple user network [12].

The current underwater FSO systems are simple point to point optical bridges, and the Visible Light Communications (VLC) consortium efforts do not properly address underwater OWC with the characteristics of standard RF communications systems (e.g., IEEE802.11, WiMAX, and LTE).

1.3 Objectives

The main objective of this thesis is to investigate Optical Wireless Communications (OWC) as a candidate solution to replace or complement MHz to GHz Radio Frequency (RF) wireless communications systems in the teleoperation of mining equipment in tunnels and underwater

environments. This objective requires the implementation of a broadband, long range, multi-user, omnidirectional OWC system demanding the development of high bandwidth OFDM LED drivers and low noise omnidirectional free space optical receivers.

1.3.1 Hypothesis

The main hypothesis is that an OWC system can replace or complement IEEE 802.11 wireless communications systems, placing the following research question:

- Is it possible to use stimulated Raman scattering or wavelength-shifting effects in optical fibers to build high gain omnidirectional photon receivers for visible light communications?

- What are the theoretical advantages of OWC systems when compared with conventional RF communications in the teleoperation of mining equipment?

This question generates the following hypothesis:

- If standard refractive or reflective optics used to concentrate photons at the photodetector are replaced with Raman scattering or wavelength-shifting fiber guides, then the field of view of the photon receiver will be higher and will offer more optical gain than a bare photodetector window.

  This hypothesis is tested in chapter three.

- When mining equipment are teleoperated in underground mines or underwater environments using optical wireless communications, a network availability higher than current RF wireless LAN systems will be obtained.

  This hypothesis is tested with underwater and tunnel OWC experiments in chapter four.

1.4 Thesis outline

With the objective of researching these technological distinct directional research hypotheses, this manuscript style dissertation has the following structure:

- Chapter two contains the literature review.
- Chapter three presents omnidirectional free space optical receivers that allow the teleoperation of vehicles using optical wireless communications.
- Chapter four reveal OWC teleoperation experimental results in atmospheric and underwater environments.
- Chapter five gives the thesis conclusions, enumerates the contributions of this work, and proposes future work to enhance the thesis contributions.

Finally, Appendix A lists the Matlab code used in WLS fiber system identification.

References

[1] Akyildiz, I. F., Jornet, J. M., and Han, C. Terahertz band: Next frontier for wireless communications. *Physical Communication 12* (2014), 16–32.

[2] Baiden, G., and Bissiri, Y. High bandwidth spherical optical wireless communication for subsea telerobotic mining. *OCEANS* (2011), 1 – 4.

[3] Federici, J., and Moeller, L. Review of terahertz and subterahertz wireless communications. *Journal of Applied Physics 107*, 11 (2010), 111101.

[4] Gordon, R. L., and Tilton, J. E. Mineral economics: Overview of a discipline. *Resources Policy 1*, 33 (2008), 4 – 11.

[5] Kristof, N. D. Death by gadget. *The New York Times 27* (2010).

[6] Logics, E. R-series, March 2015. http://www.evologics.de/en/products/acoustics/index.html.

[7] Moe, T., Maasry, C., Tang, R., and Goldman, S. *EM equity in two decades: a changing landscape*. Goldman Sachs Global Economics, Commodities and Strategy Research, 2010.

[8] Peter I. Corke, J. M. R., and Winstanley, G. J. Robotics for the mining industry. *Lecture Notes in Control and Information Sciences 236*, 33 (1998), 163 – 181.

[9] Photonics, S. Neptune underwater communications, March 2015. http://www.saphotonics.com/high-bandwidth-optical-communications/underwater.

[10] Prockter, L. Europa mission studies, December 2012. NASA, OPAG.

[11] Radenaker, M., and Kooroshy, J. The global challange of mineral scarcity in enriching the planet. *Empowering Europe* (2010), 26 – 27.

[12] Sonardyne. Bluecomm, March 2015. http://www.sonardyne.com/products/subsea-wireless-communications.html.

[13] Technologies, W. Seatooth, March 2015. http://www.wfs-tech.com/index.php/products/seatooth.

[14] Wang, J., Yang, J.-Y., Fazal, I. M., Ahmed, N., Yan, Y., Huang, H., Ren, Y., Yue, Y., Dolinar, S., Tur, M., et al. Terabit free-space data transmission employing orbital angular momentum multiplexing. *Nature Photonics 6*, 7 (2012), 488–496.

[15] Whalen, D. J. *The origins of satellite communications, 1945-1965.* Smithsonian Institution Press Washington, DC, 2002.

Chapter 2

A review of wireless communications systems

This chapter presents a historical review of the developing of wireless communication systems, giving a critical description of the physics that rule electromagnetic propagation in the implementation of optical wireless communications.

2.1 Introduction

We live in a universe made of space, time and energy, Albert Einstein's special relativity theory predicted that mass is a manifestation of energy ($E = mc^2$) in the aether (space-time fabric) with recent theories stating that matter is condensed energy in the Higgs-Field. At the present moment, physics research proved the existence of 24 fundamental particles and four fundamental forces that interact between them. These four forces are known to be originated by distinct mechanisms and are characterized by different ranges and intensity:

- Strong nuclear forces are the most intense ones, they are observable at 10^{-15} meters binding nucleons in medium sized nucleus, and binding quarks at distances less than 0.8 femto meter. The different strong nuclear forces observed in quark-gluon interactions gave birth to the theory of quantum chromodynamics.

- Weak nuclear forces have an intensity in the order of 10^{-6} when compared with strong nuclear forces, they have a 10^{-18} meters in range, they exist in neutrino interactions, using W and Z bosons as the transmission particles.

- Electromagnetic forces have an intensity in the order of $1/137$ when compared with strong nuclear forces, they have an infinite range, using the suspected massless [142] photon as the transmission particle. Photons interact with matter in a proportion related with the energy they carry, causing molecular rotation, torsion and vibration at low energy levels, and electron levels changing and ionization at higher energy levels.

- The gravitational force is the weakest one (one of the mysteries of modern physics), with an intensity in the order of 10^{-39} when compared with strong nuclear forces, it is the dominant force at the macroscopic level, and it have an infinite range. Bob McElrath suggests that gravity emerges from neutrinos [160].

2.2 Wireless Communication Technology

The main requirement of communications is range, and from the four fundamental forces, the electromagnetic force and the gravitational force are the ones that offer infinite range. Communication using gravitational waves (gravitons) is currently not feasible because the current interferometer detectors are not portable:

- the LASER Interferometer Gravitational-Wave Observatory (LIGO) experiment runs since 2002 using 2.5 miles arms and recently its advanced detector sensed the disturbances caused by the collision of two black holes.
- the Virgo interferometer gravitational wave detector that operates in Italy since May 2007 using 3000 meters long arms.

Einstein's photoelectric effect theory postulated that electromagnetic energy is transported using packets that are normally called as photons or quanta extending Max Planck theory of heat radiation. In this theory, Einstein postulates that the photon energy is proportional to its frequency (Equation 2.1).

$$E = hf \tag{2.1}$$

Where E is the photon energy, h is the Planck's constant ($6.62606957 \times 10^{-}34$ J.s) and f the photon frequency, with a recent experiment demonstrating that the Planck's constant can be a variable.

The photoelectric effect postulates the minimal energy (work function) that a photon needs to carry to eject one electron from an irradiated surface (Equation 2.2).

$$eV_o = hf - \phi \tag{2.2}$$

With e being the magnitude of electron charge, V_o the stopping potential and ϕ the work function.

Einstein's photoelectric effect discovery sponsored the developing of photodetector sensors, the LASER, and the LEDs that together with optical fiber waveguides allows broadband backbone data connections. In Optical Wireless Communications, the photoelectric effect allows the indirect detection from long-wavelength infrared (20 THz) to gamma ray wavelengths.

Current direct detection methods using heterodyne receivers at room temperature are operating above 2 THz with Silicon-Germanium RF integrated circuit designs working above 500 GHz [111].

Einstein's gravitational lensing effect was verified in 1919 and light used in free space optical communications will bend [83] as described in Einstein's field equations. This theory models the behavior of space with the presence of mass, but does not model space microscopic architecture that continues to be a big mystery to the scientific community; e.g.,:

- is vacuum filled [189] with a space-time spinfoam?
- is vacuum affected [21] by dark energy?
- does dark matter [86] fills vacuum with axions [27]?
- is vacuum made of strings [4], with light being waves [81] in the D-brane foam?

Trying to reveal more data about this mystery, diverse experiments [85] are being executed, with the LUX dark matter detector failing to detect weakly interacting massive particles (WIMPS) in 2015, and the Axion Dark Matter eXperiment (ADMX) design being questioned if it can detect a low mass axion [49].

2.2.1 History of electromagnetic wireless communications

The invention of electromagnetic wireless communications has the following technology milestones:

- Charles-Augustin de Coulomb (France) formulated in 1785 his inverse-square law that describes the electrostatic forces that exists between electrical charged particles
- Hans Christian Orsted (Denmark) discovered in 1820 that electrical currents create magnetic fields
- André-Marie Ampère (France) formulated its circuital law in 1826 relating the intensity of the magnetic field with the electrical current running in a wire
- Michael Faraday (England) in 1831 demonstrated the magnetic induction principle when in an experiment he massaged a wire with a variable magnetic field inducing an electrical field on it
- Johann Carl Friedrich Gauss (Germany) formulated in 1835 a law relating the electric charge distribution with the resulting electric field, after experimenting in 1833 with Wilhelm Eduard Weber an electromechanical telegraph over a 1200 meter wired connection
- James Clerk Maxwell (Scotland) formulated in 1865 a set of equations modeling waves with oscillating electrical and magnetic field that travel in empty space, and deducted that light was also electromagnetic radiation
- Oliver Heaviside (England) invented the transmission line model in 1880 that allowed to maximize the energy transmission in wired and wireless systems, and in 1884 reformulated Maxwell equations to the current set of four differential equations

- Heinrich Hertz (Germany) 1886 proved the existence electromagnetic waves designing the first emitter-receiver system experiment that validated Maxwell theory, and described the properties of reflection and constructive or destructive interference in the propagation of electromagnetic waves.

In the history of wireless communications development, it is known that the first electromagnetic wireless transmission of a human conversation was made using an optical wireless communication system, when Alexander Graham Bell and his assistant Charles Sumner Tainter transmitted a wireless voice telephone message in a distance of 213 meters in June 3, 1880 [183].

Sound (drums, horns and the human voice) was the first wireless communications technology to be used, and Alexander Bell's photophone and Heinrich Hertz's wireless transceiver were the first apparatus able to modulate electromagnetic waves. Before that, diverse electromagnetic communications systems using light were used, because light was the first electromagnetic radiation men was able to emit using high-temperature exothermic redox chemical reactions (combustion) or using the light of the sun (flags, mirrors):

- smoke signs [161]
- Aeneas OWC coded emission [37]
- Roman telegraph stations [69]
- Claude Chappe's optical telegraph [66]
- Colonel Mangin night and day optical telegraph [130]

2.2.2 Electromagnetic communications in free-space and in Earth's atmosphere

The main mechanism that attenuates electromagnetic waves in free space is the geometrical spreading of energy through distance, with the power density of electromagnetic waves being inversely proportional to the square of the distance from the radiation source (i.e., doubling the distance reduces the power density to one quarter). Coulombs law, gravitation and sound waves are other examples of inverse square law attenuation. Electromagnetic geometrical spreading is quantified using the Friis transmission formula (2.3) that shows that the received power Pr is proportional to the transmitted power Pt, to the area of the receiver Ar, to the area of the transmitter At, and it is inversely proportional to the square of the distance d.

$$P_r = \frac{P_t A_r A_t}{(\lambda d)^2} \tag{2.3}$$

The parameters Pt and Ar are key to the design of effective RF or free-space optical communication systems. In applications where the line-of-sight cannot be clear of obstacles, the electromagnetic radiation will be diffracted and multipath attenuation will occur, causing constructive and destructive wave interference. The radio path clearance between antennas required to reduce multipath attenuation can be calculated using the Fresnel zones formula (2.4).

$$F_n = \sqrt{\frac{n\lambda d_1 d_2}{d_1 + d_2}} \tag{2.4}$$

F_n gives the radius of the radiation volume ellipsoid [226] of the Fresnel zone n, with odd zones causing in-phase interference (0 to 180 degrees) and even zones causing out-of-phase interference (180 to 360 degrees).

In Table 2.1 we can see the advantages of using high frequencies to avoid multipath

interference, comparing the required zone 1 and 2 Fresnel clearances, for 900 MHz radios, 2.4 GHz Wi-Fi, and 450nm blue light (666.2 THz) for a free space point-to-point link.

Table 2.1: Fresnel zone clearance for RF and blue light

Frequency (GHz)	**Fresnel zone-1 (m)**	**Fresnel zone-2 (m)**
0.9	4	5.7
2.4	2.5	3.5
666,210	0.01	0.02

Fresnel zone clearance may not be possible to maintain in many communications applications, existing diverse radio propagation models (Table 2.2) to predict and budget the communication link in indoors and outdoors applications.

Table 2.2: Examples of Radio Propagation Models

Model types
Indoors:
• ITU model [209]
• Log-distance [96]
Outdoors:
• Foliage models (Weissberger [242], ITU [122])
• Terrain models (Egli [78], Longley-Rice [127], ITU [218])
• City models (Young, Okumura, Hata, COST [218])
• Band-specific models (Wi-Fi, Green-Obaidat [99])
• Environmental effects models (ITU, Crane, DAH [208])

Line-of-sight communications on Earth's surface are limited by the diffraction effects in the Fresnel zones and the radio horizon (Equation 2.5) defined by Earth's radius (R) and the height (h) of the communication tower.

$$d = \sqrt{2Rh + h^2} \tag{2.5}$$

In practice, the radio horizon is increased by the atmosphere effect that bends the waves toward Earth in a factor (K) that is weather dependent [75]. Both OWC and RF systems are affected by the properties of Earth's atmosphere with both systems requiring detailed implementation studies to achieve efficient communications channels.

2.2.3 Underwater electromagnetic propagation

Water magnetic properties are similar to vacuum (same μ in all frequencies) with the permittivity ϵ and conductivity σ variation with frequency defining the transparency windows that can be used in underwater electromagnetic communications. The frequency response of the electromagnetic propagation in pure and salt water has a large variance that can be explained as:

- the partial orientation of the permanent dipole moment of the water molecules causes a refraction index near 9 until the infrared wavelengths
- in the visible light region, the refraction index is approximately 1.34
- the infrared region is associated with molecule resonance and a great energy absorption
- between blue and green wavelengths photons have a minimal interaction with the water molecules defining the best transmission window of pure water

- above ultraviolet wavelengths the photons get a strong attenuation because they have enough energy to excite atomic transitions of water and trigger Compton scattering
- the dissolved salts increase the conductivity of seawater causing extra attenuation in all frequencies below infrared

Wireless communications in underwater environments are restricted to low bit rate magneto-Inductive transmission [101] or using the ELF/VLF spectrum allocations [28] and we can conclude that optical wireless communications using the water visible light transmission window is currently the best option to implement broadband underwater wireless communications.

2.2.4 Electromagnetic spectrum allocations

The electromagnetic spectrum can be divided in ionizing (can destroy living cells) or non-ionizing bands or divided in bands (Table 2.3) that are characterized by their human usage. The optical band is currently the electromagnetic spectrum zone that offer the highest bit rates using LASER transmission in confined space (optical fiber waveguides) or free space (optical wireless communications). NASA modulated X-ray source [93] using wide area Silicon Drift Detectors [174] is a consequence of electromagnetic spectrum depletion, that is forcing the telecommunications industry to implement wireless data transmission using ionizing radiation.

Table 2.3: Classification of radio frequency bands [225]

Frequency band	Abbreviation	Frequency range	Typical application
Extremely low	ELF	3 to 30 Hz	Underwater communications
Super low	SLF	30 to 300 Hz	Underwater communications
Ultra low	ULF	0.3 to 3 KHz	Through-the-Earth communications
Very low	VLF	3 to 30 KHz	Submarine navigation
Low	LF	30 to 300 KHz	LORAN
Medium	MF	0.3 to 3 MHz	AM broadcasting, beacons
High	HF	3 to 30 MHz	Amateur radio
Very high	VHF	30 to 300 MHz	Terrestrial communications
Ultra high	UHF	0.3 to 3 GHz	TV broadcasting
Super high	SHF	3 to 30 GHz	Wireless LAN, DBS
Extremely high	EHF	30 to 300 GHz	Millimeter wave scanner
Tremendously high	THF	0.3 to 3 THz	Medical imaging
Infrared	xIR	0.3 to 430 THz	Guided missiles
Visible radiation	color	430 to 790 THz	Illumination, VLC
Ultraviolet	xUVx	0.79 to 30 PHz	Curing
X-ray	X-ray	0.03 to 30 EHz	Medical and industrial
Gamma ray	γ	above 30 EHz	Slurry analysis

2.2.5 Channel capacity in noise affected communications

We live in a universe full of electromagnetic radiation, generated with the big bang [64], emitted by quasars [87], stars, chemical reactions [39] and technology that causes electromagnetic interference (EMI).

Unwanted radiation that interferes with the signal that carries the communication information is called noise, that can be called "white noise" when its level is independent from frequency or colored noise (non-white) when it is frequency dependent.

In communications systems diverse physical mechanisms are sources of noise, being the random movement of electrons (thermal noise) and the unpredictable fluctuations of current in electronic devices (shot noise) the two biggest white noise sources that affect communications systems.

Low frequency (below 10 KHz) communication systems are also intensively affected with two nonwhite noise sources (flicker and burst noise) when using semiconductor devices [258].

The thermal noise in a system can be modeled using thermodynamic and quantum mechanical theories [50], but the empirical model (Equation 2.6) is normally used to quantify the mean-square value of the thermal noise voltage (V^2)in a resistor with R Ohms, submitted to a temperature T (kelvin), with the Boltzmann's constant k equal to $1.38 \times 1-^{-23}$ Watts/Hz/Kelvin, the Planck's constant h equal to 6.63×10^{-34} Watt/second and B_N the bandwidth (in Hz) where the noise is evaluated.

$$E[V_T^2 N] = 4kTRB_N \tag{2.6}$$

The effect of noise in band-limited and power-limited communication channels can be modeled using the Shannon information capacity law (Equation 2.7) that models the capacity C (bits per second) of a memoryless Gaussian channel with bandwidth B (Hz), transmitting a signal X_k with power P that is affected by an additive white Gaussian noise (AWGN) with power N_o.

$$C = B.log_2(1 + \frac{P}{N_o}) \tag{2.7}$$

Shannon law demonstrates that phase shift keying (PSK) modulations offers lower bit error rate (BER) when compared with other modulation formats [109], and that having a high signal-to-noise ratio (SNR) allow the use of more spectral efficient modulations [80].

In applications where increasing the emission power is not practical (e.g., satellites), a higher SNR can be achieved in the system budget lowering the receiver operating temperature [203] to lower its internal noise sources (to minimize the Johnson noise).

Optical wireless communications are typically affected with background radiation and system noise [12]). With the first five summing junctions depending on the optoelectronic design (lens and photodetector type), on a voltage that minimizes the shot noise, rejecting lower frequencies to minimize the $\frac{1}{f}$ noise and using an effective optical filtering to minimize the optical background noise caused by natural (sun) or artificial illumination.
The electronic noise summing junction has factors common to all analog to digital (A/D) and digital to analog (D/A) systems:

- Analog to digital conversion (ADC) static and dynamic performance [173]
- ADC conversion jitter sensitivity [62]
- Digital to analog conversion (DAC) static and dynamic performance [91]
- DAC conversion phase noise [145]

2.3 Optical Wireless Communications

2.3.1 Introduction

"Future pursuit of the vision for robotic and human space exploration would utilize instruments with ever increasing capability and require orders of magnitude increase in data return rates from planetary distances. Without resorting to high-power transmitters with hundreds of watts and antenna diameters above five meters, deep-space science and exploration will rapidly encounter a bandwidth ceiling with radio frequencies of S, X, and Ka bands" [181]. Space exploration and multiple new applications [112] require supporting broadband data connections, forcing the telecommunications industries to develop communication equipment with the required bit rates. Integrated Services Digital Network (ISDN) is now an obsolete and discontinued technology and digital subscriber line (DSL) is being replaced with fiber to the home technologies [202] or hybrid fiber-coax networks [168]. As fiber replaces copper to increase the guided transmission bandwidth, in a near future Optical Wireless Communications (OWC) will replace or complement existing RF wireless communications systems and eliminate the current wireless networks bit rate bottleneck [3]. As shown in the previous sections of this literature review high frequency electromagnetic waves suffer high attenuation in underwater mediums and OWC is a solution to implement broadband wireless communications [182] for the teleoperation of mining equipment.

2.3.2 Advantages and disadvantages of OWC systems

Visible light is a high frequency electromagnetic radiation with a photon energy level near ionizing radiation, it requires special sources and detectors [186], and offers some advantages (or disadvantages) when compared with other lower frequencies.

Advantages:

- *Underwater operation:* water has a visible light transmission window that allows broadband wireless transmission
- *Unlicensed spectrum:* real-estate window taxes [56] introduced in England, Wales and France between the XVII and XX centuries were repealed, and at this moment the 430 to 790 THz frequency space (visible light) continue unlicensed
- *High bandwidth:* the current light emission technology only allows intensity modulation, and the reception technology only detects the energy effects of the photons (e.g., visible light 360 THz bandwidth allows 360 Terabit/s using Phase Shift Keying modulation)
- *Low power requirements:* using low divergence light (LASER) planetary distances can be reached using less than 1W [57]
- *No interference:* light do not penetrate opaque solids and it is easy to build interference free systems
- *Multipath fading:* the small dimensions of visible light Fresnel zones make OWC systems immune to multipath fading that plagues RF communications in tunnels [232]
- *Space diversity:* light can use time division multiplexing (TDM), frequency division multiplexing (color FDM) and its directivity properties allow easy deployment of space division multiplexing (SDM)
- *High security:* Eavesdropping shielding in OWC systems can be implemented with simple construction materials (drywall, wood, cement, fabrics, etc.)

- *Low-cost deployment:* OWC integrated in artificial illumination systems will allow to cover the largest indoor area at the minimal deployment price

- *Human body safety:* after protecting the eyes and skin from the visible light effects, this radiation is the safest radiation to use because it does not penetrate the human body, and cannot cause leukemia, cancer, and genetic damages at the risk levels of some RF systems [102].

Disadvantages:

- *Attenuation:* Dark atmospheres, turbid waters, or opaque solids can cause intense channel attenuation

- *Background noise:* Sunlight and artificial illumination require to shadow the receiver with barriers (or hats) to attenuate the interference because the option of rising the emitting power to maintain the required signal to noise ratio is not practical

- *Safety:* Strong light can damage the eyes and skin and protective measures (optical filters) need to be used during this radiation exposition (eye protection similar to the ones used in arc welding, LASER cutting, tanning beds, etc.).

2.3.3 OWC channel modeling

"The propagation of the radiation in a medium assumed to be homogeneous, isotropic, and at rest takes place in straight lines and with the same velocity in all directions, diffraction phenomena being entirely excluded. Yet, in general, each ray suffers during its propagation a certain weakening, because a certain fraction of its energy is continuously deviated from its original direction and scattered in all directions. This phenomenon of scattering, which means neither a creation nor a destruction of radiant energy but simply a change in distribution, takes place, generally speaking, in all media differing from an absolute vacuum, even in substances which are perfectly pure chemically" [195].
This text from Max Planck's book *The Theory of Heat Radiation* explains how matter affects electromagnetic propagation that in "absolute vacuum" is only affected by the inverse square law (Equation 2.8) and gravitational lensing distortion.

$$I = \frac{P}{A} = \frac{P}{4\pi r^2} \tag{2.8}$$

With P as the total power radiated by an omnidirectional isotropic source, A is the area of the sphere with radius r that has its center at the source and I as the energy density figure (power per unit of area) that is divided by the square of the distance r [210]).

2.3.4 Atmospheric OWC channel modeling

The design of OWC systems for atmospheric applications requires the creation of a functional description to customize the design to that application:

- indoor or outdoor operation
- omnidirectional or directional coverage

- line-of-sight (LOS) or non-LOS
- optical wavelength (IR-invisible, white light, or a specific color)
- type of interference (sun, artificial illumination, welding light, etc.)

After the creation of the OWC system functional description, the models to determine the range and bit rate can be summarized in two types: indoor or outdoor.

Indoor channel models

OWC channel links in indoor communications can be classified according to the degree of directionality [124], with directed links employing directional transmitters and receivers, non-directed links employing omnidirectional transmitters and receivers, with hybrid links combining sources and receptors with multiple types of directionality. Line-of-sight OWC links are implemented with a direct emitter to receiver connection, and non-LOS use one or more photon reflections from the emitter to the receptor. Ghassemlooy, Popoola and Rajbhandari [94] describe the advantages of using a small photodetector to mitigate the problems of multiples reflections and expose one problem that this thesis gives original contributions to solve: "Thus, single element receivers favor the use of large-area detectors. However, as the detector area increases so does its capacitance, which has a limiting effect on the receiver bandwidth".

In indoor OWC links the noise added by the artificial illumination can degrade the receive signal if mitigation techniques are not used. Adriano Moreira, Rui Valadas e Manuel de Oliveira Duarte [169] describe the noise effects of diverse illumination sources, quantifying background currents in a PiN photodetector between 8.2 and 5100 μA for a bare sensor and 0.4 to 1000 μA for the same sensor protected with an optical filter.

Rajbhandari, Sujan and Ghassemlooy, Zabih and Angelova and Maia [207] introduce a model for fluorescent light interference and propose a wavelet transform method to reduce artificial illumination interference in digital modulation techniques that does not have a big impact in OFDM based visible light communications [67].

The two most important technical requirements in OWC systems design is to obtain a wide frequency response and a high signal-to-noise ratio (SNR), with this thesis giving theory contributions to these two requirements in chapters 4 and 5. Joseph Kahn and John Barry article about wireless infrared communications [124] show some techniques to increase the SNR at the receiver using compound parabolic concentrators that offers wider field of view (FOV) values than Fresnel lenses [134], presenting a link budget (Equation 2.9) for indoor OWC links.

$$h(n) = \begin{cases} \frac{(m+1)A}{2\pi d^2} \cos^m \phi T_s(\psi) g(\psi) \cos\psi, & \text{if } 0 \leq \psi \leq \psi_c \\ 0, & \text{elsewhere} \end{cases} \tag{2.9}$$

With $h(n)$ as the optical DC gain, A the detector area, $\frac{(m+1)}{2\pi} \cos^m \phi$ the Lambertian radiant intensity function, $T(\psi)$ is an optical system attenuation factor (filters, coupling losses, etc.), $g(\psi)$ system optical gain (photon concentration or Raman amplification), $1/d^2$ is the inverse square law factor and the $cos\psi$ the Lambert cosine law [206].
Equation (2.9) show how critical the receiver area (A) and $g(\psi)$ are to maximize the signal at the photo-detector, two parameters that this thesis gives contributions to the theory of designing large area receivers with wide field of view (ψ_c).

Outdoor channel models

The importance of increasing the receiver area to maintain a desirable SNR is described by Kaur, Bhardwaj and Soni articles [128] [229], a design parameter that is critical in long range outdoor OWC channels.

Laser communications in atmosphere are common with diverse commercial systems available to install point-to-pint links [228] and a large number of articles about channel modeling of outdoor OWC links.

The link budget for outdoor channel [38] links can be an adaptation of equation 2.9 with an exponential decay described with Beer's law, with Scott Bloom article [35] presenting a link budget equation (2.10) adapted for laser communications.

$$P_{received} = P_{transmitted} \frac{A_{receiver}}{(d.Divergence)^2} e^{-\alpha.d} \tag{2.10}$$

In this equation the Laser divergence multiplies with the distance d to quantifying the geometrical attenuation factor, with $e^{-\alpha.d}$ as Beer's law attenuation at communication distance d times α the atmospheric attenuation factor that can reach values over 225dB/Km in low visibility conditions [35].

Scott Bloom article [35] also refers the choice of an optimal wavelength in atmospheric transmission, customized to the typical molecular content of the atmosphere, a subject that Manor and Arnon [159] study in their article, concluding that there is no magic wavelength [2, 10, 135, 141] for atmospheric OWC links.

Erich Leitgeb co-author several articles [175, 42, 177, 196, 9, 200, 150, 132, 92, 23] that describe models for fog, rain, snow and scintillation.

Atmosphere does not have a magic wavelength and Laser communications can be customized for the sensor maximum responsivity (infrared band) or to achieve sunlight background noise immunity, described in literature as ultraviolet solar blind optical communications [251, 250, 172, 123]. OWC systems using solar blind ultraviolet wavelengths can be an alternative to RF in the implementation of vehicle collision avoidance systems [180] in autonomous mining vehicles fleets [25] on planet Earth or others celestial bodies [151]; e.g., help the human species expand to Mars [137].

2.3.5 Underwater OWC channel modeling

"Once photons penetrate the air-water interface of aquatic systems they may only be scattered or absorbed. The extent to which either of these phenomena may occur is governed by three parameters: absorption coefficient, scattering coefficient, and the volume scattering function. These three parameters are often referred to as inherent optical properties because they only depend on constituents of the aquatic medium and not on the geometry of the light field" [244]. Curtis Mobley book "Light and water: radiative transfer in natural waters" [165] divide the optical properties of water in two sets [165] of parameters: inherent optical properties (IOP) and apparent optical properties (AOP). The two fundamental IOP used in underwater OWC link budget modeling are the absorption coefficient and volume scattering function that are calculated from the ratios between emitted $\Phi_i(\lambda)$, absorbed $\Phi_a(\lambda)$, scattered $\Phi_s(\lambda)$ and transmitted $\Phi_t(\lambda)$ radiant powers [165]. IOP and AOP are frequently used parameters in many studies of the bio-optical properties of oceanic waters, with AOP values less trivial to model than IOP, causing a diversity of theories and critics about AOP models [171]. The absorption ($a(\lambda)$) and scattering ($b(\lambda)$) coefficients define the beam attenuation coefficient ($c(\lambda)$) frequently used in Beer's law link attenuation models, and the AOP values

depend on the light source direction, normally the sun in other non-OWC applications, with AOP values being always a ratio of two radiometric variables.The AOP downwelling plane irradiance $K_d(\lambda; z)$ is one of the most commonly used parameter to evaluate the water body optical propagation window that will specify the OWC emitter (Laser or LED) wavelength and the receiver type (blue or red region sensitivity). $K_d(\lambda; z)$ is considered to have a high independence from environmental effects [152] and because of that was used by Nils Gunnar Jerlov [117] to develop a water type classification scheme [164]. Jerlov water mass classification shows that the red to orange wavelength band is the optimal choice to develop a short range OWC system that operates in any type of water and that wavelengths between 350 and 500 nm offer the maximum range in clear water types (I, IA, IB, II).

Main factors that affect optical propagation in underwater mediums

The exponential decay caused by the beam attenuation coefficient ($c(\lambda)$) have the consequence to define maximum downwelling ranges for OWC systems that based in diving experience is near 200 meters in clear waters and 50 meters in some coastal waters [185].
Using a simple cause-effect model, the main factors that affect IOP, AOP and the optical propagation in underwater mediums can be reduced to:

- water body chemical constituents variability
- turbulence of the water body
- pressure effect in the refraction index
- sunlight or artificial illumination background noise
- obstacles (marine life, divers, etc.)

Ocean water is made with diverse chemical constituents [219, 34] in a quantity that depends on the location and depth of the water body, being pure water, chlorophyll content [239, 18, 7, 44], humic and fulvic acids [48] that are the constituents that have a higher influence in the optical transmission properties of the water body. Turbulence causes bubbles [104] and intense variation in the refraction index that is also influenced by temperature and salinity fluctuations [157]. Robin Pope and Edward Fry pure water integrating cavity study [199] show that the purest ocean waters may offer low attenuations starting at UV wavelengths (380 nm), with 417 nm being the wavelength that offer the lowest attenuation, values very similar to Laura Johnson PhD research findings [120], Raymond Smith et Baker [222], Morel at al [170] and Tedetti et al [235] articles.

The radiance transfer equation

The equation that links all the IOPs to generate the radiance distribution function is called the radiance transfer equation (RTE) that in a customization [163] for horizontal homogeneous water bodies that do not vary with time (no turbulence or temperature variations) can assume the form of the integro-differential equation 2.11 that can be solved using Monte Carlo methods [136], discrete ordinates [115] or invariant imbedding [166].

$$\begin{aligned}\cos\theta\frac{dL(z,\theta,\varphi,\lambda)}{dz} = -c(z,\lambda)L(z,\theta,\varphi,\lambda) + \int_0^{4\pi} L(z,\theta',\varphi',\lambda) \\ \times\beta(z;\theta',\varphi\rightarrow\theta,\phi;\lambda)d\Omega' + S(z,\theta,\phi,\varphi,\lambda)\end{aligned} \tag{2.11}$$

With (θ',φ') as the incidence direction, (θ,φ) as the scattered direction and $S(z,\theta,\phi,\varphi,\lambda)$ the water body bioluminescence.

The implementation of underwater OWC systems require a perfect knowledge of the

radiance transfer equation of the water body and the use of a professional software like "HydroLight" [167] is required to specify water properties customized optical components.

Underwater link budget equation

The modeling of an underwater link budget equation can be the adaption of equations 2.9 or 2.10, replacing the atmospheric attenuation factors by the underwater attenuation factor $c(\lambda) = a(\lambda) + b(\lambda)$, being $a(\lambda)$ the absorption coefficient and $b(\lambda)$ the scattering coefficient. Diverse articles present this type of link budget equation based in the inverse square law, Lambert cosine law and Beer's law [20, 19, 88, 95, 144, 16, 106] with multiple Monte-Carlo characterization studies [89, 59, 90] for the underwater Beer's law attenuation factor. Underwater OWC systems suffer from multiple scattering in participating media, starting in the LED external quantum efficiency [216] and ending in the photodetector [205] cause intense inter symbol interference (ISI) that can be minimized using a cellular structure [8].

Doniec, Angermann and Rus article [71] present the results of an OWC underwater experiment presenting data from the AquaOptical-II modem, demonstrating that a Beer's law based link budget model (Equation 2.12) offer acceptable precision in clear water bodies.

$$P(\theta, \phi, d) = I(\theta)\frac{exp(cr)}{r^2}S(\phi)A_d\cos(\phi) \tag{2.12}$$

With P (in Watts) as the radiance power arriving to the photodetector, d the OWC distance, θ the transmission angle (beam collimation), ϕ the incident angle at the photon receiver surface, c the absorption coefficient of the water ($\frac{1}{36}m^{-1}$ in this experiment), A_d the photodetector area, $I(\theta)$ is the source radiant intensity function (equivalent to atmospheric equation 2.9) and $S(\phi)$ is the photon receiver angular sensitivity function.

2.3.6 OWC safety and legislation

High power lights can cause injury to eyes and skin, with low divergence LASERs being the most dangerous light source because of its high-density radiation levels. ANSI Z136 LASER safety standard is followed by the United States Department of Labor Occupational Safety & Health Administration (OSHA) that describes in its technical manual (OTM) a summary of biological effects of light in skin and eyes (Table 2.4).

Table 2.4: Summary of basic biological effects of light [184]

Photobiological spectral domain	**Eye effects**	**Skin effects**
Ultraviolet C (0.200 to 0.280 μm)	Photokeratitis	Erythema (sunburn), Skin cancer
Ultraviolet B (0.280 to 315 μm)	Photokeratitis	Accelerated skin aging, Increased pigmentation
Ultraviolet A (0.315 to 0.400 μm)	Photochemical UV cataract	Pigment darkening, Skin burn
Visible (0.400 to 0.780 μm)	Photochemical and thermal retinal injury	Photosensitive reactions, Skin burn
Infrared A (0.780 to 1.400 μm)	Cataract, retinal burns	Skin burn
Infrared B (1.400 to 3.00 μm)	Corneal burn, Aqueous flare, IR cataract	Skin burn
Infrared C (3.00 to 1000 μm)	Corneal burn only	Skin burn

Studies show that wavelengths between 400nm and 1400nm are focused in the eye retina causing it damage [116], and that infrared radiation does not reach the retina but damage the cornea [118]. Below 400nnm the maximum permissible exposure (MPE) is below 1 mW/cm^2 for skin or retinal damage [55] requiring to increase the safety procedures when operating low divergence LASERs or tight collimated LEDs.

Effective eyewear need to be used to protect the eyes from damage, and the European norm EN207 [30] is currently the standard more demanding for eyewear effectiveness against different LASER classes (Table 2.5).

Table 2.5: IEC60825-1 - Safety of Laser Products

Classification	**Outline of risk assessment**
Class 1	Lasers that are safe under reasonably foreseeable conditions of operation, including the use of optical instruments for intra-beam viewing.
Class 1M	Lasers emitting in the wavelength range from 302.5 to 4,000 nm which are safe under reasonably foreseeable conditions of operation, but may be hazardous if the user employs optics within the beam.
Class 2	Lasers that emit visible radiation in the wavelength range from 400 to 700 nm where eye protection is normally afforded by aversion responses, including the blink reflex. This reaction may be expected to provide adequate protection under reasonably foreseeable conditions of operation including the use of optical instruments for intra-beam viewing
Class 2M	Lasers that emit visible radiation in the wavelength range from 400 to 700 nm where eye protection is normally afforded by aversion responses including the blink reflex. However, viewing of the output may be more hazardous if the user employs optics within the beam.
Class 3R	Lasers that emit in the wavelength rage from 302.5 to 106 nm where direct intra-beam viewing is potentially hazardous but the risk is lower than for Class 3B lasers.
Class 3B	Lasers that are normally hazardous when direct intra-beam exposure occurs. Viewing diffuse reflections is normally safe.
Class 4	Lasers that are also capable of producing hazardous diffuse reflections. They may cause skin injuries and could also constitute a fire hazard. Their use requires extreme caution.

2.3.7 Optical detection in OWC systems

Measuring the effects of photons in matter is currently the best method to detect high frequency radiation, because current technology does not allow OWC receivers using direct-conversion (homodyne), overcoming the responsivity limitations of photodetectors at low signal levels [213]. Recent research experiments in the area of optical heterodyne receivers [24] and optical parametric amplification (OPA) resulted in the development of technologies [255] with potential to implement homodyne or heterodyne detection in OWC systems [240].

Full photonic devices are the ideal components to implement OWC systems, but their nonexistence at the present moment [191] force the use of an Electrical-Optical-Electrical (E-O-E) dual transformation connection, with an electrical modulating signal controlling a LED or laser-diode programmable power source or external spatial light modulator [77]. After the beam of light propagates the free space optical (FSO) medium (vacuum, air, water, etc.), the photons will be collected and transported to the photodetector using conventional refractive, reflective or optical fiber waveguides, thus implementing a concentrating stage at the OWC receiver that will be characterized by its photon collecting area, FOV and optical losses. The OWC receiver optical concentrating stage will collect photons from an input area and transfer them into the smaller optical detector active area that may use a photoconductive, photovoltaic, photoemissive or thermal detection technique.

Broadband OWC systems using OFDM require bandwidth that thermal detectors do not offer, forcing the use of semiconductor photoconductive or photovoltaic [241] photodetectors. Non-solid state devices like the photoemissive photomultiplier tube (PMT) can offer more performance [230] in complete darkness mediums, where PMT low dark noise, high gain and large area photocathode responsivity to blue wavelengths have no semiconductor match.

High bandwidth OWC photodetection, in particular, indoor VLC is normally done using unity gain PiN diodes [22], with avalanche photodiodes [84] and superconducting nanowire single photon detectors (SNSPD) more suited for long range OWC. The SNSPD is currently the fastest single-photon detector [103] used in OWC systems, but its requirements for cryogenic cooling makes it not practical in multiple OWC applications. New materials with high quantum efficiency at room temperatures are being researched, which include the carbon allotrope graphene that is a promising material that offers potential to manufacture photodetectors that cover all optical spectrum [204]. Such a solution offers a responsivity that can be enhanced using quantum dots [155] or be used as photoluminescence doping material in WLS optical receivers [233].

NASA's Lunar Laser Communication Demonstration (LLCD) [133] is currently the longest range OWC experiment. The LLCD uses SNSPD photodetection with four 40 cm telescopes [133] that concentrate the low divergence infrared laser light shot by the Lunar Lasercom Space Terminal (LLST) from a satellite orbiting the moon into a cryogenic refrigerated SNSPD quad detector array coupled to a bundle of multimode fiber [100]. The LLCD experiment offers more bandwidth and uses less power than current radio links, but this design is very specific for satellite communications and it is not appropriate to be used on earth surface OWC applications because of the bulkiness of the cryogenic receiver and the SNSPD maximum responsivity [178] at infrared wavelengths not suited be used in the underwater optical transmission window [121].

NASA confined space optics (optical waveguides) solution to pipe the light focused by the four receiving telescopes using a bundle of multimode fiber demonstrated the advantages of all optical amplification technique in FSO.

2.3.8 Optical amplification in OWC systems

Following the FSO amplification approach of LLCD NASA experiment, we investigated the feasibility to use stimulated Raman scattering (SRS) to implement free space optical amplification. Diverse technical literature report optical amplifiers using SRS at near blue wavelengths implemented in pressurized gases [143] or silica fiber [192]. Parallel with Raman FSO amplification, we also experimented if WLS fluorescent fiber Stoke‘s shift and propagation properties allow the design of high gain omnidirectional OWC receivers and if transparent optical waveguides coated with WLS materials can be used as an OWC leaky feeder for longitudinal wireless communications in tunnels [223] [76].

2.3.9 Photon detection using WLS materials

The responsivity of several fluorescent organic materials is described in organic photochemistry literature [60], with diverse organic compounds quantum yield (ϕ) for fluorescence (Equation 2.13) being described by Carsten Achenbach [1] and Pla-Dalmau et al. [193] [194].

$$\phi = \frac{EmmitedPhotons}{AbsorbedPhotons} \tag{2.13}$$

WLS fibers are used in diverse physics experiments [63] like the large hadron collider (LHC) calorimeter, but the behavior of WLS fibers when used as a receiver for LED intensity modulated (IM) OFDM-OWC is not known.

The LHC project is WLS fiber widest literature source, with Gomes et al. [97], presenting a comparative study of WLS fibers from three different manufacturers, giving experimental results for ten types of WLS fibers measuring their light output (Equation 2.14) as a function of short (L_1) and long (L_2) attenuation lengths, fluorescence dopant concentration and fiber

cladding.

$$I(x) = I_{01}e^{\frac{x}{L_1}} + I_{02}e^{\frac{x}{L_2}} \tag{2.14}$$

The decay time of WLS fibers can be modeled by the equation 2.15, with τ_r as the rise time that typically is below 1ns, and a fall time τ_f that can be low as 3ns, as described by Brekhovskikh et al. [43] and Baumbaugh et al. [29].

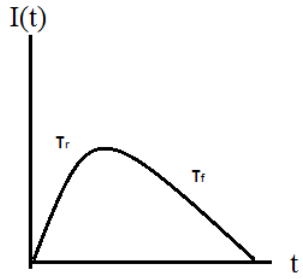

Figure 2.1: Time dependence of WLS emitted light

Figure 2.1 describe the characteristic time response of WLS [231] emitted light and equation 2.16 describes the rise time with a Gaussian function $f(t)$ characterized by a standard deviation σ_{ET} [138].

$$I(t) = I_0(e^{-\frac{t}{\tau_f}} - e^{-\frac{t}{\tau_r}}) \tag{2.15}$$

$$I(t) = I_0 e^{-\frac{t}{\tau_f}} f(t) \tag{2.16}$$

2.3.10 Selection of photodetectors for OWC systems

The decision to use a cooled SNSPD as the photodetector for an interplanetary OWC system required a trade-off study that is common to other OWC applications [114]. The choice for the OWC system photodetector depends on the application bit rate and range [146], background illumination noise [249] and financial budget; here are some application examples:

- Charge-coupled-devices (CCD) for short range and low bandwidth [156] [113]
- Avalanche photodiodes (APD) for medium range and high bandwidth [41]
- PMT in applications with minimal background illumination [197]
- Silicon Photomultiplier (SiPM) for indoor VLC [14].

Time-correlated single-photon counting photodetectors [125] is an example of sensor that is used in physics experiments [40] [119] [188], radiation detectors [46] and nuclear medicine [253], having the potential to be used in OWC system design. The selection of the OWC photodetector will requires a trade-off between the following characteristics:

- Quantum Efficiency η, that measures the ratio between incident photons and generated electrons (expressed in %)
- Spectral Responsivity $\mathcal{R}$, that measures the ratio between the generated photocurrent and the incident light power (usually expressed in A/W)
- Internal gain (e.g., PMT and SiPM)
- Optical-to-electrical signal bandwidth, pulse rise and fall timing values
- Noise-equivalent power (NEP), that is the minimum power of the input signal to be detectable (expressed in W or $W/\sqrt{Hz}$).

The Quantum Efficiency η is the ratio between the electron generation rate (photoelectrons) and the photon incidence rate (Equation 2.17), that in semiconductor [98] or PMT photodetectors is related with the spectral responsivity $\mathcal{R}$ that defines the photocurrent I_p when the active area is exposed to P_r radiometric power ($I_p = \mathcal{R}P_r$).

$$\eta = \frac{\sum electrons}{\sum photons} = \mathcal{R}\frac{h\nu}{q} \tag{2.17}$$

With h as the Planck's constant, q the electron charge and ν the photon frequency that multiplied with the Planck's constant defines the semiconductor bandgap minimal energy to define a photon-electron generation responsivity.

The Optical-to-Electrical (OE) signal bandwidth and pulse timing of different types of photodetectors depend on the technology and its implementation. A trade-off between large detection area and fast timing exists in PiN diodes and APD, where the diode reverse capacitance is associated to the device area, reverse bias voltage and junction thickness. In APDs, excess noise factor, gain, bandwidth and gain-bandwidth product are the most important OWC system design parameters that can be enhanced, using an optimized device layout and semiconductor process [47] [11].

High gain photodetectors also have timing optimized devices, with PMT with photoelectron reduced transit and spread time [105], and SiPM with a fast output terminal [252] that nulls the delay of the internal quenching resistance [68].

The Noise-Equivalent Power "is the input power that gives a signal equal to that of the noise" [245], defining a figure of merit that is dependent on the wavelength of the optical signal λ, how the light intensity modulation frequency f affects the photodetector gain (Equation 2.18) and from quantitative and qualitative characteristics of the existing noise sources.

$$NEP(\lambda, f) = \frac{\sum Noise}{\mathcal{R}(\lambda)Gain(f)} \tag{2.18}$$

Lowering the NEP value in an OWC receiver allow to increase the communications range without rising the photonic emitted power, and that can be done reducing the level of system noise or increasing the $\mathcal{R}(\lambda)Gain(f)$ product.

In low light photodetection, PMT have less noise than APD and because the product $\mathcal{R}(\lambda)Gain(f)$ in PMT is higher than in APD, the low PMT quantum efficiency [162] can be ignored.

APD and PiN photodetectors have a NEP that is affected by shot noise (dark current and photocurrent), Johnson noise from the thermal variations of the diode junction, with APDs having an additional noise source (excess noise) caused by the avalanche gain that also generates a high dark count rate in SiPM devices [139].

PMT photodetectors noise mechanisms are not "solid state" generated, with the main noise factor being caused by the thermionic emission of single electrons from the cathode and dynodes [82]. These technology differences, distinct noise sources and levels in OWC photodetection, force the definition of an OWC system NEP that is a quadratic sum of all individual NEP values (Equation 2.19) presents in the OE conversion [212].

$$SystemNEP^2 = \sum (NEP_1)^2 + \sum (NEP_2)^2 ... + \sum (NEP_n)^2 \tag{2.19}$$

Using Beer's law for mediums with exponential attenuation and equations 2.17, 2.18, 2.19 and 2.20 we can define a photodetector technology independent model [147] for FSO receiver signal-to-noise ratio (SNR) values in atmospheric or underwater omnidirectional OWC links:

$$SNR(P_t, r, c, D, NEP, \phi, \theta) = \left(\frac{P_t e^{-cr} D^2 \cos\phi}{4r^2 \tan^2\theta NEP} \right)^2 \tag{2.20}$$

with P_t as the optical transmitting power, r the OWC link distance, c the atmospheric or underwater attenuation coefficients [243], D the circular shaped receiver diameter, θ the half angle of the transmitter beam width and ϕ the angle between the receiver normal and the photon emission line-of-sight.

Equation 2.20 can be used to predict SNR in different OWC environments and help defining a strategy of modulation techniques [33] to optimize the link bit error rate (BER).

2.3.11 Survey of research and development efforts in OWC systems

OWC is a research objective to hundreds of individuals that Karunatilaka et al. [126], summarize in a literature review survey focused in the time period 1979 to 2014. An updated and more compact version of that survey including a compilation of the most cited articles and known systems is summarized in table 2.6, with table 2.7 presenting a list of PhD thesis related with the research present in this document.

Table 2.6: Connection performance of diverse OWC experiments and systems

Authors	**Range (m)**	**Bit rate**	**Notes**
Snow et al. [224]	9	50 Mbit/s	Underwater, Laser
Bales et al. [26]	20	10 Mbit/s	Underwater, Laser
Tivey et al. [237]	2.7	14.4 Kbit/s	Underwater, LED
Schill et al. [214]	2	57.6 Kbit/s	Underwater, LED
Mark Chancey [51]	12	10 Mbit/s	Underwater, LED
Cochenour et al. [53]	3.6	5 Mbit/s	Underwater, LED
Hanson et al. [107]	2	1 Gbit/s	Underwater, Laser
Heather Brundage [45]	13	3 Mbit/s	Underwater, LED
Simpson et al. [221]	7.7	5 Mbit/s	Underwater, LED
Woods Hole [198]	200	5 Mbit/s	Underwater, LED, PMT
Doniec et al. [72]	30	1.2 Mbit/s	Underwater, LED
Cossu et al. [58]	2.5	58 Mbit/s	Underwater, LED
Oubei et al. [187]	7	2.3 Gbit/s	Underwater, Laser
SA Photonics [190]	200	250 Mbit/s	Underwater, Laser
UON Technologies [234]	40	115 Kbit/s	Underwater, LED
NASA LLCD [36]	400M	622 Mbit/s	Atmosphere, Laser

Table 2.7: PhD thesis (2003 to 2016) complementary to this research

Author	Date	Title	Main contributions
Alqudah [15]	2003	Space diversity techniques in indoor broadband optical wireless communications	FOV
Zand [254]	2003	High-speed Optical Wireless Communications Using Reduced-state Sequence Detection	hardware
Dikmelik [65]	2005	Dember effect photodetectors and the effects of turbulence on free-space optical communication systems	detection
Ketprom [131]	2005	Line-of-sight propagation of optical wave through multiple-scatter channel in optical wireless communication system	channel modeling
Komine [140]	2005	Visible light wireless communications and its fundamental study	VLC modeling
Kedar [129]	2006	Optical Wireless Communication Through Multi-scattering Channels	reception models
Trisno [238]	2006	Design and analysis of advanced free space optical communication systems	omnidirectional receiver
Cole [54]	2006	Estimation and detection of signals in a turbulent free space optical communications channel using array detectors	array detection
Alhammadi [13]	2006	Applying wide field of view retroreflector technology to free space optical robotic communications	cat eye receiver
Anguita [17]	2007	Characterization and advanced communication techniques for free-space optical channels	OAM model
Schill [215]	2007	Distributed communication in swarms of autonomous underwater vehicles	protocol
Binbin [246]	2007	Free-space optical communications through the scattering medium: analysis of signal characteristics	channel model
Lee [149]	2009	Discrete multitone modulation for short-range optical communications	modulations
Popoola [201]	2009	Subcarrier intensity modulated free-space optical communication systems	modulations
Reinhardt [211]	2010	Atmospheric channel modeling and estimation for free-space optical communications systems in adverse visibility using radiative transfer theory	channel model
Hashmi [108]	2010	Novel architectures for broadband free-space optical communications: deep-space and terrestrial optical links	channel model
Son [227]	2010	Design and optimization of free space optical networks	protocol
Lyke [158]	2010	Statistics of the received power for free space optical channels	PDF model
Elgala [79]	2010	A Study on the Impact of Nonlinear Characteristics of LEDs on Optical OFDM	hardware
Liao [154]	2010	Design, fabrication and packaging of dual-mode radio frequency (RF)/free space optical (FSO) wireless communication modules	hardware
Li [153]	2011	MAC Design for Optical Wireless Communications	protocol
Wu [247]	2011	Free space optical networking with visible light: A multi-hop multi-access solution	protocol
Tellez [236]	2011	Integrated approach to free space optical communications in strong turbulence	PDF model
Xiaoyan [248]	2011	Performance Analysis of Multiple Input Multiple Output Free Space Optical Communication Systems	Link model
Drexler [74]	2012	Utilizing Gaussian-Schell model beams to mitigate atmospheric turbulence in free space optical communications	modulations
Ben Naila [32]	2012	Studies on RF signals transmission over a turbulent free space optical channel	receptor modeling
Cox Jr [59]	2012	Simulation, modeling, and design of underwater optical communication systems	underwater channel modeling
He [110]	2012	Performance Limits of Outdoor Wireless Optical Communication Links through Scattering and Turbulent Channels	channel modeling
Cui [61]	2012	Physical layer characteristics and techniques for visible light communications	channel modeling
Simpson [220]	2012	Underwater Free-Space Optical Communication Using Smart Transmitters and Receivers	omnidirectional OWC
Zhou [257]	2013	Broadband Optical Wireless Communications	fly eye receiver
Nelson [179]	2013	Experiments in Optimization of Free Space Optical Communication Links for Applications in a Maritime Environment	channel modeling
Muralidharan [176]	2013	Light emitting diode designs and modulation schemes for dual illumination and visible light communication applications	hardware
Doniec [73]	2013	Autonomous underwater data muling using wireless optical communication and agile AUV control	data mulling
Ahmad [6]	2013	Underwater optical wireless sensor network	hardware
Zhou [256]	2013	Wireless optical transceiver design, link analisys and alignment control for mobile communication	receiver model
Sevincer [217]	2013	Transceiver Selection for Multi-Element Free-Space-Optical Communications	receiver model
Dong [70]	2014	Integrated Transceiver Design for Visible Light Communication System	hardware
Bedi [31]	2014	A new generation of IC based beam steering devices for free-space optical communication	fly-eye FOV
Chowdhury [52]	2014	High-speed Indoor Optical Wireless Communications-Channel Modeling Methods and Applications	channel model
Lee [148]	2014	Free-Space Optical Communication Systems with a Partially Coherent Gaussian Beam and Media Diversity	channel modeling
Johnson [120]	2015	Optical property variability in the underwater optical wireless channel	underwater channel modeling
Ahdi [5]	2016	Reliability and Capacity Planning in Hybrid Optical Networks	hybrid optical protocols

References

[1] Achenbach, C. P. Active optical fibres in modern particle physics experiments. *arXiv preprint nucl-ex/0404008* (2004).

[2] Achour, M. Free-space optics wavelength selection: 10 μm versus shorter wavelengths [invited]. *Journal of optical networking 2*, 6 (2003), 127–143.

[3] Adeyemi-Ejeye, A. O., and Walker, S. D. Ultra-high definition wireless video transmission using h. 264 over 802.11 n wlan: Challenges and performance evaluation. In *Telecommunications (ConTEL), 2013 12th International Conference on* (2013), IEEE, pp. 109–114.

[4] Aharony, O., Gubser, S. S., Maldacena, J., Ooguri, H., and Oz, Y. Large n field theories, string theory and gravity. *Physics Reports 323*, 3 (2000), 183–386.

[5] Ahdi, F. *Reliability and Capacity Planning in Hybrid Optical Networks*. PhD thesis, THE GEORGE WASHINGTON UNIVERSITY, 2016.

[6] Ahmad, Z. U. *Underwater optical wireless sensor network*. PhD thesis, University of Warwick, 2013.

[7] Ahn, Y.-H., Bricaud, A., and Morel, A. Light backscattering efficiency and related properties of some phytoplankters. *Deep Sea Research Part A. Oceanographic Research Papers 39*, 11-12 (1992), 1835–1855.

[8] Akhoundi, F., Salehi, J. A., and Tashakori, A. Cellular underwater wireless optical cdma network: Performance analysis and implementation concepts. *Communications, IEEE Transactions on 63*, 3 (2015), 882–891.

[9] Al Naboulsi, M., de Fornel, F., Sizun, H., Gebhart, M., Leitgeb, E., Muhammad, S. S., Flecker, B., and Chlestil, C. Measured and predicted light attenuation in dense coastal upslope fog at 650, 850, and 950nm for free-space optics applications. *Optical Engineering 47*, 3 (2008), 036001–036001–14.

[10] Al Naboulsi, M. C., Sizun, H., and de Fornel, F. Wavelength selection for the free space optical telecommunication technology. In *Photonics Europe* (2004), International Society for Optics and Photonics, pp. 168–179.

[11] Alaie, Z., Nejad, S. M., and Yousefi, M. Recent advances in ultraviolet photodetectors. *Materials Science in Semiconductor Processing 29* (2015), 16–55.

[12] Alexander, S. B. *Optical communication receiver design*. SPIE Optical engineering press Bellingham, Washington, USA, 1997.

[13] Alhammadi, K. *Applying wide field of view retroreflector technology to free space optical robotic communications*. ProQuest, 2006.

[14] Almer, O., Tsonev, D., Dutton, N. A., Al Abbas, T., Videv, S., Gnecchi, S., Haas, H., and Henderson, R. K. A SPAD-based visible light communications receiver employing higher order modulation. In *2015 IEEE Global Communications Conference (GLOBECOM)* (2015), IEEE, pp. 1–6.

[15] Alqudah, Y. A. *Space diversity techniques in indoor broadband optical wireless communications*. PhD thesis, The Pennsylvania State University, 2003.

[16] Anguita, D., Brizzolara, D., Parodi, G., and Hu, Q. Optical wireless underwater communication for AUV: Preliminary simulation and experimental results. In *OCEANS, 2011 IEEE-Spain* (2011), IEEE, pp. 1–5.

[17] Anguita, J. A. *Characterization and advanced communication techniques for free-space optical channels*. ProQuest, 2007.

[18] Antoine, D., Morel, A., Gentili, B., Gordon, H. R., Banzon, V. F., Evans, R. H., Brown, J. W., Walsh, S., Baringer, W., and Li, A. In search of long-term trends in ocean color. *EOS, Transactions American Geophysical Union 84*, 32 (2003), 301–309.

[19] Arnon, S. Underwater optical wireless communication network. *Optical Engineering 49*, 1 (2010), 015001–015001.

[20] Arnon, S., Barry, J., Karagiannidis, G., Schober, R., and Uysal, M. *Advanced optical wireless communication systems*. Cambridge university press, 2012.

[21] Ashtekar, A., Bonga, B., and Kesavan, A. Gravitational waves from isolated systems: Surprising consequences of a positive cosmological constant. *Physical Review Letters 116*, 5 (2016), 051101.

[22] Atabaki, A. H., Meng, H., Alloatti, L., and Ram, R. J. A High-Speed Photodetector for Telecom, Ethernet, and FTTH applications in zero-change CMOS process. In *Optical Fiber Communication Conference* (2016), Optical Society of America, pp. Tu2D–7.

[23] Awan, M. S., Horwath, L. C., Muhammad, S. S., Leitgeb, E., Nadeem, F., and Khan, M. S. Characterization of fog and snow attenuations for free-space optical propagation. *Journal of communications 4*, 8 (2009), 533–545.

[24] Bai, F., Su, Y., and Sato, T. Performance analysis of heterodyne-detected OCDMA systems using PolSK modulation over a free-space optical turbulence channel. *Electronics 4*, 4 (2015), 785–798.

[25] Bakambu, J. N., Polotski, V., and Cohen, P. Heading-aided odometry and range-data integration for positioning of autonomous mining vehicles. In *Control Applications, 2000. Proceedings of the 2000 IEEE International Conference on* (2000), IEEE, pp. 279–284.

[26] Bales, J. W., and Chrissostomidis, C. High-bandwidth, low-power, short-range optical communication underwater. In *International Symposium on Unmanned Untethered Submersible Technology* (1995), UNIVERSITY OF NEW HAMPSHIRE-MARINE SYSTEMS, pp. 406–415.

[27] Ballesteros, G., Redondo, J., Ringwald, A., and Tamarit, C. Standard model-axion-seesaw-higgs portal inflation. five problems of particle physics and cosmology solved in one stroke. *arXiv preprint arXiv:1610.01639* (2016).

[28] Bannister, P., Harrison, J., Rupp, C., King, R., Cosmo, M., Lorenzini, E., Dyer, C., and Grossi, M. Orbiting transmitter and antenna for spaceborne communications at ELF/VLF to submerged submarines. In *In AGARD, ELF/VLF/LF Radio Propagation and Systems Aspects 14 p (SEE N93-30727 11-32)* (1993), vol. 1.

[29] Baumbaugh, B. W., Baumbaugh, T. A., Brushwyler, T. R., Daily, K. S., Fidler, E. D., Kirzeder, M. B., Lohr, E. E., Marchant, J. M., Mathews, S. S., Ruchti, R. C., et al. Studies of SiPM and scintillation plates with waveshifter fiber and SiPM readout. In *2009 IEEE Nuclear Science Symposium Conference Record (NSS/MIC)* (2009), IEEE, pp. 846–849.

[30] Bäumler, W. Safety/eye protection. In *Laser and IPL Technology in Dermatology and Aesthetic Medicine*. Springer, 2011, pp. 383–393.

[31] Bedi, V. *A new generation of IC based beam steering devices for free-space optical communication*. 2014.

[32] Ben Naila, C. Studies on RF signals transmission over a turbulent free space optical channel.

[33] Bhambare, R. R., and Raut, R. D. A survey on digital modulation techniques for software defined radio applications. *IRACST, ISSN* (2013), 2250–3501.

[34] Bissett, W., Carder, K., Walsh, J., and Dieterle, D. Carbon cycling in the upper waters of the sargasso sea: Ii. numerical simulation of apparent and inherent optical properties. *Deep Sea Research Part I: Oceanographic Research Papers 46*, 2 (1999), 271–317.

[35] Bloom, S. The physics of free space optics. *Air Fiber white paper, available online at http://www. airfiber. com* (2002).

[36] Boroson, D. M., Scozzafava, J. J., Murphy, D. V., Robinson, B. S., and Shaw, H. The lunar laser communications demonstration (llcd). In *Space Mission Challenges for Information Technology, 2009. SMC-IT 2009. Third IEEE International Conference on* (2009), IEEE, pp. 23–28.

[37] Bouchet, O. *Wireless Optical Communications*. John Wiley & Sons, 2013.

[38] Bouchet, O., Sizun, H., Boisrobert, C., and De Fornel, F. *Free-space optics: propagation and communication*, vol. 91. John Wiley & Sons, 2010.

[39] Boveris, A., Cadenas, E., and Chance, B. Ultraweak chemiluminescence: a sensitive assay for oxidative radical reactions. In *Federation proceedings* (1981), vol. 40, pp. 195–198.

[40] Braem, A., Joram, C., Piuz, F., Schyns, E., and Seguinot, J. Technology of photocathode production. *Nuclear Instruments and Methods in Physics Research Section A: Accelerators, Spectrometers, Detectors and Associated Equipment 502*, 1 (2003), 205–210.

[41] Brandl, P., Enne, R., Jukic, T., and Zimmermann, H. OWC using a fully integrated optical receiver with large-diameter APD. *Photonics Technology Letters, IEEE 27*, 5 (2015), 482–485.

[42] Brandl, P., Plank, T., and Leitgeb, E. Optical wireless links in future space communications with high data rate demands. In *Satellite and Space Communications, 2009. IWSSC 2009. International Workshop on* (2009), IEEE, pp. 305–309.

[43] Brekhovskikh, V., Konoplyannikov, A., Rykaline, V., and Dzhelyadin, R. The WLS fiber time properties study. Tech. rep., 2000.

[44] Bricaud, A., Morel, A., Babin, M., Allali, K., and Claustre, H. Variations of light absorption by suspended particles with chlorophyll a concentration in oceanic (case 1) waters: Analysis and implications for bio-optical models. *Journal of Geophysical Research: Oceans 103*, C13 (1998), 31033–31044.

[45] Brundage, H. *Designing a wireless underwater optical communication system*. PhD thesis, Massachusetts Institute of Technology, 2010.

[46] Buzhan, P., Dolgoshein, B., Filatov, L., Ilyin, A., Kantzerov, V., Kaplin, V., Karakash, A., Kayumov, F., Klemin, S., Popova, E., et al. Silicon photomultiplier and its possible applications. *Nuclear Instruments and Methods in Physics Research Section A: Accelerators, Spectrometers, Detectors and Associated Equipment 504*, 1 (2003), 48–52.

[47] Campbell, J. C. Recent advances in avalanche photodiodes. *Journal of Lightwave Technology 34*, 2 (2016), 278–285.

[48] Carder, K. L., Steward, R. G., Harvey, G. R., and Ortner, P. B. Marine humic and fulvic acids: Their effects on remote sensing of ocean chlorophyll. *Limnology and oceanography 34*, 1 (1989), 68–81.

[49] Castelvecchi, D. Axion alert! Exotic-particle detector may miss out on dark matter, November 2016. http://www.nature.com/news/axion-alert-exotic-particle-detector-may-miss-out-on-dark-matter-1.20925.

[50] Caves, C. M. Quantum-mechanical noise in an interferometer. *Physical Review D 23*, 8 (1981), 1693.

[51] Chancey, M. A. Short range underwater optical communication links.

[52] Chowdhury, M. I. S. *HIGH-SPEED INDOOR OPTICAL WIRELESS COMMUNICATIONS–CHANNEL MODELING METHODS AND APPLICATIONS*. PhD thesis, The Pennsylvania State University, 2014.

[53] Cochenour, B., Mullen, L., and Laux, A. *Phase coherent digital communications for wireless optical links in turbid underwater environments*. IEEE, 2007.

[54] Cole, M. *Estimation and detection of signals in a turbulent free space optical communications channel using array detectors*, vol. 68. 2006.

[55] Corbett, J., Woods, M., et al. UV laser radiation: Skin hazards and skin protection controls. Tech. rep., SLAC National Accelerator Laboratory (SLAC), 2013.

[56] Corkery, J., Forder, J., Svantesson, D., and Mercuri, E. Taxes, the internet and the digital economy. *Revenue Law Journal 23*, 1 (2015), 7.

[57] Cornwell, D. Laser communication from the moon at 622mb/s, 2014.

[58] Cossu, G., Corsini, R., Khalid, A., Balestrino, S., Coppelli, A., Caiti, A., and Ciaramella, E. Experimental demonstration of high speed underwater visible light communications. In *Optical Wireless Communications (IWOW), 2013 2nd International Workshop on* (2013), IEEE, pp. 11–15.

[59] Cox Jr, W. C. *Simulation, modeling, and design of underwater optical communication systems*. North Carolina State University, 2012.

[60] Coyle, J. D. *Introduction to organic photochemistry*. John Wiley & Sons, 1986.

[61] Cui, K. Physical layer characteristics and techniques for visible light communications.

[62] Da Dalt, N., Harteneck, M., Sandner, C., and Wiesbauer, A. On the jitter requirements of the sampling clock for analog-to-digital converters. *Circuits and Systems I: Fundamental Theory and Applications, IEEE Transactions on 49*, 9 (2002), 1354–1360.

[63] Danilov, M., representing the CALICE collaboration, et al. Scintillator tile hadron calorimeter with novel SiPM readout. *Nuclear Instruments and Methods*

in Physics Research Section A: Accelerators, Spectrometers, Detectors and Associated Equipment 581, 1 (2007), 451–456.

[64] de Bernardis, P., Ade, P. A., Bock, J., Bond, J., Borrill, J., Boscaleri, A., Coble, K., Crill, B., De Gasperis, G., Farese, P., et al. A flat universe from high-resolution maps of the cosmic microwave background radiation. *Nature 404*, 6781 (2000), 955–959.

[65] Dikmelik, Y. *Dember effect photodetectors and the effects of turbulence on free-space optical communication systems*. 2005.

[66] Dilhac, J. The telegraph of claude chappe-an optical telecommunication network for the xviiith century. *Institut National des Sciences Appliquées de Toulouse* (2001).

[67] Dissanayake, S. D., and Armstrong, J. Comparison of ACO-OFDM, DCO-OFDM and ADO-OFDM in IM/DD systems. *Journal of lightwave technology 31*, 7 (2013), 1063–1072.

[68] Dolinsky, S., Fu, G., and Ivan, A. Timing resolution performance comparison for fast and standard outputs of SensL SiPM. In *Nuclear Science Symposium and Medical Imaging Conference (NSS/MIC), 2013 IEEE* (2013), IEEE, pp. 1–6.

[69] Donaldson, G. Signalling communications and the roman imperial army. *Britannia 19* (1988), 349–356.

[70] Dong, Z. Integrated transceiver design for visible light communication system.

[71] Doniec, M., Angermann, M., and Rus, D. An end-to-end signal strength model for underwater optical communications. *Oceanic Engineering, IEEE Journal of 38*, 4 (2013), 743–757.

[72] Doniec, M., Detweiler, C., Vasilescu, I., and Rus, D. Using optical communication for remote underwater robot operation. In *Intelligent Robots and Systems (IROS), 2010 IEEE/RSJ International Conference on* (2010), IEEE, pp. 4017–4022.

[73] Doniec, M. W. *Autonomous underwater data muling using wireless optical communication and agile AUV control*. PhD thesis, Massachusetts Institute of Technology, 2013.

[74] Drexler, K. R. *Utilizing Gaussian-Schell model beams to mitigate atmospheric turbulence in free space optical communications*. 2012.

[75] Du Castel, F. *Tropospheric Radiowave Propagation Beyond the Horizon: International Series of Monographs in Electromagnetic Waves*. Elsevier, 2013.

[76] Dudley, S. E., Quinlan, T. J., and Walker, S. D. Ultrabroadband wireless–optical transmission links using axial slot leaky feeders and optical fiber for underground transport topologies. *IEEE Transactions on Vehicular Technology 57*, 6 (2008), 3471–3476.

[77] Efron, U. *Spatial light modulator technology: materials, devices, and applications*, vol. 47. CRC Press, 1994.

[78] Egli, J. J. Radio propagation above 40 mc over irregular terrain. *Proceedings of the IRE 45*, 10 (1957), 1383–1391.

[79] Elgala, H. *A Study on the Impact of Nonlinear Characteristics of LEDs on Optical OFDM*. PhD thesis, Jacobs University Bremen, 2010.

[80] Eliaz, A., and Reuven, I. Highly-spectrally-efficient reception using orthogonal frequency division multiplexing, Oct. 30 2014. US Patent 20,140,321,525.

[81] Ellis, J. R., Mavromatos, N., and Nanopoulos, D. Probing models of quantum spacetime foam. Tech. rep., 1999.

[82] Engstrom, R. W. Multiplier photo-tube characteristics: Application to low light levels. *JOSA 37*, 6 (1947), 420–431.

[83] Falkowski, A., and Pérez-Victoria, M. Electroweak precision observables and the unhiggs. *Journal of High Energy Physics 2009*, 12 (2009), 061.

[84] Ferraro, M. S., Rabinovich, W. S., Clark, W. R., Waters, W. D., Campbell, J. C., Mahon, R., Vaccaro, K., and Krejca, B. D. Impact ionization engineered avalanche photodiode arrays for free space optical communication. In *SPIE LASE* (2016), International Society for Optics and Photonics, pp. 97390S–97390S.

[85] Font-Ribera, A., McDonald, P., Mostek, N., Reid, B. A., Seo, H.-J., and Slosar, A. Desi and other dark energy experiments in the era of neutrino mass measurements. *Journal of Cosmology and Astroparticle Physics 2014*, 05 (2014), 023.

[86] for the DEAP Collaboration, B. C., et al. The DEAP-3600 dark matter experiment. *arXiv preprint arXiv:1511.00949* (2015).

[87] Francis, P. J., Hewett, P. C., Foltz, C. B., Chaffee, F. H., Weymann, R. J., and Morris, S. L. A high signal-to-noise ratio composite quasar spectrum. *The Astrophysical Journal 373* (1991), 465–470.

[88] Gabriel, C., Khalighi, M.-A., Bourennane, S., Leon, P., and Rigaud, V. Channel modeling for underwater optical communication. In *GLOBECOM Workshops (GC Wkshps), 2011 IEEE* (2011), IEEE, pp. 833–837.

[89] Gabriel, C., Khalighi, M.-A., Bourennane, S., Léon, P., and Rigaud, V. Monte-carlo-based channel characterization for underwater optical communication systems. *Journal of Optical Communications and Networking 5*, 1 (2013), 1–12.

[90] Gabriel, C., Khalighi, M. A., Bourennane, S., Lon, P., and Rigaud, V. Misalignment considerations in point-to-point underwater wireless optical links. In *OCEANS - Bergen, 2013 MTS/IEEE* (June 2013), pp. 1–5.

[91] Galton, I. Spectral shaping of circuit errors in digital-to-analog converters. *Circuits and Systems II: Analog and digital signal processing, IEEE Transactions on 44*, 10 (1997), 808–817.

[92] Gebhart, M., Leitgeb, E., Muhammad, S. S., Flecker, B., Chlestil, C., Al Naboulsi, M., de Fornel, F., and Sizun, H. Measurement of light attenuation in dense fog conditions for fso applications. In *Optics & Photonics 2005* (2005), International Society for Optics and Photonics, pp. 58910K–58910K.

[93] Gendreau, K. C., Arzoumanian, Z., Kenyon, S. J., and Spartana, N. S. Miniaturized high-speed modulated x-ray source, Aug. 25 2015. US Patent 9,117,622.

[94] Ghassemlooy, Z., Popoola, W., and Rajbhandari, S. *Optical wireless communications: system and channel modelling with Matlab®*. CRC Press, 2012.

[95] Giles, J. W., and Bankman, I. N. Underwater optical communications systems. part 2: basic design considerations. In *Military Communications Conference, 2005. MILCOM 2005. IEEE* (2005), IEEE, pp. 1700–1705.

[96] Goldhirsh, J., and Vogel, W. J. Handbook of propagation effects for vehicular and personal mobile satellite systems. *NASA Reference Publication 1274* (1998), 40–67.

[97] Gomes, A., David, M., Henriques, A., and Maio, A. Comparative study of WLS fibres for the ATLAS tile calorimeter. *Nuclear Physics B-Proceedings Supplements 61*, 3 (1998), 106–111.

[98] Govind, P. A. Fiber-optic communication systems. *John Wiley, New York* (2002).

[99] Green, D. B., and Obaidat, A. An accurate line of sight propagation performance model for ad-hoc 802.11 wireless lan (wlan) devices. In *Communications, 2002. ICC 2002. IEEE International Conference on* (2002), vol. 5, IEEE, pp. 3424–3428.

[100] Grein, M. E., Kerman, A. J., Dauler, E. A., Shatrovoy, O., Molnar, R. J., Rosenberg, D., Yoon, J., DeVoe, C. E., Murphy, D. V., Robinson, B. S., et al. Design of a ground-based optical receiver for the lunar laser communications demonstration. In *Space Optical Systems and Applications (ICSOS), 2011 International Conference on* (2011), IEEE, pp. 78–82.

[101] Gulbahar, B., and Akan, O. B. A communication theoretical modeling and analysis of underwater magneto-inductive wireless channels. *Wireless Communications, IEEE Transactions on 11*, 9 (2012), 3326–3334.

[102] Güler, G., Tomruk, A., Ozgur, E., Sahin, D., Sepici, A., Altan, N., and Seyhan, N. The effect of radiofrequency radiation on dna and lipid damage in female and male infant rabbits. *International journal of radiation biology 88*, 4 (2012), 367–373.

[103] Hadfield, R. H., and Johansson, G. Superconducting devices in Quantum optics, 2016.

[104] Hagem, R. M., Thiel, D. V., O'Keefe, S. G., and Fickenscher, T. The effect of air bubbles on an underwater optical communications system for wireless sensor network applications. *Microwave and Optical Technology Letters 54*, 3 (2012), 729–732.

[105] Hamamatsu Photonics, K. Photomultiplier tubes: Basics and applications. *Edition 3a* (2006).

[106] Hamza, T., Khalighi, M.-A., Bourennane, S., Léon, P., and Opderbecke, J. Investigation of solar noise impact on the performance of underwater wireless optical communication links. *Opt. Express 24*, 22 (Oct 2016), 25832–25845.

[107] Hanson, F., and Radic, S. High bandwidth underwater optical communication. *Applied optics 47*, 2 (2008), 277–283.

[108] Hashmi, A. J. Novel architectures for broadband free-space optical communications: deep-space and terrestrial optical links.

[109] Haykin, S. S., Moher, M., and Song, T. *An introduction to analog and digital communications*, vol. 1. Wiley New York, 1989.

[110] He, Q. Performance limits of outdoor wireless optical communication links through scattering and turbulent channels.

[111] Hillger, P., Grzyb, J., Lachner, R., and Pfeiffer, U. An antenna-coupled 0.49 thz sige hbt source for active illumination in terahertz imaging applications. In *Microwave Integrated Circuits Conference (EuMIC), 2015 10th European* (2015), IEEE, pp. 180–183.

[112] Holub, P., Šrom, M., Pulec, M., Matela, J., and Jirman, M. Gpu-accelerated dxt and jpeg compression schemes for low-latency network transmissions of hd, 2k, and 4k video. *Future Generation Computer Systems 29*, 8 (2013), 1991–2006.

[113] Iwase, D., Kasai, M., Yendo, T., Arai, S., Yamazato, T., Okada, H., and Fujii, T. Improving communication rate of visible light communication system using high-speed camera. In *Circuits and Systems (APCCAS), 2014 IEEE Asia Pacific Conference on* (Nov 2014), pp. 336–339.

[114] Jakšić, Z. *Micro and Nanophotonics for Semiconductor Infrared Detectors: Towards an Ultimate Uncooled Device*. Springer, 2014.

[115] Jaruwatanadilok, S. Underwater wireless optical communication channel modeling and performance evaluation using vector radiative transfer theory. *Selected Areas in Communications, IEEE Journal on 26*, 9 (2008), 1620–1627.

[116] Jeon, S., and Lee, W. K. inner retinal damage after exposure to green diode laser during a laser show. *Clinical ophthalmology (Auckland, NZ) 8* (2014), 2467.

[117] Jerlov, N. G. *Marine optics*, vol. 14. Elsevier, 1976.

[118] Jiao, L.-G., Wang, J.-R., Yang, J.-G., and Yang, Z.-F. Ocular damage induced by a vis-infrared supercontinuum source. *Journal of biomedical optics 19*, 12 (2014), 120503–120503.

[119] Jillings, C., Ford, R., Hallin, A., Harvey, P., MacLeod, R., Mak, H., Skensved, P., and Stevenson, R. The photomultiplier tube testing facility for the Sudbury neutrino observatory. *Nuclear Instruments and Methods in Physics Research Section A: Accelerators, Spectrometers, Detectors and Associated Equipment 373*, 3 (1996), 421–429.

[120] Johnson, L. J. *Optical property variability in the underwater optical wireless channel*. PhD thesis, University of Warwick, 2015.

[121] Johnson, L. J., Jasman, F., Green, R. J., and Leeson, M. S. Recent advances in underwater optical wireless communications. *Underwater Technology 32*, 3 (2014), 167–175.

[122] Joshi, M. S. Outdoor propagation models: A literature review. *International Journal on Computer Science and Engineering 4*, 2 (2012).

[123] Ju, Z., Shan, C., Jiang, D., Zhang, J., Yao, B., Zhao, D., Shen, D., and Fan, X. Mg zn1- o-based photodetectors covering the whole solar-blind spectrum range. *Applied Physics Letters 93*, 17 (2008).

[124] Kahn, J. M., and Barry, J. R. Wireless infrared communications. *Proceedings of the IEEE 85*, 2 (1997), 265–298.

[125] Kapusta, P., Wahl, M., and Erdmann, R. *Advanced Photon Counting: Applications, Methods, Instrumentation*, vol. 15. Springer, 2015.

[126] Karunatilaka, D., Zafar, F., Kalavally, V., and Parthiban, R. LED based indoor visible light communications: State of the art. *IEEE Communications Surveys & Tutorials 17*, 3 (2015), 1649–1678.

[127] Kasampalis, S., Lazaridis, P. I., Zaharis, Z. D., Bizopoulos, A., Zettas, S., and Cosmas, J. Comparison of longley-rice, itu-r p. 1546 and hata-davidson propagation models for dvb-t coverage prediction. In *Broadband Multimedia Systems and Broadcasting (BMSB), 2014 IEEE International Symposium on* (2014), IEEE, pp. 1–4.

[128] Kaur, H., Bhardwaj, A., and Soni, G. Performance improvement of free space optical link by varying transmitter and receiver aperture diameter. In *Communication Technologies (GCCT), 2015 Global Conference on* (2015), IEEE, pp. 761–766.

[129] Kedar, D. *Optical Wireless Communication Through Multi-scattering Channels*. PhD thesis, Ben-Gurion University of the Negev, 2006.

[130] Kennedy, C. Army signalling and its use in war. *The RUSI Journal 41*, 234 (1897), 969–998.

[131] Ketprom, U. *Line-of-sight propagation of optical wave through multiple-scatter channel in optical wireless communication system*. PhD thesis, University of Washington, 2005.

[132] Khan, M. S., Awan, M. S., Muhammad, S. S., Faisal, M., Marzuki, M., Nadeem, F., and Leitgeb, E. Probabilistic model for free-space optical links under continental fog conditions. *Radioengineering 19*, 3 (2010), 460–465.

[133] Khatri, F. I., Robinson, B. S., Semprucci, M. D., and Boroson, D. M. Lunar laser communication demonstration operations architecture. *Acta Astronautica 111* (2015), 77–83.

[134] Killinger, D. Free space optics for laser communication through the air. *Optics and Photonics News 13*, 10 (2002), 36–42.

[135] Kim, I. I., McArthur, B., and Korevaar, E. Comparison of laser beam propagation at 785 nm and 1550 nm in fog and haze for optical wireless communications. In *proc. SPIE* (2001), vol. 4214, pp. 26–37.

[136] Kirk, J. Monte carlo study of the nature of the underwater light field in, and the relationships between optical properties of, turbid yellow waters. *Marine and Freshwater Research 32*, 4 (1981), 517–532.

[137] Knapp, A. SpaceX billionaire Elon Musk wants a Martian colony of 80,000 people, 2012.

[138] Knoll, G. F. *Radiation detection and measurement*. John Wiley & Sons, 2010.

[139] Kolb, A., Lorenz, E., Judenhofer, M. S., Renker, D., Lankes, K., and Pichler, B. J. Evaluation of geiger-mode APDs for PET block detector designs. *Physics in medicine and biology 55*, 7 (2010), 1815.

[140] Komine, T. *Visible light wireless communications and its fundamental study*. PhD thesis, Ph. D. dissertation, Keio University, 2005.

[141] Korevaar, E. J., Kim, I. I., and McArthur, B. Debunking the recurring myth of a magic wavelength for free-space optics. In *ITCom 2002: The Convergence of Information Technologies and Communications* (2002), International Society for Optics and Photonics, pp. 155–166.

[142] Kouwn, S., Oh, P., and Park, C.-G. Massive photon and dark energy. *arXiv preprint arXiv:1512.00541* (2015).

[143] Krylov, V., Ollikainen, O., Wild, U. P., Rebane, A., Bespalov, V. G., and Staselko, D. I. Femtosecond stimulated Raman scattering in pressurized gases in the ultraviolet and visible spectral ranges. *JOSA B 15*, 12 (1998), 2910–2916.

[144] Kumar, P. V., Praneeth, S., and Narender, R. B. Analysis of optical wireless communication for underwater wireless communication. *Int. J. Sci. Eng. Res. 2* (2011), 1–9.

[145] Kurosawa, N., Kobayashi, H., Kogure, H., Komuro, T., and Sakayori, H. Sampling clock jitter effects in digital-to-analog converters. *Measurement 31*, 3 (2002), 187–199.

[146] LANGER, K.-D., and GROBE, L. Recent results & emerging solutions in opt. wireless indoor communications.

[147] Lanzagorta, M. Underwater communications. *Synthesis Lectures on Communications 5*, 2 (2012), 1–129.

[148] Lee, I. E. *Free-Space Optical Communication Systems with a Partially Coherent Gaussian Beam and Media Diversity*. PhD thesis, Northumbria University, 2014.

[149] Lee, J. Discrete multitone modulation for short-range optical communications. *Eindhoven: Technische Universiteit Eindhoven* (2009).

[150] Leitgeb, E., Plank, T., Awan, M., Brandl, P., Popoola, W., Ghassemlooy, Z., Ozek, F., and Wittig, M. Analysis and evaluation of optimum wavelengths for free-space optical transceivers. In *Transparent Optical Networks (ICTON), 2010 12th International Conference on* (2010), IEEE, pp. 1–7.

[151] Lever, P. J., and Wang, F.-Y. Intelligent excavator control system for lunar mining system. *Journal of Aerospace Engineering 8*, 1 (1995), 16–24.

[152] Lewis, M. The measurement of apparent optical properties for the diagnosis of harmful algal blooms. *Real-time Coastal Observing Systems for Marine Ecosystem Dynamics and Harmful Algal Blooms: Theory, Instrumentation and Modelling, edited by: Babin, M., Roesler, CS, and Cullen, JJ, UNESCO, Paris* (2008), 207–236.

[153] Li, Y. Mac design for optical wireless communications.

[154] Liao, J. *Design, fabrication and packaging of dual-mode radio frequency (RF)/free space optical (FSO) wireless communication modules*. PhD thesis, RENSSELAER POLYTECHNIC INSTITUTE, 2010.

[155] Liu, C.-H., Chang, Y.-C., Norris, T. B., and Zhong, Z. Graphene photodetectors with ultra-broadband and high responsivity at room temperature. *Nature nanotechnology 9*, 4 (2014), 273–278.

[156] Liu, Y. Decoding mobile-phone image sensor rolling shutter effect for visible light communications. *Optical Engineering 55*, 1 (2016), 016103–016103.

[157] Lu, W., Liu, L., and Sun, J. Influence of temperature and salinity fluctuations on propagation behaviour of partially coherent beams in oceanic turbulence. *Journal of Optics A: Pure and Applied Optics 8*, 12 (2006), 1052.

[158] Lyke, S. D. Statistics of the received power for free space optical channels.

[159] Manor, H., and Arnon, S. Performance of an optical wireless communication system as a function of wavelength. *Applied optics 42*, 21 (2003), 4285–4294.

[160] McElrath, B. Emergent electroweak gravity. *arXiv preprint arXiv:0812.2696* (2008).

[161] Miranda, L. C., and Lima, C. A. Trends and cycles of the internet evolution and worldwide impacts. *Technological Forecasting and Social Change 79*, 4 (2012), 744–765.

[162] Mirzoyan, R., Laatiaoui, M., and Teshima, M. Very high quantum efficiency PMTs with bialkali photo-cathode. *Nuclear Instruments and Methods in Physics Research Section A: Accelerators, Spectrometers, Detectors and Associated Equipment 567*, 1 (2006), 230–232.

[163] Mobley, C. Radiative transfer in the ocean. *Encyclopedia of ocean sciences 4* (2001), 2321.

[164] Mobley, C., Boss, E., and Roesler, C. Ocean optics web book, 2010.

[165] Mobley, C. D. *Light and water: radiative transfer in natural waters*. Academic press, 1994.

[166] Mobley, C. D., Gentili, B., Gordon, H. R., Jin, Z., Kattawar, G. W., Morel, A., Reinersman, P., Stamnes, K., and Stavn, R. H. Comparison of numerical models for computing underwater light fields. *Applied Optics 32*, 36 (1993), 7484–7504.

[167] Mobley, C. D., and Sundman, L. K. Hydrolight 5, ecolight 5, technical documentation. sequoia scientific. *Inc, Bellevue* (2008).

[168] Morant, M., Llorente, R., Herrera, J., Alves, T., Cartaxo, A., and Herman, M. Integrated FTTH and in-building fiber-coax OFDM field trial.

[169] Moreira, A. J., Valadas, R. T., and de Oliveira Duarte, A. Optical interference produced by artificial light. *Wireless Networks 3*, 2 (1997), 131–140.

[170] Morel, A., Gentili, B., Claustre, H., Babin, M., Bricaud, A., Ras, J., and Tieche, F. Optical properties of the clearest natural waters. *Limnology and oceanography 52*, 1 (2007), 217–229.

[171] Morel, A., and Maritorena, S. Bio-optical properties of oceanic waters- a reappraisal. *Journal of Geophysical research 106*, C4 (2001), 7163–7180.

[172] Moriarty, D., and Hombs, B. System design of tactical communications with solar blind ultraviolet non line-of-sight systems. In *Military Communications Conference, 2009. MILCOM 2009. IEEE* (2009), IEEE, pp. 1–7.

[173] Moschitta, A., and Petri, D. Wideband communication system sensitivity to overloading quantization noise [adc characterization]. *Instrumentation and Measurement, IEEE Transactions on 52*, 4 (2003), 1302–1307.

[174] Moszynski, M., Plettner, C., Nassalski, A., Szczesniak, T., Swiderski, L., Syntfeld-Kazuch, A., Czarnacki, W., Pausch, G., Stein, J., Niculae, A., et al. A comparative study of silicon drift detectors with photomultipliers, avalanche photodiodes and pin photodiodes in gamma spectrometry with labr3 crystals. *IEEE Transactions on Nuclear Science 56*, 3 (2009), 1006.

[175] Muhammad, S. S., Köhldorfer, P., and Leitgeb, E. Channel modeling for terrestrial free space optical links. In *Transparent Optical Networks, 2005, Proceedings of 2005 7th International Conference* (2005), vol. 1, IEEE, pp. 407–410.

[176] Muralidharan, S. *Light emitting diode designs and modulation schemes for dual illumination and visible light communication applications.* PhD thesis, RENSSELAER POLYTECHNIC INSTITUTE, 2013.

[177] Nadeem, F., Kvicera, V., Awan, M. S., Leitgeb, E., Muhammad, S. S., and Kandus, G. Weather effects on hybrid FSO/RF communication link. *Selected Areas in Communications, IEEE Journal on 27*, 9 (2009), 1687–1697.

[178] Natarajan, C. M., Tanner, M. G., and Hadfield, R. H. Superconducting nanowire single-photon detectors: physics and applications. *Superconductor science and technology 25*, 6 (2012), 063001.

[179] Nelson, C. *Experiments in Optimization of Free Space Optical Communication Links for Applications in a Maritime Environment.* PhD thesis, dissertation from John Hopkins University, 2013.

[180] Nieto, A., and Dagdelen, K. Development and testing of a vehicle collision avoidance system based on gps and wireless networks for open-pit mines. In *31st International Symposium on Applications of Computers in the Minerals Industries-APCOM* (2003), Citeseer, p. 50.

[181] Njoku, E., Abrams, M. J., Asrar, G. R., Marzano, F. S., Minnett, P. J., Salomonson, V. V., Singhroy, V. H., and Turk, F. J. *Encyclopedia of Remote Sensing.* Springer, 2014.

[182] O'Brien, D. C., Zeng, L., Le-Minh, H., Faulkner, G., Walewski, J. W., and Randel, S. Visible light communications: Challenges and possibilities. In

Personal, Indoor and Mobile Radio Communications, 2008. PIMRC 2008. IEEE 19th International Symposium on (2008), IEEE, pp. 1–5.

[183] of Australia, W. I. Modulated light, June 2005. http://modulatedlight.org/Modulated_Light_DX/GrothArticle1.html.

[184] of Labor Occupational Safety & Health Administration, U. S. D. Osha technical manual, March 2015. https://www.osha.gov/dts/osta/otm/otm_iii/otm_iii_6.html#3.

[185] of Ocean Exploration, T. N. O., and Research. Depth at which different colors of light penetrate ocean waters, May 2016. http://oceanexplorer.noaa.gov/explorations/04deepscope/background/deeplight/media/diagram3.html.

[186] O'Sullivan, C. M., and Murphy, J. A. Field guide to terahertz sources, detectors, and optics. SPIE.

[187] Oubei, H. M., Li, C., Park, K.-H., Ng, T. K., Alouini, M.-S., and Ooi, B. S. 2.3 Gbit/s underwater wireless optical communications using directly modulated 520 nm laser diode. *Optics express 23*, 16 (2015), 20743–20748.

[188] Pansart, J. Avalanche photodiodes for particle detection. *Nuclear Instruments and Methods in Physics Research Section A: Accelerators, Spectrometers, Detectors and Associated Equipment 387*, 1 (1997), 186–193.

[189] Perez, A. Spin foam models for quantum gravity. *Classical and Quantum Gravity 20*, 6 (2003), R43.

[190] Photonics, S. Neptune underwater optical communications.

[191] Pile, D. Microprocessors: Electronic-photonic chip. *Nature Photonics 10*, 3 (2016), 145–145.

[192] Pini, R., Salimbeni, R., Matera, M., and Lin, C. Ultraviolet four-photon mixing in a multimode silica fiber Raman amplifier. *Optics Communications 47*, 3 (1983), 226–229.

[193] Pla-Dalmau, A., Foster, G., and Zhang, G. Coumarins as wavelength shifters in polystyrene. *Nuclear Instruments and Methods in Physics Research Section A: Accelerators, Spectrometers, Detectors and Associated Equipment 361*, 1 (1995), 192–196.

[194] Pla-Dalmau, A., Zhang, G., and Foster, G. Searching for new green wavelength shifters in polystyrene. Tech. rep., 1993.

[195] Planck, M. *The theory of heat radiation*. Courier Corporation, 2013.

[196] Plank, T., Leitgeb, E., and Loeschnigg, M. Recent developments on free space optical links and wavelength analysis. In *Space Optical Systems and Applications (ICSOS), 2011 International Conference on* (2011), IEEE, pp. 14–20.

[197] Pontbriand, C., Farr, N., Hansen, J., Kinsey, J. C., Pelletier, L.-P., Ware, J., and Fourie, D. Wireless data harvesting using the AUV sentry and WHOI optical modem. In *OCEANS 2015-MTS/IEEE Washington* (2015), IEEE, pp. 1–6.

[198] Pontbriand, C., Farr, N., Ware, J., Preisig, J., and Popenoe, H. Diffuse high-bandwidth optical communications. In *OCEANS 2008* (2008), IEEE, pp. 1–4.

[199] Pope, R. M., and Fry, E. S. Absorption spectrum (380–700 nm) of pure water. ii. integrating cavity measurements. *Applied optics 36*, 33 (1997), 8710–8723.

[200] Popoola, W., Ghassemlooy, Z., Awan, M., and Leitgeb, E. Atmospheric channel effects on terrestrial free space optical communication links. In *Proceedings of 3rd International Conference on Electronics, Computers and Artificial Intelligence* (2009), pp. 17–23.

[201] Popoola, W. O. *Subcarrier intensity modulated free-space optical communication systems*. PhD thesis, Northumbria University, 2009.

[202] Popov, M. The convergence of wired and wireless services delivery in access and home networks. In *Optical Fiber Communication Conference* (2010), Optical Society of America, p. OWQ6.

[203] Pospieszalski, M. W. Extremely low-noise amplification with cryogenic FETs and HFETs: 1970-2004. *Microwave Magazine, IEEE 6*, 3 (2005), 62–75.

[204] Pospischil, A., Humer, M., Furchi, M. M., Bachmann, D., Guider, R., Fromherz, T., and Mueller, T. CMOS-compatible graphene photodetector covering all optical communication bands. *Nature Photonics 7*, 11 (2013), 892–896.

[205] Premože, S., Ashikhmin, M., Tessendorf, J., Ramamoorthi, R., and Nayar, S. Practical rendering of multiple scattering effects in participating media. In *Proceedings of the Fifteenth Eurographics conference on Rendering Techniques* (2004), pp. 363–374.

[206] Quan, J., Li, Y., and Zhang, Y. Configuring indoor visible light communication networks. In *Communications in China Workshops (ICCC), 2012 1st IEEE International Conference on* (2012), IEEE, pp. 54–58.

[207] Rajbhandari, S., Ghassemlooy, Z., and Angelova, M. Effective denoising and adaptive equalization of indoor optical wireless channel with artificial light using the discrete wavelet transform and artificial neural network. *Journal of Lightwave technology 27*, 20 (2009), 4493–4500.

[208] Recommendation, U. 838-3. specific attenuation model for rain for use in prediction methods. *International Telecommunication Union, Geneva* (2005).

[209] Recommendations, I. Propagation data and prediction methods for the planning of indoor radiocommunication systems and radio local area networks in the frequency range 900mhz to 100ghz. *ITU Recommendations* (2001).

[210] Reed, M., Simon, B., Reed, M., and Simon, B. Methods of modern mathematical physics, vol. iii, scattering theory. *Bull. Amer. Math. Soc 2* (1980), 0273–0979.

[211] Reinhardt, C. N. *Atmospheric channel modeling and estimation for free-space optical communications systems in adverse visibility using radiative transfer theory.* UNIVERSITY OF WASHINGTON, 2010.

[212] Rieke, G. *Detection of Light: from the Ultraviolet to the Submillimeter.* Cambridge University Press, 2003.

[213] Säckinger, E. *Broadband circuits for optical fiber communication.* John Wiley & Sons, 2005.

[214] Schill, F., Zimmer, U. R., and Trumpf, J. Visible spectrum optical communication and distance sensing for underwater applications. In *Proceedings of ACRA* (2004), pp. 1–8.

[215] Schill, F. S. Distributed communication in swarms of autonomous underwater vehicles. Tech. rep., The Australian National University, 2007.

[216] Schnitzer, I., Yablonovitch, E., Caneau, C., Gmitter, T., and Scherer, A. 30% external quantum efficiency from surface textured, thin-film light-emitting diodes. *Applied Physics Letters 63*, 16 (1993), 2174–2176.

[217] Sevincer, A. *Transceiver Selection for Multi-Element Free-Space-Optical Communications*. UNIVERSITY OF NEVADA, RENO, 2013.

[218] Seybold, J. S. *Introduction to RF propagation*. John Wiley & Sons, 2005.

[219] Shifrin, K. *Physical optics of ocean water*. Springer Science & Business Media, 1988.

[220] Simpson, J. A. *Underwater Free-Space Optical Communication Using Smart Transmitters and Receivers*. North Carolina State University, 2012.

[221] Simpson, J. A., Cox, W. C., Krier, J. R., Cochenour, B., Hughes, B. L., and Muth, J. F. 5 mbps optical wireless communication with error correction coding for underwater sensor nodes. In *OCEANS 2010* (2010), IEEE, pp. 1–4.

[222] Smith, R. C., and Baker, K. S. Optical properties of the clearest natural waters (200–800 nm). *Applied optics 20*, 2 (1981), 177–184.

[223] Smyth, P. P., Wood, D., Ritchie, S., and Cassidy, S. Optical wireless: New enabling transmitter technologies. In *Communications, 1993. ICC'93 Geneva. Technical Program, Conference Record, IEEE International Conference on* (1993), vol. 1, IEEE, pp. 562–566.

[224] Snow, J. B., Flatley, J. P., Freeman, D. E., Landry, M. A., Lindstrom, C. E., Longacre, J. R., and Schwartz, J. A. Underwater propagation of high-data-rate laser communications pulses. In *San Diego'92* (1992), International Society for Optics and Photonics, pp. 419–427.

[225] Sobot, R. *Wireless Communication Electronics: Introduction to RF Circuits and Design Techniques*. Springer Science & Business Media, 2012.

[226] Solutions, G. Fresnel zones, March 2015. http://www.4gon.co.uk/solutions/technical_fresnel_zones.php.

[227] Son, I. K. *Design and optimization of free space optical networks*. PhD thesis, Auburn University, 2010.

[228] Song, X., and Cheng, J. Optical communication using subcarrier intensity modulation in strong atmospheric turbulence. *Journal of Lightwave Technology 30*, 22 (2012), 3484–3493.

[229] Soni, G., and Malhotra, J. Free space optics system:performance and link availability. *International Journal of Computing and Corporate Research 1*, 3 (2011).

[230] Spicer, W. E., and Herrera-Gomez, A. Modern theory and applications of photocathodes. In *SPIE's 1993 International Symposium on Optics, Imaging, and Instrumentation* (1993), International Society for Optics and Photonics, pp. 18–35.

[231] Spieler, H. Introduction to radiation detectors and electronics. *VI. Position-Sensitive Detectors* (1998).

[232] Sun, Z., and Akyildiz, I. F. Channel modeling and analysis for wireless networks in underground mines and road tunnels. *Communications, IEEE Transactions on 58*, 6 (2010), 1758–1768.

[233] Tang, L., Ji, R., Cao, X., Lin, J., Jiang, H., Li, X., Teng, K. S., Luk, C. M., Zeng, S., Hao, J., et al. Deep ultraviolet photoluminescence of water-soluble self-passivated graphene quantum dots. *ACS nano 6*, 6 (2012), 5102–5110.

[234] Technologies, U. Optical modem module, May 2016. http://www.uontechnologies.com/products.php.

[235] Tedetti, M., Sempéré, R., Vasilkov, A., Charriere, B., Nérini, D., Miller, W. L., Kawamura, K., and Raimbault, P. High penetration of ultraviolet radiation in the south east pacific waters. *Geophysical research letters 34*, 12 (2007).

[236] Tellez, J. A. Integrated approach to free space optical communications in strong turbulence. Tech. rep., DTIC Document, 2011.

[237] Tivey, M., Fucile, P., and Sichel, E. A low power, low cost, underwater optical communication system. *Ridge 1* (2000), 27–29.

[238] Trisno, S. Design and analysis of advanced free space optical communication systems.

[239] Uitz, J., Claustre, H., Morel, A., and Hooker, S. B. Vertical distribution of phytoplankton communities in open ocean: An assessment based on surface chlorophyll. *Journal of Geophysical Research: Oceans 111*, C8 (2006).

[240] Vitelli, C., Toffoli, L., Sciarrino, F., and De Martini, F. Efficient long range communication by Quantum injected optical parametric amplification. In *Personal Satellite Services*. Springer, 2010, pp. 330–339.

[241] Wang, Z., Tsonev, D., Videv, S., and Haas, H. On the design of a solar-panel receiver for optical wireless communications with simultaneous energy harvesting. *Selected Areas in Communications, IEEE Journal on 33*, 8 (2015), 1612–1623.

[242] Weissberger, M. A. An initial critical summary of models for predicting the attenuation of radio waves by trees. Tech. rep., DTIC Document, 1982.

[243] Willebrand, H., and Ghuman, B. S. *Free space optics: enabling optical connectivity in today's networks*. SAMS publishing, 2002.

[244] Williamson, C. E., Morris, D. P., Pace, M. L., and Olson, O. G. Dissolved organic carbon and nutrients as regulators of lake ecosystems: resurrection of a more integrated paradigm. *Limnology and Oceanography 44*, 3part2 (1999), 795–803.

[245] Witteman, W. J. *Detection and Signal Processing*. Springer, 2006.

[246] Wu, B. *Free-space optical communications through the scattering medium: analysis of signal characteristics*. PhD thesis, The Pennsylvania State University, 2007.

[247] Wu, Z. *Free space optical networking with visible light: A multi-hop multi-access solution*. PhD thesis, BOSTON UNIVERSITY, 2011.

[248] Xiaoyan, W. *Performance Analysis of Multiple Input Multiple Output Free Space Optical Communication Systems*. 2011.

[249] Xu, F., Khalighi, M.-A., and Bourennane, S. Impact of different noise sources on the performance of PIN-and APD-based FSO receivers. In *Telecommunications (ConTEL), Proceedings of the 2011 11th International Conference on* (2011), IEEE, pp. 211–218.

[250] Xu, Z., Ding, H., Sadler, B. M., and Chen, G. Analytical performance study of solar blind non-line-of-sight ultraviolet short-range communication links. *Optics letters 33*, 16 (2008), 1860–1862.

[251] Yan, F., Luo, Y., Zhao, J., and Olsen, G. 4H-SiC visible blind UV avalanche photodiode. *Electronics Letters 35*, 11 (1999), 929–930.

[252] Yeom, J.-Y., Vinke, R., Pavlov, N., Bellis, S., O'Neill, K., Jackson, C., and Levin, C. S. Performance of fast timing silicon photomultipliers for scintillation detectors. In *Nuclear Science Symposium and Medical Imaging Conference (NSS/MIC), 2012 IEEE* (2012), IEEE, pp. 2845–2847.

[253] Yoon, H. S., Ko, G. B., Kwon, S. I., Lee, C. M., Ito, M., Song, I. C., Lee, D. S., Hong, S. J., and Lee, J. S. Initial results of simultaneous PET/MRI experiments with an MRI-compatible silicon photomultiplier PET scanner. *Journal of Nuclear Medicine 53*, 4 (2012), 608–614.

[254] Zand, B. *High-speed Optical Wireless Communications Using Reduced-state Sequence Detection*. National Library of Canada= Bibliothèque nationale du Canada, 2003.

[255] Zhang, Y., Manjavacas, A., Hogan, N. J., Zhou, L., Ayala-Orozco, C., Dong, L., Day, J. K., Nordlander, P., and Halas, N. J. Toward surface plasmon-enhanced optical parametric amplification (SPOPA) with engineered

nanoparticles: A nanoscale tunable infrared source. *Nano letters 16*, 5 (2016), 3373–3378.

[256] Zhou, D. *Wireless optical transceiver design, link analisys and alignment control for mobile communication.* 2013.

[257] Zhou, Z. *Broadband Optical Wireless Communications.* PhD thesis, The Pennsylvania State University, 2013.

[258] Ziemer, R., and Tranter, W. H. *Principles Of Communications: System Modulation And Noise.* John Wiley & Sons, 2006.

Chapter 3

Optical Wireless Communications Omnidirectional Receivers for Vehicular Teleoperation

3.1 Abstract

Wide aperture omnidirectional free-space optical (FSO) receivers using wavelength shifting (WLS) fibers that enable the use of small active area high-speed photodetectors in optical wireless communications, are presented. In particular, the influence of WLS fiber decay time in the bit rate is evaluated when receiving intensity modulated light generated with commercial off-the-shelf light-emitting diodes. The option of increasing the photon collecting area of a $7mm^2$ active area avalanche photodiode using WLS fiber, gave a 300% improvement in the bit rate, when compared with the option of using a bare $31mm^2$ active area avalanche photodiode. It was also experimentally verified, that a WLS spiral receiver mounted over a reflective base gave more gain than simulated Lambert's cosine law, proving that reflective optics can be used to increase the WLS-FSO receiver aperture.

3.1.1 Contributions of Authors

Alberto Rui Frutuoso Barroso

- Concept generation
- Experiment design, planning and implementation
- Data analysis

Dr. Gregory Baiden

- Identified the research problem of omnidirectional reception in OWC systems
- Analyzed results and suggested improvements for the experimental procedures
- Patent application for systems and methods invented in this research
- Review and approval of the article for publication.

Dr. Julia Johnson

- Analyzed results and suggested article structure
- Article proofreading

Publication Status

Under review at the Elsevier AEU International Journal of Electronics and Communications (submitted in 27 November 2016, Ref: AEUE_2016_971)

Partial publication in two patents:

- OMNIDIRECTIONAL OPTICAL WIRELESS COMMUNICATIONS RECEIVER & SYSTEM (Publication number WO2016154742)
- OPTICAL RECEIVER (Publication number WO2015179961)

3.2 Introduction

The tetherless teleoperation of vehicles [3] using high-definition video, dense LIDAR data [22] and haptic virtual telepresence needs the existence of a broadband omnidirectional wireless system, whose implementation in tunnels, requires the use of optical wireless communications (OWC) to mitigate the intense attenuation that non-optical wavelengths have in those environments [9]. Tunnels are a common traffic infrastructure, with many not designed for high traffic volumes, forcing the implementation of vehicle-to-vehicle (V2V) and vehicle-to-infrastructure (V2I) visible light communications (VLC) integrated [8] in cooperative intelligent transportation systems (ITS). Vehicular communications using VLC-ITS, obligate the development of omnidirectional free-space optical (OFSO) receivers to mitigate the effects of turbulence [16] and pointing errors [28] in the propagation channel [30]. Targeting that objective, this work presents high aperture and field-of-view (FOV) FSO receivers using wavelength shifting (WLS) fibers with fluorescence and lifetime [17] characteristics compatible with high speed photodetectors. The sensitivities of these WLS-OFSO receivers are evaluated with light generated by blue light-emitting diodes (LED), modulated with continuous sine waves or pulsed Direct-Current biased Optical Orthogonal Frequency Division Multiplexing (DCO-OFDM) signals.

3.3 OFSO photodetection theoretical considerations

The two most important characteristics of an OFSO receiver are the receiving area (aperture) and FOV that are inversely related in geometrical optics because of the conservation of the etendue of light [20]. Standard flat photodetectors have a maximum FOV equal to half a sphere (2π sr), with that value being reduced when the semiconductor die is mounted inside a deep cavity in a windowed case.

The photon radiant flux received in the area of flat photodetectors falls with the cosine of the angle of incidence, requiring the use of multiple photodetectors to balance the sensitivity inside the FOV of the OWC omnidirectional receiver used in vehicular teleoperation [24, 32]. Cylindrical geometries for photodetectors were proposed [27], but currently, the widest omnidirectional response photodetection is achieved using hemispherical shaped [12] photomultiplier tubes (PMT). Photodetection using PMT is not an effective design choice to implement OWC systems because of its fragility to mechanical vibrations, frequent permanent damage when exposed to intense light [13] and sensitivity to magnetic fields.

The nonexistence of cylindrical or hemispherical shaped semiconductor photodetectors to implement omnidirectional photon receivers is a technological obstacle for the implementation of OWC supporting the teleoperation of vehicles, with diverse solutions being researched by academia [29, 10, 7, 18, 2] and industry [15]. For example, omnidirectional photon receivers replicating optical properties of the fly-eye were investigated by Yun and Kavehrad [33], Sterckx et al. [26] and Al-Ghamdi et al. [1] as alternative solutions for diversity receivers [19, 5, 4, 6, 25]. Kahn et al. [14], divides the different configurations of FSO receivers in three types as seen in figure 3.1, with type-2 and 3 describing multiple FOV and off-axis diversity implementations.

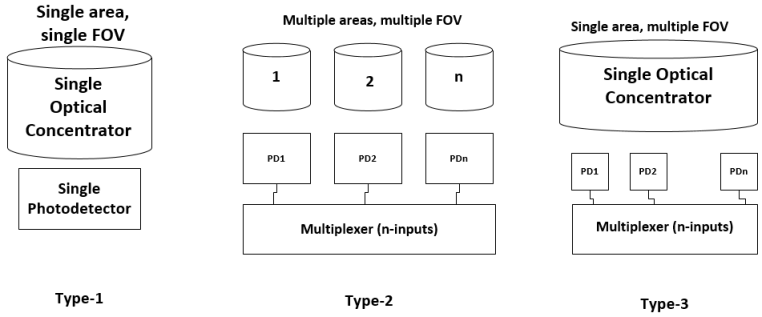

Figure 3.1: Types of free-space optical receivers

The use of diversity receivers [23] in FSO vehicular communications requires handover multiplexing circuits, with a complexity related with the number of photodetection channels and the operational speed of the vehicle. FSO communications for high speed vehicles promote the use of type-1 receivers with a wide FOV, that the sphere, torus and cylinder shapes offer without requiring an optimization angle to maximize the photon receiving area [31].

3.4 Method

Experiments were undertaken with four different avalanche photodiodes (APD) described in table 3.1 coupled to Saint-Gobain BCF-91A and BCF-92 WLS fibers, with 12 and 2.7ns decay time, respectively. Four types of single cladding WLS fiber with 0.8mm diameters were ordered, evaluating the BCF-92 fiber doped with different levels of fluorescent dye concentrations (standard, half, double), and the photodetectors were selected for an enhanced responsivity in the blue region. The chosen photodetector was tested coupled to WLS fiber, bare, and paired, to evaluate the alternative of using multiple APD to increase the photodetection area. A 36dB coaxial amplifier (ZX60-100VH) was used to amplify the output of the three types of photodetectors, using customized impedance matching circuits to adapt the photodetector junction capacitances.

Table 3.1: Photodetectors used in this study

Type	**Part Number**	**Gain**	$\mathcal{R}$**(A/W) at 450nm**	**Active area**(mm^2)
APD	C5331-11	30	6	0.79
APD	C5331-04	30	6	7
APD	S8664-30K	50	15	7
APD	C3079	200	52	31

3.4.1 Measurement setup

Two experimental measurement setups were used:

- Multiple 0.5meter length samples of single WLS fibers were coupled to a Hamamatsu short-wavelength C5331 Avalanche Photodiode (APD) module receiving intensity modulated light from 12 Watt of uncollimated 450nm LED blue light at a range of 3 meters, measuring its electrical-optical-electrical (E-O-E) response using a Copper Mountain Technologies TR1300/1 network analyzer controlled by Matlab™.

- A pair of field-programmable gate arrays (FPGA) modules programmed as transparent Ethernet bridges modulating (DCO-OFDM) the intensity of 24-LED modules (450nm) able to emit 24 Watts of radiometric power, and receiving FSO signals at 1 to 120 meters distances using WLS fiber receivers or bare photodetectors.

The network analyzer acquired data to evaluate the WLS fiber in an E-O-E response constituted by a cascade of three individual transfer functions: LED, WLS fiber and APD photodetector.

In an attempt to remove the effect of the Hamamatsu APD and DCO-OFDM LED modules transfer functions from the measured data, those two blocks were characterized without WLS fiber, resulting in a cascade function that was inverted and inserted in the forward path of a Matlab processing script (Appendix A).

The bit rate results were obtained for the characterized APDs, using an FPGA implemented OFDM-Ethernet bridge, amplifying the photodetector output with a fixed 36dB amplifier with no automatic gain control (AGC). The OFDM carrier modulation type was automatically selected based in a software implemented Signal-to-Noise (SNR) look-up table.

3.5 Results and discussion

An evaluation procedure was executed to identify a WLS fiber suitable for use in the implementation of OFSO receivers. Frequency response characterizations were made with two different decay time fluorescent materials used in the BCF-91A and BCF-92 fibers, and the influence of BCF-92 fiber fluorescent dye concentration in the OWC receiver optical gain, was measured. Together with this WLS fiber OWC characterization, a procedure to identify a photodetector that allows bit rates above 100 Mbps was executed, evaluating the bit rate of OFDM based OWC selecting two APD photodetectors with the highest gain. The APD that offered more bit rate was experimented in a single photodetector configuration, or connected with a second device evaluating parallel and series APD bundling.

Finally, the selected pair (photodetector, WLS fiber) was used to build OFSO receivers for OWC systems that were evaluated using DCO-OFDM LED modulations, in 1 to 120 meter communication range experiments.

In the remainder of this section, the bit rate and omnidirectional response of spiral and toroidal WLS OFSO receivers are compared and discussed.

3.5.1 DCO-OFDM bit rate evaluation using APD photodetectors

Based on the gain and responsivity to blue to green wavelengths of the avalanche photodiodes described in table 3.1, it was decided to evaluate the C3079 and S8664-30K devices receiving DCO-OFDM LED modulated light.

C3079 Avalanche Photodiode (APD) photodetector

Figure 3.2 reveals a bit rate maximum reached at 40 meters range, showing the effects of not having an AGC, with the typical low bit rate values in short ranges caused by distortion; these results were obtained using 24W of 12 degrees collimated 450nm LED light.

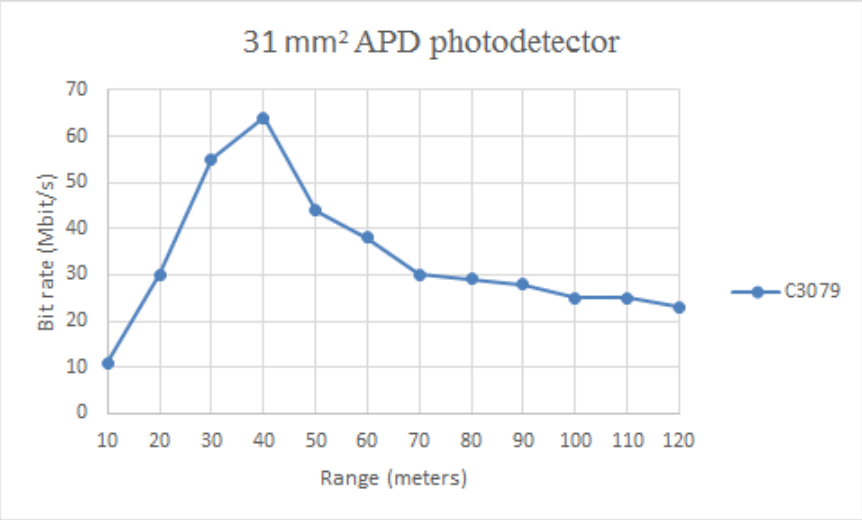

Figure 3.2: C3079 APD photodetector line-of-sight bit rate evaluation

This experiment shows the disadvantages of using large area APD photodetectors with an associated high junction capacitance.

The C3079 APD was operated with 400 Volts of reverse bias voltage, forming a 60pF junction capacitance that limited the OWC bit rate to values below 65 Mbit/s.

S8664-30K APD photodetector

This experiment used 24 Watts of uncollimated 450nm LED light, illuminating a bare (no optical gain) Hamamatsu S8664-30K APD, which was preferred to the C5331 series APD devices because of a higher gain. Figure 3.3 shows that a single APD using this LED setup does not requires an AGC circuit, and that low bit rates are measured in distances inferior to 22 meters for the double APD (series or parallel) configurations. The experiments with APD association in series (direct) or parallel (with a buffered current summing junction to avoid adding photodetectors capacitance), confirmed that the series association offers a bandwidth superior than the buffered-parallel. Wilkinson and Granlund combination techniques were also experimented to bundle APD photodetectors, with both adding techniques showing noise levels higher than a single APD photodetection circuit.

This experiment identified the S8664-30K APD as the photodetector to be used in the construction of WLS OFSO receivers for OWC experiments.

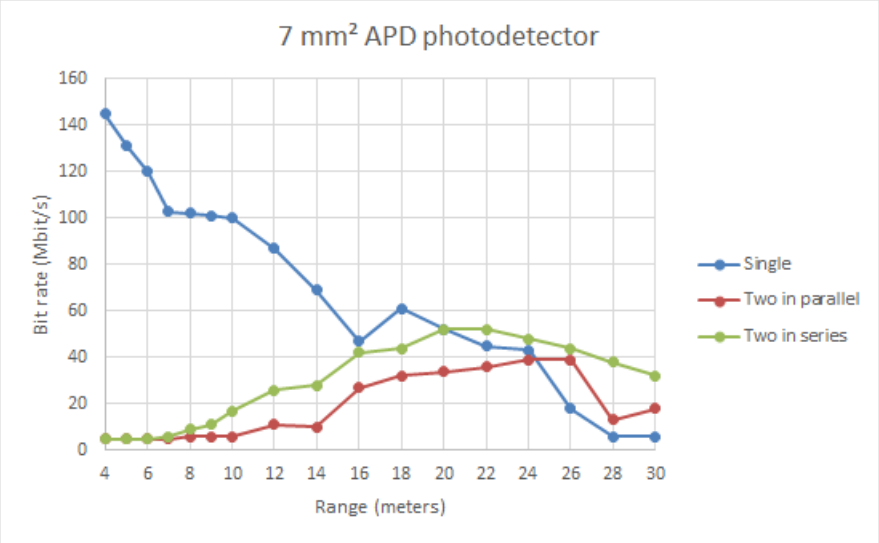

Figure 3.3: S8664-30K APD photodetector line-of-sight bit rate evaluation

3.5.2 BCF-91A WLS fiber frequency and time response evaluation

This experiment was accomplished by analyzing rough-cut unpolished termination WLS fiber samples from a population of 600, quantifying APD coupling losses, gain and frequency response.

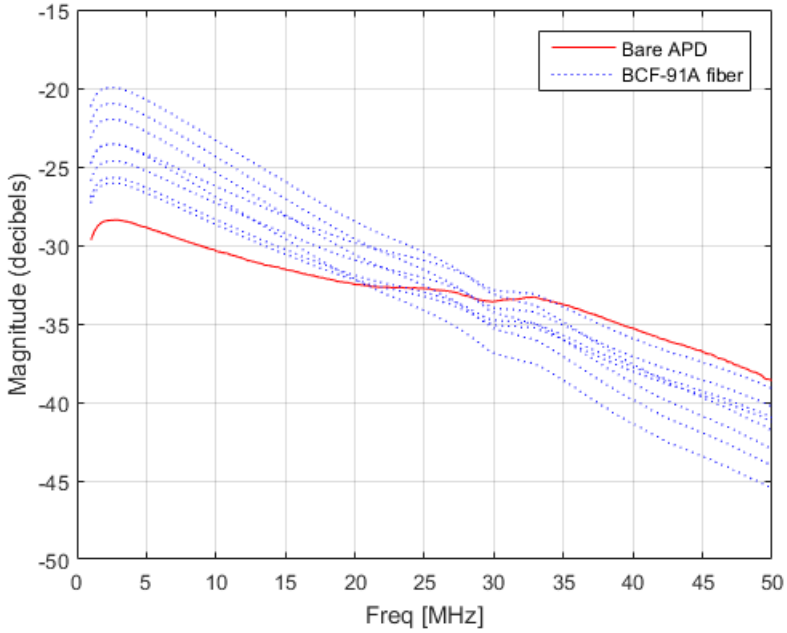

Figure 3.4: BCF-91A WLS fiber frequency response

Figure 3.4 compares the BCF-91A fiber frequency response with the exposed $0.79mm^2$ C5331-11 APD active area, and shows more than 5dB of fiber-to-fiber gain variance.

It was demonstrated that one segment of 0.5meter length of 0.8mm diameter BCF-91A fiber ($400mm^2$ of active area) can give 1.5 times more gain than a $0.79mm^2$ APD active area. It was also confirmed, that this fiber behaves as a narrow band optical filter in the blue region, showing its potential for indoor VLC systems using phosphor converted white LEDs.

The obtained geometrical area gain (WLS fiber/APD) was 500, a value that was reduced by: unpolished fiber termination coupling losses, 6% capture efficiency for single clad WLS fiber, and a propagation attenuation length of 3.5 meters (where 1/e of the guided light is attenuated by the fluorescent dye).

Figure 3.4 also confirms the 12ns decay time announced in the manufacturer datasheet, because all fiber gain measurements become inferior to the bare APD after 30MHz, a value that correlates with the 10 to 90% rise time (t_r) formula: BW(Hz)=$0.35/t_r$.

Zeng et al. [34], modified rational function modeling technique (Equation 3.1) was used to characterize the cascade E-O-E transfer function (TF).

$$f(s) = (\sum_{j=1}^{N} \frac{C_j}{s - a_j} + d)e^{-st_d} \tag{3.1}$$

The complete system required eleven poles to fit, the effects of the WLS fiber in the TF were not easily identified, and because of that, the inverted transfer function of the LED driver and APD frontend was inserted in the TF cascade during Matlab processing. After the extraction of LED/APD unwanted TFs, two poles were found describing the WLS fiber TF, fitting the extracted WLS fiber TF with the precision displayed in figure 3.5. The extracted transfer function was chosen to fit from 2 to 30MHz, due to the lower limit of the network analyzer (300 KHz), the DCO-OFDM implementation in the FPGA kit was not programed to generate OFDM carriers below 2MHz, and the BFC-91A fiber does not offer significant gain for frequencies above 30MHz.

$$f(s) = I_o(\frac{C_1}{s - short} + \frac{C_2}{s - long}) \tag{3.2}$$

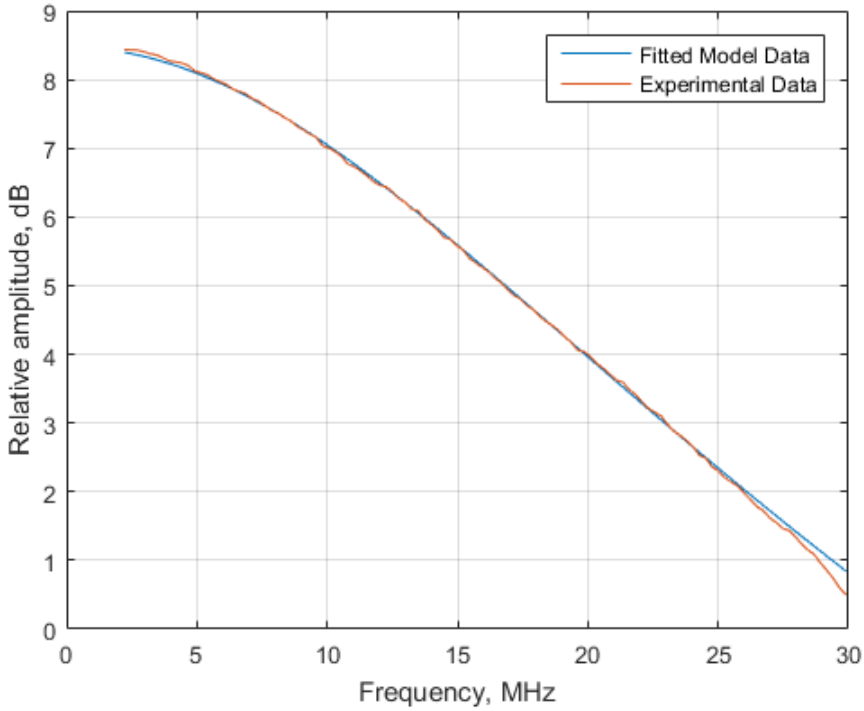

Figure 3.5: BCF-91A transfer function 2-poles fitting

Equation 3.2 was obtained as the fitted model of frequency response for this type of WLS fiber, where I_o, C_1, C_2, *short* and *long* are constants that can also be obtained from the frequency domain counterpart of the intensity model (Equation 3.3) presented by Gomes et al. [11]. Their experimental results model WLS fiber light output as a function of short (L_1) and long (L_2) attenuation lengths.

$$I(x) = I_{01}e^{\frac{x}{L_1}} + I_{02}e^{\frac{x}{L_2}} \tag{3.3}$$

Using this equation as the model structure for a gray-box modeling strategy, system parameters were estimated using the Matlab function "rationalfit".

The obtained WLS fiber rational fit is shown in figure 3.5 with a time step response plotted in figure 3.6, confirming the BCF-91A 12ns rise time.

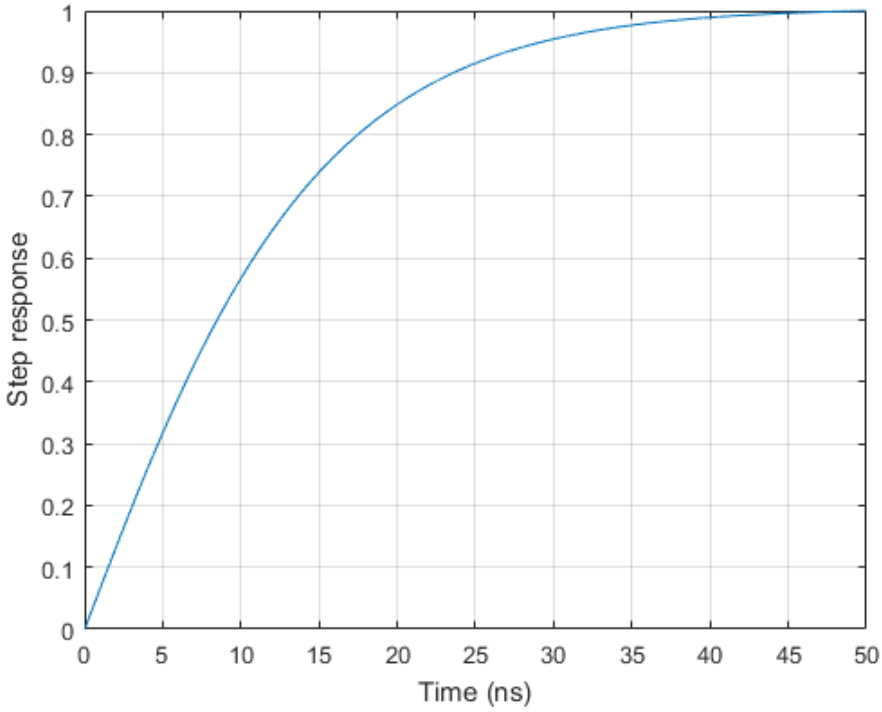

Figure 3.6: BCF-91A step response

3.5.3 BCF-92 WLS fiber frequency and time response evaluation

Similar experimental procedures used to evaluate the BCF-91A fiber were undertaken for three populations of BCF-92 with different doping levels.

In this section, an estimate of the effect of fiber fluorescent doping level has in the blue-to-green wavelength shifting efficiency is presented, and the influence of the fast BCF-92 decay time (2.7 ns) in the E-O-E bandwidth is evaluated.

BCF-92 (100 ppm)

Figure 3.7 shows that half doped (100 ppm) WLS fiber does not allow area gains for an OWC receiver using a single strand, and that the fiber-to-fiber gain variance is more than 7dB.

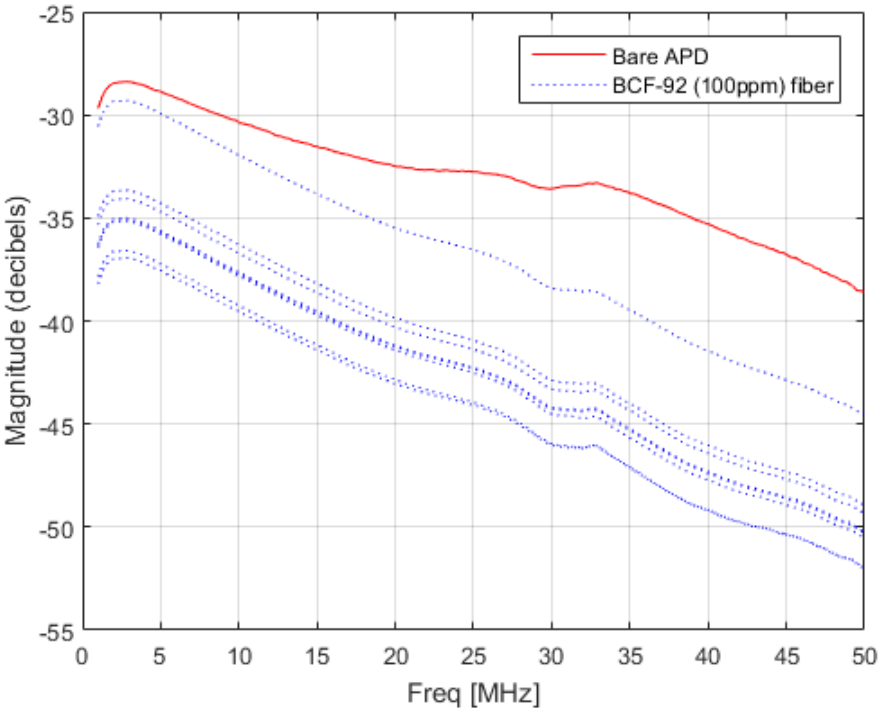

Figure 3.7: BCF-92 (100ppm) WLS fiber frequency response

BCF-92 (200 ppm)

Figure 3.8 demonstrates that standard doped (200 ppm) WLS fiber can offer more than 7dB of gain when compared with the 100 ppm counterparts. The 200ppm doping reduces the fiber-to-fiber gain variance to 4dB.

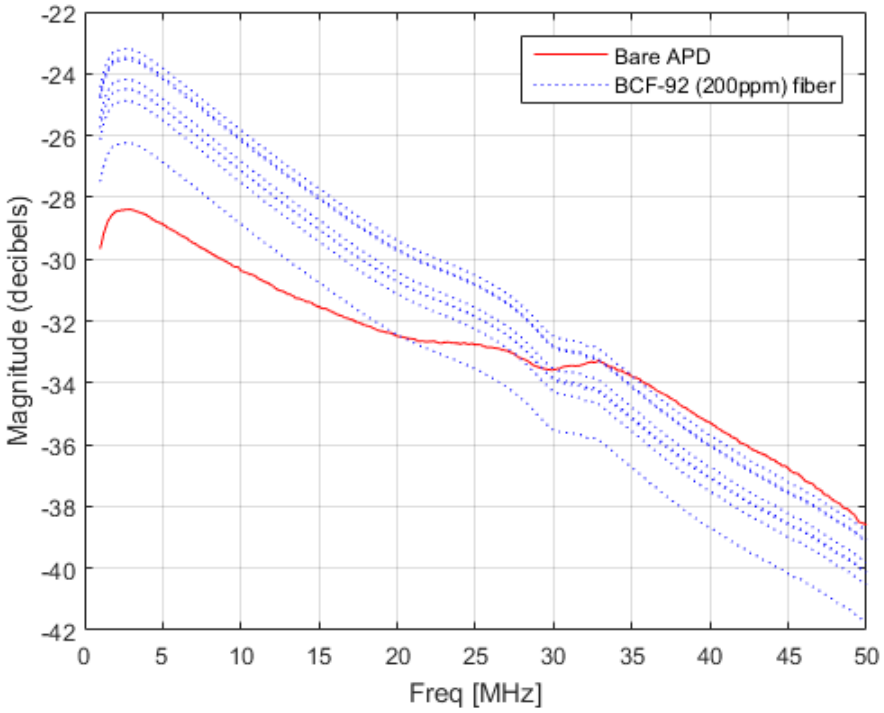

Figure 3.8: BCF-92 (200ppm) WLS fiber frequency response

BCF-92 (400 ppm)

The test results for the double doped (400 ppm) BCF-92 WLS fiber are illustrated in figure 3.9. We found that the 200 ppm and 400 pm maximum gain are equivalent, and that the advantage of the 400ppm doping is a fiber-to-fiber gain variance inferior to 2dB.

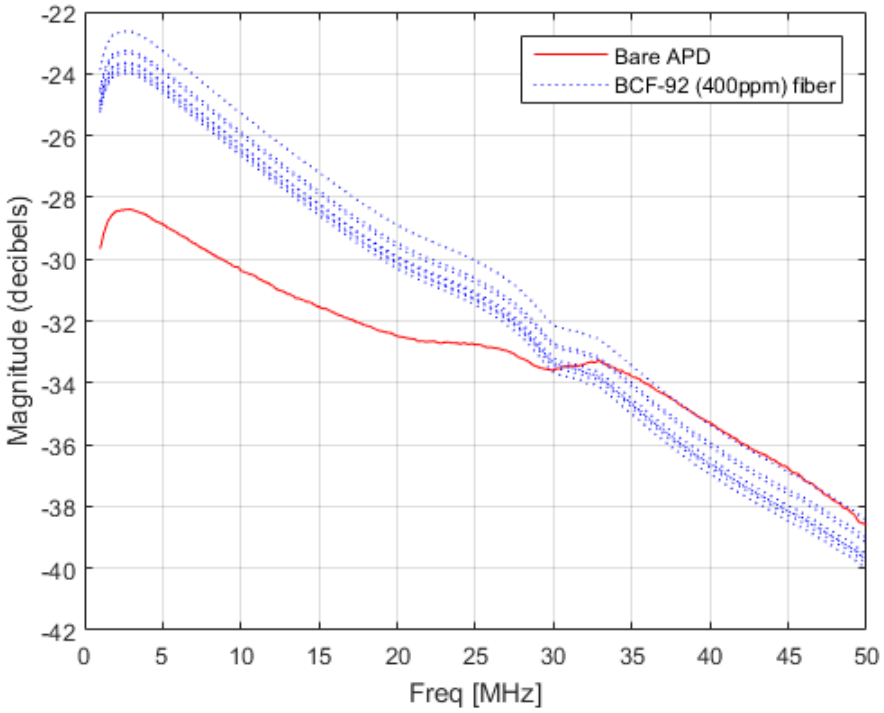

Figure 3.9: BCF-92 (400ppm) WLS fiber frequency response

This WLS fiber study confirmed that BCF-91A fluorescent die offer the highest light output (Figure 3.10) and a slower pulse response when compared with the fluorescent die used in the BCF-92 WLS fiber.

These experimental results determined that the BCF-92 WLS fiber with a 400 ppm fluorescent die doping level offers the highest frequency response and gain stability, suited to design OFSO receivers for broadband OWC systems.

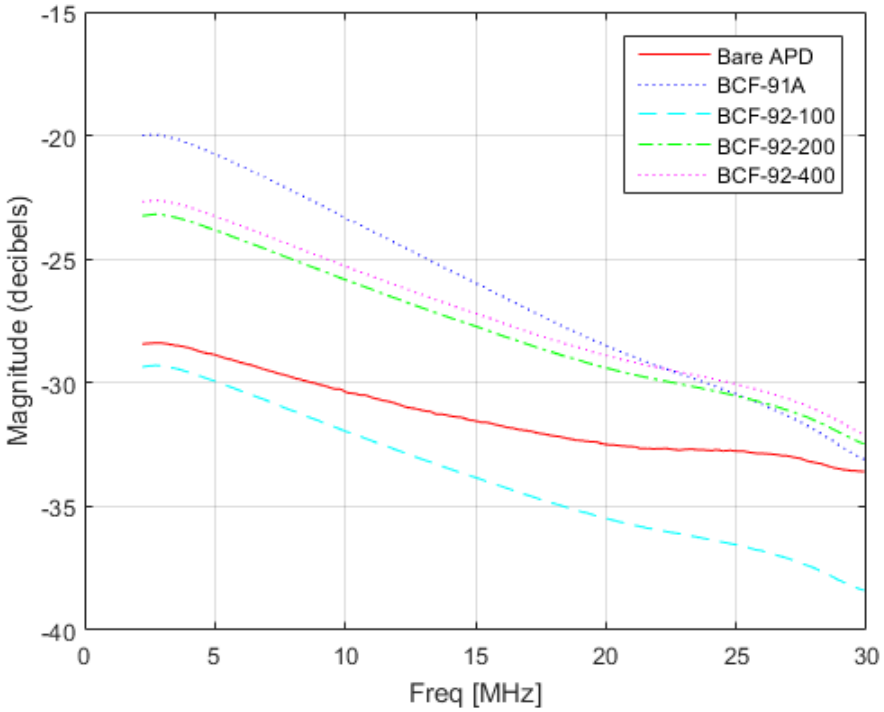

Figure 3.10: WLS fiber frequency response comparison

3.5.4 Bit rate evaluation of WLS OFSO receivers

The previous characterizations determined BCF-92 and the Hamamatsu S8664-30K as the best components to design OFSO receivers, with the objective to be used in vehicular communications using blue or phosphor converted white LEDs.

Spherical WLS-OFSO receiver

The first 4π sr WLS-OFSO receiver studied and simulated in this work was a spherical shaped solid, with the project name WLS-balloon. This experimental apparatus is illustrated in figure 3.11, and its developing was abandoned because it required an excessive quantity of fiber, that caused a big termination bundle forcing the use of an inefficient and bulky lens holder to collimate the 35.7 degrees output divergence of the BCF-92 WLS fiber (also confirmed by Peyronel et. al, [21]).

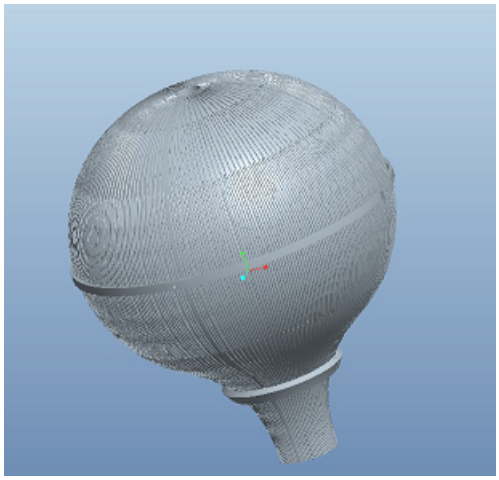

Figure 3.11: A prototype of a 10-inch diameter balloon WLS FSO receiver

In this experimental phase, we decided to replace bulky imaging optics with reflective and refractive compound parabolic concentrators (CPC), choosing models with acceptance angles compatible with the WLS fiber divergence, and with input-to-output diameter ratios near two. CPCs with more than three input-to-output diameter ratios were analyzed in a trade-off between the losses caused by an acceptance angle lower than the fiber divergence, and the gain of bundling more fibers to increase the photodetection area.

Spiral WLS-OFSO receiver

Figure 3.12: Spiral WLS free space optical receiver

Simulations and laboratory experiments demonstrated that the previous balloon shaped WLS-OFSO receiver failed to give more gain than the bare photodetector, because the WLS fiber area near the APD that offers the highest signal level was not being properly exposed. The fluorescent dye in the WLS fiber causes an intense longitudinal transmission attenuation, a characteristic that needs to be regarded in the design of FSO receivers using WLS fibers. Respecting this design restriction, we decided to invert the balloon fiber routing with the objective to expose the WLS fiber near the APD coupling zone.

The spiral WLS receiver was the first experiment maximizing the exposure of the WLS fiber near the photodetector, which also included two additional optimizations: short length WLS fiber segment usage and a higher count of fibers (rejecting the option of using longer lengths to expand the photodetection area). This spiral experiment (Figure 3.12) is a hemispherical (2π sr) receiver that routes a bundle of 36 segments (500mm length) of WLS fiber in a spiral trajectory with minimal bending losses (datasheet recommended value), focusing its output in the active area of one S8664-30K APD expanded with a refractive compound parabolic concentrator (CPC).

Two spiral prototypes were built to evaluate the BCF-91A and BCF-92 fibers receiving OFDM LED modulations, the experimental results were compared with a bare C3079 APD and a Fresnel collimated (25mm diameter) S8664-30K APD.

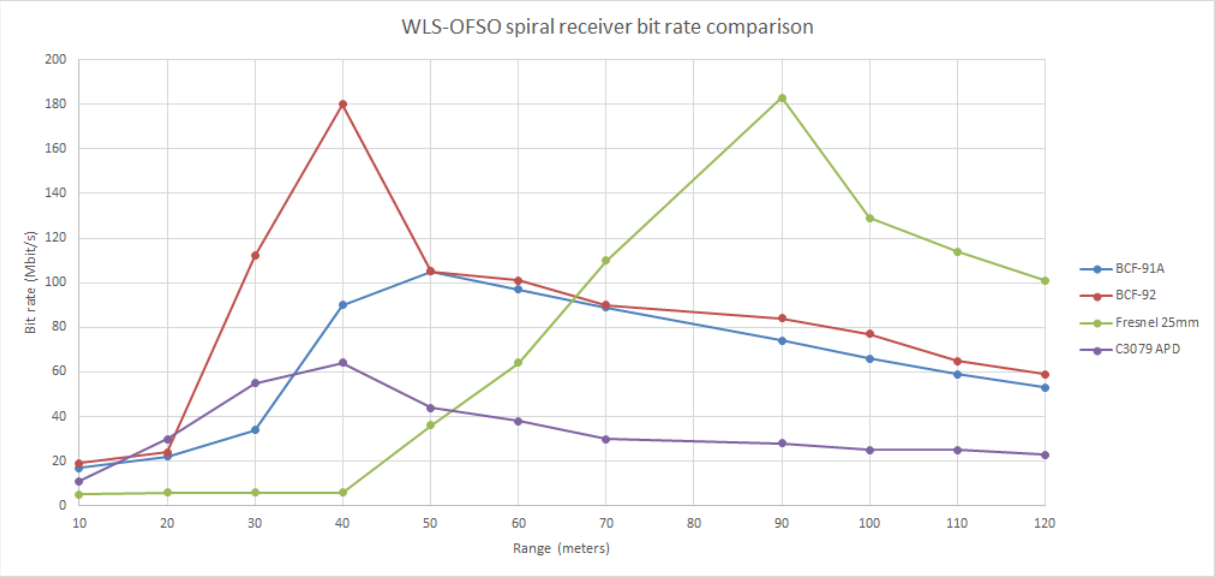

Figure 3.13: OWC bit rate experimental results

In figure 3.13 we confirm that the BCF-92 fiber offers more bit rate than BCF-91 due to its lower decay time. We verify that the BCF-92 fiber was not a bandwidth bottleneck in this experiment, because its maximum bit rate is equal to the values obtained with a standard refractive 25mm diameter Fresnel collimating lens. The bit rate was limited in all experiments by the frequency response of the LED driver module.

Figure 3.14 demonstrates that this receiver gives better responsivity than a Lambertian cosine law, because the fiber was mounted over a reflective surface that redirects lost photons back to the fiber.

Measured-1 data were collected in total darkness, measured-2 data were obtained under electronic ballast fluorescent indoor illumination with an intensity of $0.78\mu mol$ of photosynthetically active radiation (PAR), and the angular sensitivity of a 25mm Fresnel lens is plotted as a comparison of this spiral with standard refractive optics.

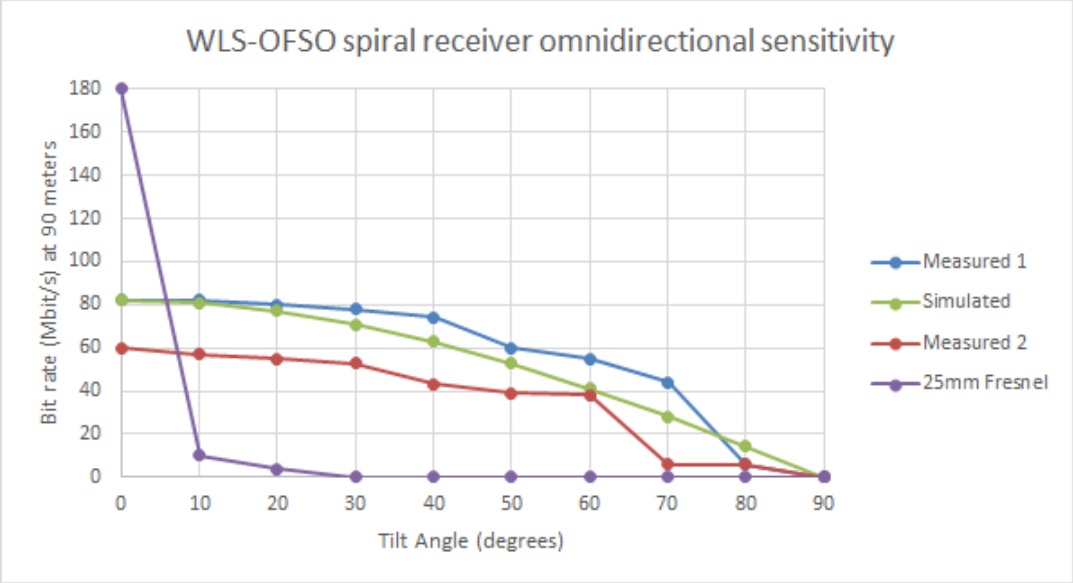

Figure 3.14: Spiral WLS (BCF-92) horizontal angular sensitivity at 90 meters ranges

Toroidal WLS-OFSO receiver

Following the design strategy of the spiral receiver, a toroidal shape receiver was experimented with both single and double WLS fiber termination.

The toroidal receiver (Figure 3.15) was tested with the following design restrictions:

- minimize fiber count to use small CPC collimation
- maximize the intersection of the WLS fiber with the OWC light trajectory
- route the fiber minimizing bending attenuation
- maximize the exposure of the fiber zones coupled to the APD
- use double termination for longer segments of fiber.

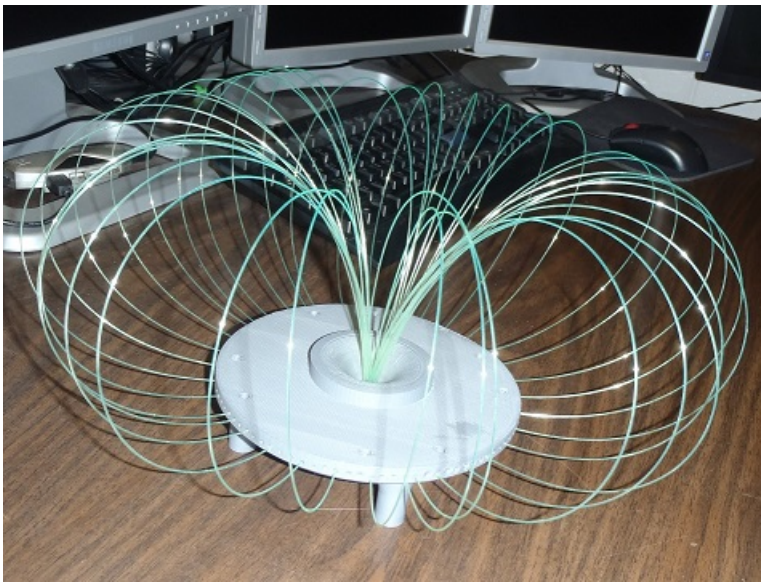

Figure 3.15: Toroidal WLS free space optical receiver

Figure 3.16 shows the bit rate experimental results at 90 meters range using one 24-LED module collimated at 12 degrees, for the single and double terminated toroid receiver, comparing the obtained bit rates with the spiral receiver. The X-axis (tilt angle) in figure 3.16 represent the polar angle θ of the toroid, with the Z-axis coming from the center of the toroid or spiral receiver. The zero to 360-degree azimuthal ϕ angle bit rate response of the spiral is zero because the used casing is opaque (an aluminum frame), and it is a flat 45 Mbit/s in the toroidal receiver.

The flat azimuthal angular bit rate response of the toroidal receiver is present in figure 3.16 for the tilt angle of 90 degrees, a value inferior to the peak of the polar response (at 45 degrees), because the inner part of the WLS fiber is not exposed when θ=90 degrees.

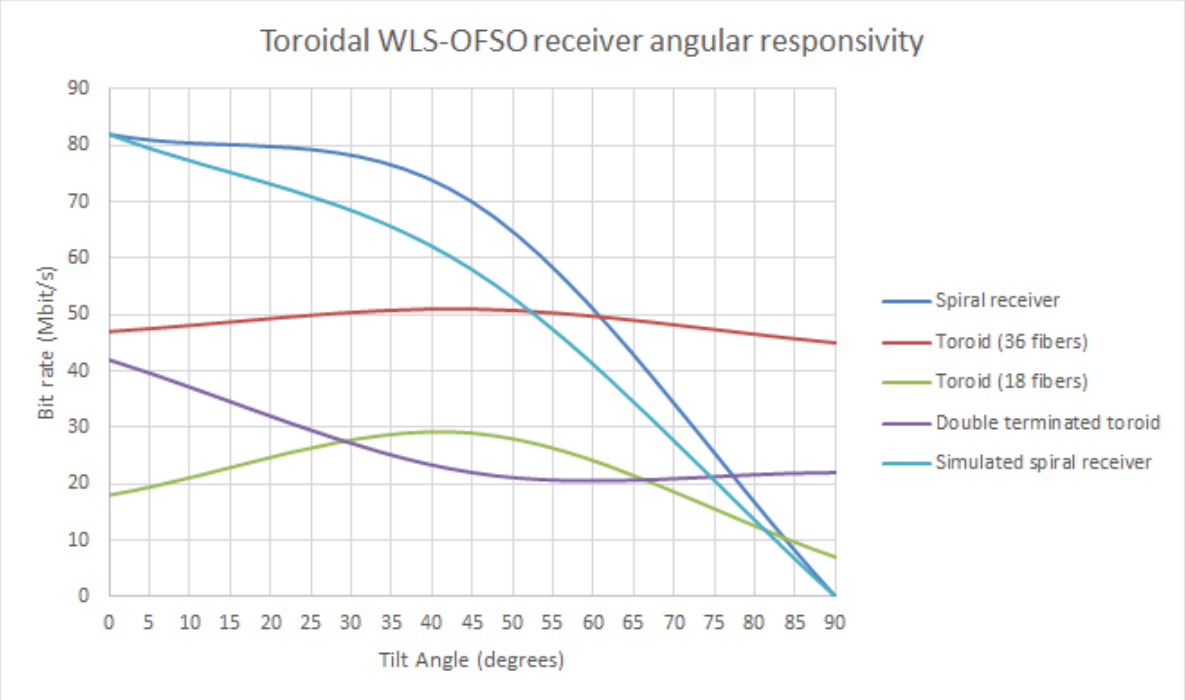

Figure 3.16: Toroidal and spiral WLS-OFSO receivers angular responsivity comparison

3.6 Conclusions

Our subject has been the development of OFSO receivers for vehicular OWC where the field of vision is normally limited with implementation restrictions. The 0 to 360 degrees flat gain of the toroidal receiver demonstrates its potential for use in V2I-OWC, to complement the more sensitive spiral arrangement that was developed with the intention to be integrated in vehicles where a 360-degree line-of-sight does not exist. V2V communication for tunnel traffic control is an application example, where individual spiral receivers would be installed on the front and on the back of the automated vehicle. In warehouse teleoperated vehicles, a single roof installed spiral receiver can be used in tall ceilings environments, and in more restrictive scenarios, a single toroidal WLS receiver or individual line-of-sight spiral receivers can be enabled using a standard antenna diversity selection method, or using the data from a local inertial navigation sensor.

Based in the experimental results we arrived at the following conclusions:

- Simulation and experimental results of the frequency response of BCF-92 WLS fiber, proved that this fiber type does not cause a bit rate bottleneck in LED OWC.
- WLS fibers can be used to build high gain OFSO receivers if the fiber zone near the photodetector is exposed and fiber light output divergence is mitigated.
- OFSO receivers using WLS fiber can increase its aperture without reducing the FOV, allowing the use of small active area (and high bandwidth) avalanche photodiodes (APD).
- The bit rate of a two APD array was inferior to a single device, due to APD noise floor summing and an increased jitter.

- It was confirmed that the wavelength shifting noise of BCF91A and BCF-92 fibers can be neglected in the design of OFSO receivers, being the photodetector noise the dominant source.

- The 36 fibers toroidal shaped receiver proved that V2V and V2I 4π sr VLC receivers can be built using WLS fiber.

References

[1] Al-Ghamdi, A. G., and Elmirghani, J. M. Performance evaluation of a triangular pyramidal fly-eye diversity detector for optical wireless communications. *Communications Magazine, IEEE 41*, 3 (2003), 80–86.

[2] Arnon, S., Barry, J., Karagiannidis, G., Schober, R., and Uysal, M. *Advanced optical wireless communication systems*. Cambridge university press, 2012.

[3] Barroso, A. R. F., Baiden, G., and Johnson, J. Teleoperation of mining equipment using optical wireless communications. In *2015 Seventh International Conference on Ubiquitous and Future Networks* (2015), IEEE, pp. 727–733.

[4] Cap, G. A., Refai, H. H., and Sluss Jr, J. J. Omnidirectional free-space optical (FSO) receivers. In *Defense and Security Symposium* (2007), International Society for Optics and Photonics, pp. 65510O–65510O.

[5] Chadha, D. *Terrestrial wireless optical communication*. McGraw Hill Professional, 2013.

[6] Chen, T., Liu, L., Tu, B., Zheng, Z., and Hu, W. High-spatial-diversity imaging receiver using fisheye lens for indoor MIMO VLCs. *Photonics Technology Letters, IEEE 26*, 22 (2014), 2260–2263.

[7] Chen, Z., Serafimovski, N., and Haas, H. Angle diversity for an indoor cellular visible light communication system. In *Vehicular Technology Conference (VTC Spring), 2014 IEEE 79th* (2014), IEEE, pp. 1–5.

[8] Falcitelli, M., and Pagano, P. Visible light communication for cooperative ITS. In *Intelligent Transportation Systems* (2016), Springer, pp. 19–47.

[9] Forooshani, A. E., Bashir, S., Michelson, D. G., and Noghanian, S. A survey of wireless communications and propagation modeling in underground mines. *Communications Surveys & Tutorials, IEEE 15*, 4 (2013), 1524–1545.

[10] Ghosh, A. K., Kunta, S., Verma, P., and Huck, R. C. Free-space optics based sensor network design using angle-diversity photodiode arrays. In *SPIE Optical Engineering+ Applications* (2010), International Society for Optics and Photonics, pp. 78140U–78140U.

[11] Gomes, A., David, M., Henriques, A., and Maio, A. Comparative study of WLS fibres for the ATLAS tile calorimeter. *Nuclear Physics B-Proceedings Supplements 61*, 3 (1998), 106–111.

[12] Hirota, S., Nishimura, Y., Suda, Y., Okajima, Y., Shiozawa, M., Nakayama, S., Tanaka, H., Hayato, Y., Ikeda, M., Nakahata, M., et al. New large aperture, hybrid photo-detector and photo multiplier tube for a gigantic water Cherenkov ring imaging detector. *Nuclear Instruments and Methods in Physics Research Section A: Accelerators, Spectrometers, Detectors and Associated Equipment 766* (2014), 152–155.

[13] Hobbs, P. C. *Building electro-optical systems: making it all work*, vol. 71. John Wiley & Sons, 2011.

[14] Kahn, J. M., You, R., Djahani, P., Weisbin, A. G., Teik, B. K., and Tang, A. Imaging diversity receivers for high-speed infrared wireless communication. *Communications Magazine, IEEE 36*, 12 (1998), 88–94.

[15] Khalighi, M.-A., Gabriel, C., Hamza, T., Bourennane, S., Leon, P., and Rigaud, V. Underwater wireless optical communication; recent advances and remaining challenges. In *Transparent Optical Networks (ICTON), 2014 16th International Conference on* (2014), IEEE, pp. 1–4.

[16] Klaus, W. Development of LC optics for free-space laser communications. *AEU-International Journal of Electronics and Communications 56*, 4 (2002), 243–253.

[17] Mahnke, M., Wiechmann, S., Heider, H., Blume, O., and Müller, J. Aluminum oxide doped with erbium, titanium and chromium for active integrated optical applications. *AEU-International Journal of Electronics and Communications 55*, 5 (2001), 342–348.

[18] Mmbaga, P. F., Thompson, J., and Haas, H. Performance analysis of indoor diffuse VLC MIMO channels using angular diversity detectors. *Journal of Lightwave Technology 34*, 4 (2016), 1254–1266.

[19] Nakhkoob, B., Bilgi, M., Yuksel, M., and Hella, M. Multi-transceiver optical wireless spherical structures for MANETs. *Selected Areas in Communications, IEEE Journal on 27*, 9 (2009), 1612–1622.

[20] Nilsson, J. *Optical design and characterization of solar concentrators for photovoltaics*. 2005.

[21] Peyronel, T., Quirk, K., Wang, S., and Tiecke, T. Luminescent detector for free-space optical communication. *Optica 3*, 7 (2016), 787–792.

[22] Saadatseresht, M., Talebi, R., Johnson, J., and Abdel-Dayem, A. Chapter 37 - Practical issues for binary code pattern unwrapping in fringe projection method.

In *Emerging Trends in Image Processing, Computer Vision and Pattern Recognition*, L. Deligiannidis and H. R. Arabnia, Eds. Morgan Kaufmann, 2015, pp. 561 – 581.

[23] Samimi, H., and Azmi, P. Performance analysis of equal-gain diversity receivers over generalized gamma fading channels. *AEU-International Journal of Electronics and Communications 62*, 7 (2008), 496–505.

[24] Sevincer, A., Bilgi, M., Yuksel, M., and Pala, N. Prototyping multi-transceiver free-space optical communication structures. In *Communications (ICC), 2010 IEEE International Conference on* (2010), IEEE, pp. 1–5.

[25] Shang, T., Yang, Y., Li, W., Wang, X., and Jia, J. An omni-directional optical antenna and its beam control method based on the EC-KPA algorithm for mobile FSO. *Optics express 21*, 2 (2013), 2307–2323.

[26] Sterckx, K. L., Elmirghani, J. M., and Cryan, R. A. Pyramidal fly-eye detection antenna for optical wireless systems. In *Optical Wireless Communications (Ref. No. 1999/128), IEE Colloquium on* (1999), IET, pp. 5–1.

[27] Szmulowicz, F., and Chandler, T. C. Proposal for a new cylindrical geometry for transverse infrared photodetectors. *IEEE Transactions on Electron Devices 28*, 7 (Jul 1981), 772–776.

[28] Trung, H. D., Pham, A. T., et al. Pointing error effects on performance of free-space optical communication systems using SC-QAM signals over atmospheric turbulence channels. *AEU-International Journal of Electronics and Communications 68*, 9 (2014), 869–876.

[29] Tsonev, D., Sinanovic, S., and Haas, H. Practical MIMO capacity for indoor optical wireless communication with white LEDs. In *Vehicular Technology Conference (VTC Spring), 2013 IEEE 77th* (2013), IEEE, pp. 1–5.

[30] Vellakudiyan, J., Muthuchidambaranathan, P., Bui, F. M., and Palliyembil, V. Performance of a subcarrier intensity modulated differential phase-shift keying over generalized turbulence channel. *AEU-International Journal of Electronics and Communications 69*, 11 (2015), 1569–1573.

[31] Yadav, A. K., and Chandel, S. Tilt angle optimization to maximize incident solar radiation: A review. *Renewable and Sustainable Energy Reviews 23* (2013), 503–513.

[32] Yuksel, M., Akella, J., Kalyanaraman, S., and Dutta, P. Free-space-optical mobile ad hoc networks: Auto-configurable building blocks. *Wireless Networks 15*, 3 (2009), 295–312.

[33] Yun, G., and Kavehrad, M. Spot-diffusing and fly-eye receivers for indoor infrared wireless communications. In *Wireless Communications, 1992. Conference Proceedings., 1992 IEEE International Conference on Selected Topics in* (1992), IEEE, pp. 262–265.

[34] Zeng, R. X., and Sinsky, J. H. Modified rational function modeling technique for high speed circuits. In *2006 IEEE MTT-S International Microwave Symposium Digest* (2006), IEEE, pp. 1951–1954.

Chapter 4

Teleoperation of Mining Equipment Using Optical Wireless Communications

4.1 Abstract

Penguin Automated Systems Inc. is presently evaluating the world's first omnidirectional Optical Wireless Communications (OWC) network customized to teleoperate mobile equipment in surface, underground and underwater mining operations. Experimental results of novel technologies that made this possible are presented here: a mode programmable On-Off-Keying (OOK), Orthogonal Frequency Division Modulations (OFDM) Half-Duplex LED driver, and a single photodetector Free Space Optical (FSO) receiver. Experimentation demonstrated viability of this OWC system in its intended environments.

4.1.1 Contributions of Authors

Alberto Rui Frutuoso Barroso

- Concept generation
- Experiment design, planning and implementation
- Data analysis

Dr. Gregory Baiden

- Identified the advantages of using OWC systems in mining operations
- Analyzed results and suggested improvements for the experimental procedures
- Patent application for systems and methods invented in this research
- Review and approval of the article for publication.

Dr. Julia Johnson

- Analyzed results and suggested article structure
- Article proofreading

Publication Status

Published (compact version) at the IEEE 2015 Seventh International Conference on Ubiquitous and Future Networks, pages 727–733.

4.2 Introduction

The depletion and scarcity of high-grade mineral deposits in dry land is forcing the Natural Resources industry to look for alternate sources to assist a sustainable worldwide economic growth. Underwater and space (near-Earth objects) are humanity's next exploration frontier [5], and that requires the creation of reliable broadband omnidirectional wireless communication systems to teleoperate equipment in those environments. The electromagnetic spectrum below 3 THz [6] is allocated to diverse radio communications services, requiring use of spectrum below ionizing radiation frequencies to implement more services and provide more bandwidth. Optical wireless communications (OWC) offer important advantages over standard RF communication systems, having the potential of bitrates above multiple Terabit/s in space, atmosphere and underwater environments.

The 2013 NASA Lunar Laser Communications Demonstration (LLCD) [38] showed that a 0.5W Laser was able to transmit 622 Mbps in a 400 thousand kilometer link into a 0.8 meter photon collection receiver, a technology more efficient than NASA standard Ka-band 40W radios that require an Earth receiving station equipped with 18 meter diameter parabolic antennas. The LLCD proves the superiority of current OWC technologies when compared with standard RF in point-to-point links, but gimbals aligned Lasers used in the LLCD are not always possible to implement in mobile mining equipment, and an omnidirectional OWC system is mandatory to allow the teleoperation of mobile equipment.

Currently, leaky feeder (radiant coaxial cable) is the most prevalent communications infrastructure present in underground mines [7], but this infrastructure is often not installed in temporary areas like ore body fronts, block caving draw bells and room & pillar zones, for example.

Diverse wireless systems working in bands from Very High Frequencies (VHF) to microwave [24] are used in the zones not covered by the leaky feeder, but multiple studies show that the teleoperation of mining equipment in underground and underwater environments using those bands is not reliable.

Akyildiz, Sun and Vuran [1] present models characterizing Wireless Underground Communications Networks (WUCNS) in tunnels and room & pillar areas, concluding that intense attenuation and fluctuations exist in the near region, and that the tunnel size and antenna positioning are critical. This lack of network reliability limits the teleoperation of mining equipment, a problem that Hakem, Delisle and Coulibaly [18] quantify, measuring path losses above 85 dB at 20 meters distances in tunnels with 25 cm of surface irregularities, and concluding that 2.4 GHz gives more network availability than 5.8 or 60 GHz systems.

RF performance in underwater communications is even more limited [21], forcing the use of low frequencies [29], magnetic induction [45], acoustic communications [32], Laser OWC [37] or hybrid (acoustic-OWC) systems [40].

This paper presents field test results of novel technologies that address the two biggest problems to implement OWC teleoperation enabled networks: nonexistence of high bandwidth omnidirectional FSO receivers and inefficient OWC LED modulation drivers.

4.3 Experimental Methodology

Data collected from atmospheric and underwater experiments using different types of LED drivers and FSO receivers was obtained from an OWC OFDM modulator implemented in a Field Programmable Gate Array (FPGA), with the following communication statistics collected from it: uncoded bitrate, modulation density (bits/Hz), and signal to noise per OFDM carrier. Field tests were executed indoors (tunnels) and outdoors using a pontoon boat (Figure 4.1) customized for atmospheric and underwater OWC experiments.

Figure 4.1: Penguin ASI OWC research pontoon boat [36]

4.3.1 OFDM modulator

The OFDM modulator was implemented using a Wireless Open-Access research platform (WARP) FPGA board (Figure 4.2) with custom designed AD and DA daughter boards: a Multiple-In (MI) daughter board using one octal LNA/VGA/AAF/ADC device (AD9272), and a Multiple-Out (MO) daughter board using four dual 12-Bit, 125Msps digital to analog converters (DAC2902).

The main blocks synthesized in the FPGA were:

- DDR2 memory controller
- PowerPC 405 processor
- Pre-distorted OFDM LED modulator
- OOK modulator
- Half-Duplex packet controller

The following packet based OFDM modulations schemes were implemented: 1024/256/64/8-QAM, 16-APSK, QPSK and BPSK, capable of the bandwidth efficiency present in table 4.1.

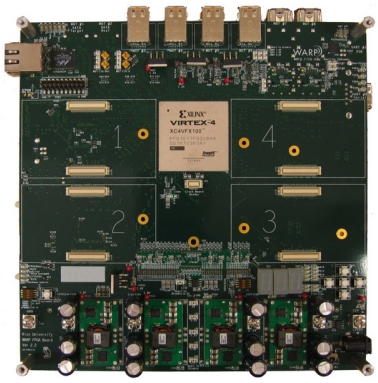

Figure 4.2: WARP: Virtex-4 FPGA board v2.2 [44]

Table 4.1: FPGA OFDM modulator capabilities

E-O-E Bandwidth (MHz)	**Bitrate (Mbps)**	**Efficiency (bit/Hz)**
6	56	9.3
15	175	11.6
30	292	9.7
50	494	9.9

4.3.2 OWC LED driver

A LED driver for OWC communications need to integrate the following features:

- Pulsed time digital modulations (OOK, Manchester, PPM, etc.)
- Pulsed time (framing), frequency and amplitude modulations (ASK, FSK, PSK, QAM, APSK, etc.)
- LED dimming for VLC applications
- RGB Colour Shift Keying (CSK)
- Half-Duplex and Full-Duplex modes
- LED temperature monitoring and over current protection

It was determined during this research that efficient and versatile LED drivers for OWC do not exist, with the catalogs of the current leaders of Mixed Signal Logic Products (MSLP) offering only LED drivers for illumination applications.

After executing a literature review about the problems that affect the use of LEDs in OWC, nonlinearities [10] [20] [41] and LED frequency response [26] [27] [30] were identified as main performance limiting factors. To address these two problems, equalization and pre-distortion schemes for LED OFDM modulation were implemented in the FPGA.

One Texas Instruments MSP430F2619 Mixed Signal Microcontroller (MSM) was used to supervise the temperature and current of the LED array that integrates a GaN control FET in an Integrated OWC Circuit (IOWCC) structure.

The FPGA communicates with the IOWCC with three 50 Ohms OFDM coaxial links to support Color Shift Keying (CSK) [34] modulations, one Local Interconnect Network (LIN) bus to monitor and control the IOWCC features (LED bias point, OOK mode, analog OFDM and VLC dimming mode), and one LVDS pair to control the OFDM half-duplex framing or OOK modulations.

It was observed that the IOWCC gives a superior frequency response (Figure 4.3) when compared with our previous prototypes that used the industry standard bias tee to inject the AC OFDM component in the LED serial array.

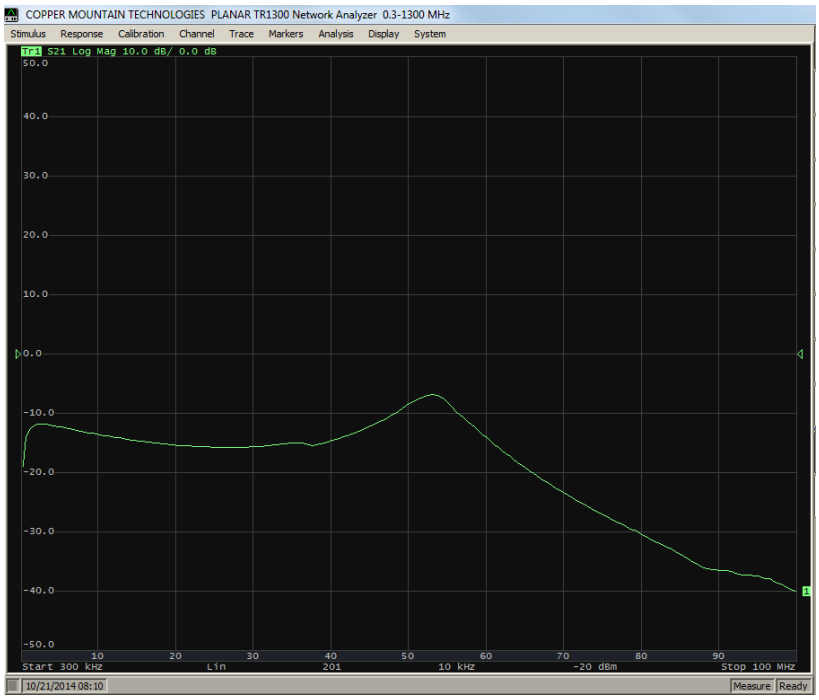

Figure 4.3: IOWCC E-O-E frequency response

The IOWCC superior frequency response resulted from the absence of the bias tee capacitor and its undesired Equivalent Series Resistance (ESR), and by programming the MSM with a full Safe Operating Area (SOA) temperature and current control strategy, to maximize the LED DC power parameter P_{DC} (Equation 4.1) in the LED frequency response model [4].

$$P(\omega) = \frac{P_{\mathrm{DC}}}{\sqrt{1 + (\omega\tau)^2}} \tag{4.1}$$

4.3.3 Omnidirectional OWC receiver

The teleoperation of mobile mining equipment using an OWC system requires the usage of wide aperture large Field of View (FOV) photon receivers, and standard reflective or refractive optical technologies do not offer efficient solutions for that requirement. The most commonly used technologies to implement large aperture FSO receivers are:

- large Hemispherical Photomultiplier Tubes (PMT) [11]
- fish-eye lens [8]
- Compound Parabolic Concentrators (CPC) [43]
- multiple detectors connected to a Received Signal Strength Indicator (RSSI) controlled selector/combiner [22].
- Fresnel lens [14]

The main limitations of these omnidirectional implementations are summarized in table 4.2.

Table 4.2: OWC omnidirectional receiver technologies

Technology	**Undesired characteristics**
PMT	fragile, price, bulky
Fish-eye lens	low gain, fragile
CPC	low acceptance angle, bulky
Array of sensors	price, mechanical complexity
Fresnel lens	bulky, narrow FOV

A variety of experiments of omnidirectional optical receivers using refractive and reflective optics were undertaken, integrating photodetector arrays [2], PMT sensors, Silicon Photomultiplier Diodes [17], and wavelength shifting (WS) fibers [33]. The biological optics [28] of three species (Figure 4.4) were replicated using WS fibers, mimicking the FOV of the eye [42] of the owl, pigeon, and arthropods.

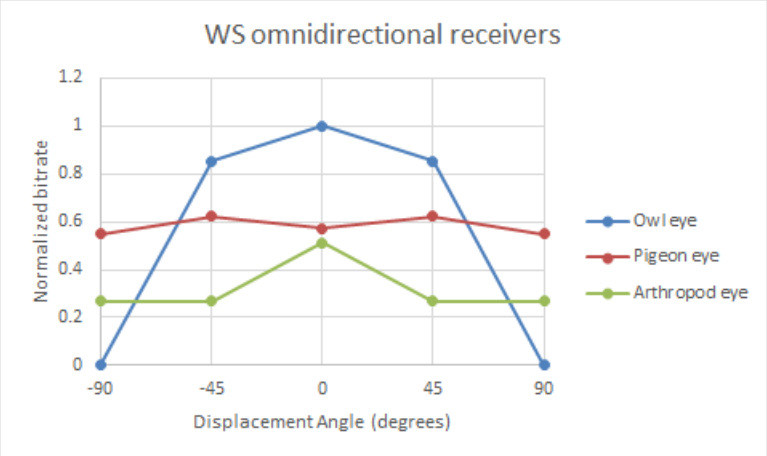

Figure 4.4: WS modeled biological eyes

Zemax OpticStudio was used to model OWC receivers replicating the owl, pigeon, and diverse arthropods eyes, and it was concluded that the owl eye is the optical shape more effective to be integrated on the side of vehicles where a central top point is not available.

The simulations also proved that the pigeon monocular vision (Figure 4.5) offer an optimal omnidirectional reception in vehicles with one or two available central points.

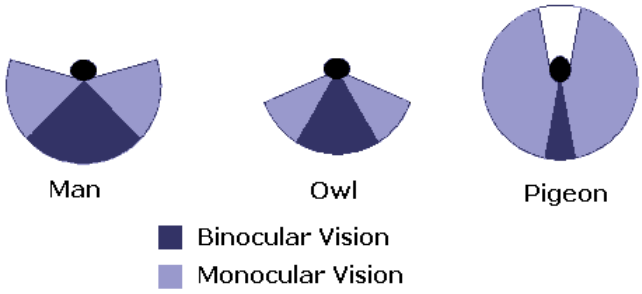

Figure 4.5: Pigeon vision [31]

Figure 4.6: 150 meters range atmospheric test using 8 blue LEDs

4.4 Results and discussion

In the process of system modeling and prototype experimentation, an ideal setting was established for the implementation of vehicle to infrastructure (V2I) optical wireless communications with the required performance to teleoperate mobile equipment in the mining industry. The requirements for achieving that ideal experimental environment are highlighted in this section. Long range and high bitrates are the objectives for the implementation of V2I-OWC networks, in surface, underground and underwater mining operations.

The bitrate and range of OWC networks depends on parameters that characterize the transmitter, the propagation medium, and the receiver (Figure 4.7).

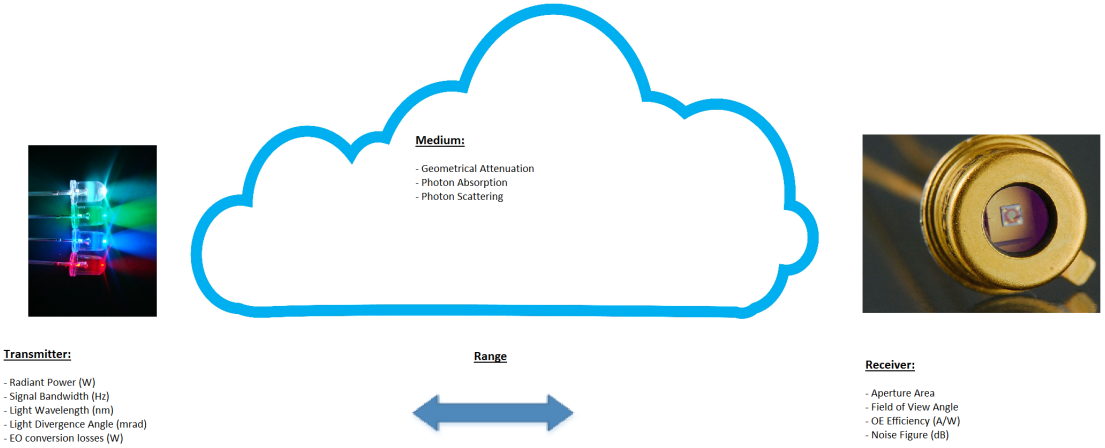

Figure 4.7: OWC Propagation model

In the transmitter the radiant power and emission divergence are the main design parameters that need to be chosen to obtain the desired range and omnidirectional coverage. The choice for the light beam spreading varies between a low divergence Laser and a 180 degrees uncollimated LED, with intermediary divergences obtained using refractive or reflective optics.

The specification of the wavelength for light emission in vacuum (outer space) is only restricted by the Photodetector color responsivity (A/W), its Quantum efficiency (%), the LED or Laser diode (LD) radiometric power, and other electro-mechanical parameters. Choosing the wavelength of emission for atmosphere or underwater OWC is more complex, because a careful study of the medium [3] is required, followed by customized optoelectronic design. A gain parameter was modeled for the receiver (OE gain), and OWC link budget calculators were programmed in Matlab to model the bitrate of the system in different types of atmosphere (fog, rain, snow) and Jerlov [14] water types.

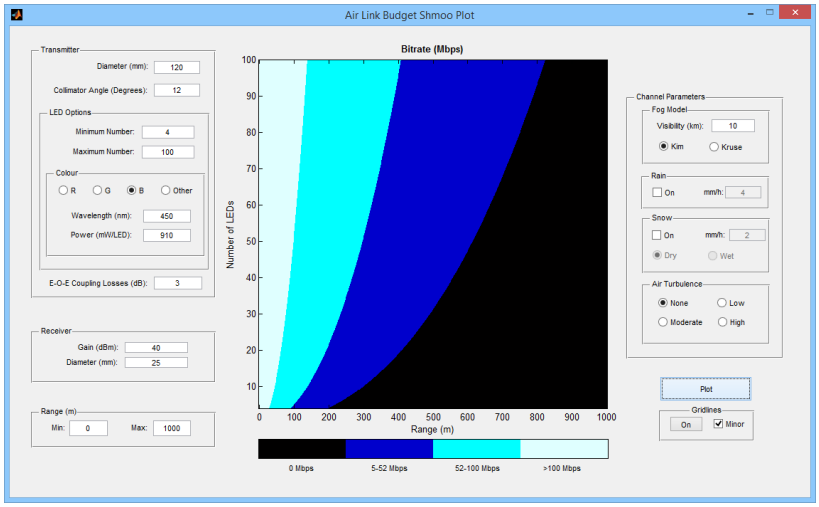

Figure 4.8: Atmospheric link budget calculator

The air link budget calculator (Figure 4.8) accounts for all parameters P_{n} (Equation 4.2): radiometric power of the LEDs, geometric attenuation, fog, rain, snow [35].

$$P\mathrm{receiver}(dBm) = \sum P\mathrm{n}(dB) \tag{4.2}$$

The underwater link budget calculator (Figure 4.9) replaces the atmospheric attenuation with Beer-Lambert law (Equation 4.3), and uses the Photonator Monte Carlo simulator [9] to increase the prediction precision for the range and bitrate.

Both link budget simulators give small errors between the predicted and measured values, but new versions are being developed to include detector (APD, SiPMD, WS fiber) specifications and the temperature de-rating that affects the frequency response of the IOWCC.

$$\frac{I}{I_0} = \exp(-\gamma L) \tag{4.3}$$

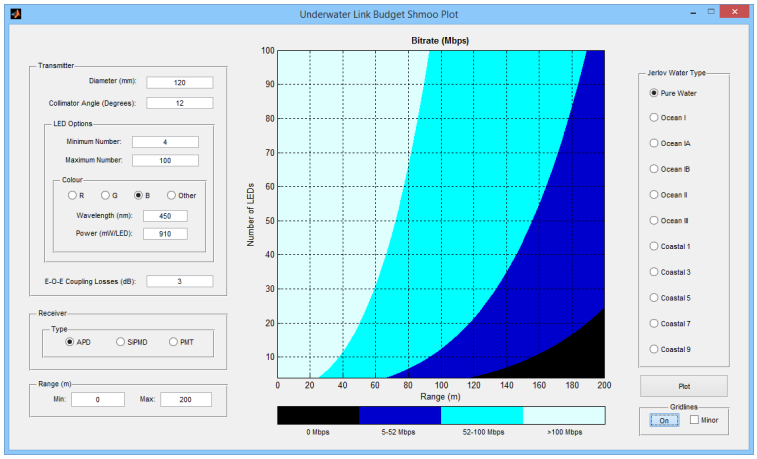

Figure 4.9: Underwater link budget calculator

To experimentally validate these OWC link budget models, atmospheric tests were executed in a 130 meters long corridor with wall irregularities below one meter, and underwater tests were run inside Laurentian University (LU) 50 meters length Olympic pool (Figure 4.15) filled with crystalline water similar to deep ocean waters. Long Lake (Ontario, Figure 4.1) was used to run experiments in a turbid water equivalent to the type present in coastal breakwater harbors, and coastal water experiments were made in unfiltered tap water pools and in the Florida Keys [46].

4.4.1 Atmospheric experiments

A test was run at 100 meters range with minimal environmental light (less than 1 micromole of photons) and a small offset error (Figure 4.10) was observed between the measured and predicted values, error that was attributed to inexistent thermal parameters in the link budget modeling.

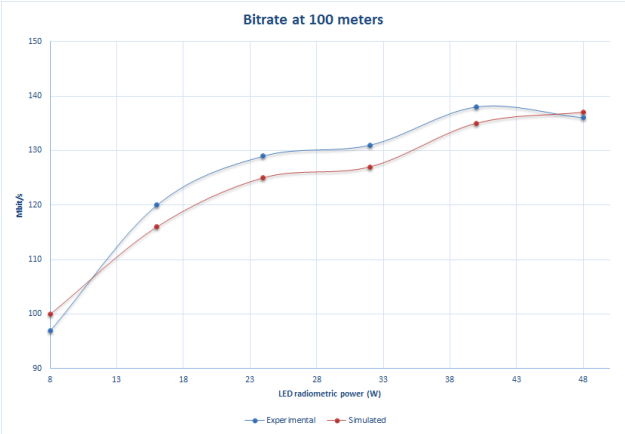

Figure 4.10: OWC bitrate at 100 meters (night tests)

The experimental tests with the owl-eye omnidirectional receiver (Figure 4.11) show that an optical antenna with 120 degrees vertical and 360 degrees horizontal can be designed using 3 receivers covering 120 degrees each.

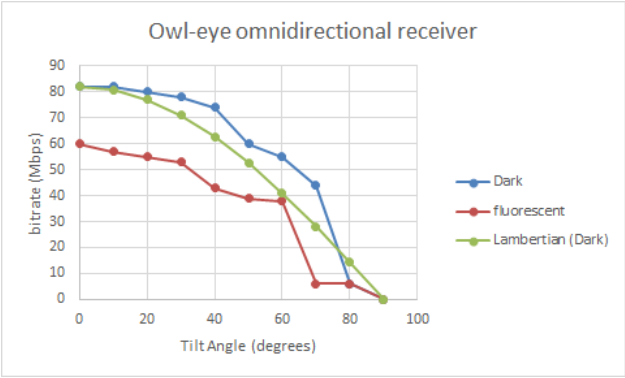

Figure 4.11: Owl-Eye Omnidirectional Receiver

The owl-eye omnidirectional receiver allows higher bitrates than IEEE 802.11 (no channel bonding) in Tunnels with lengths above 120 meters (Figure 4.12). An inappropriate AGC circuit causes the low bitrate between 0 and 25 meters.

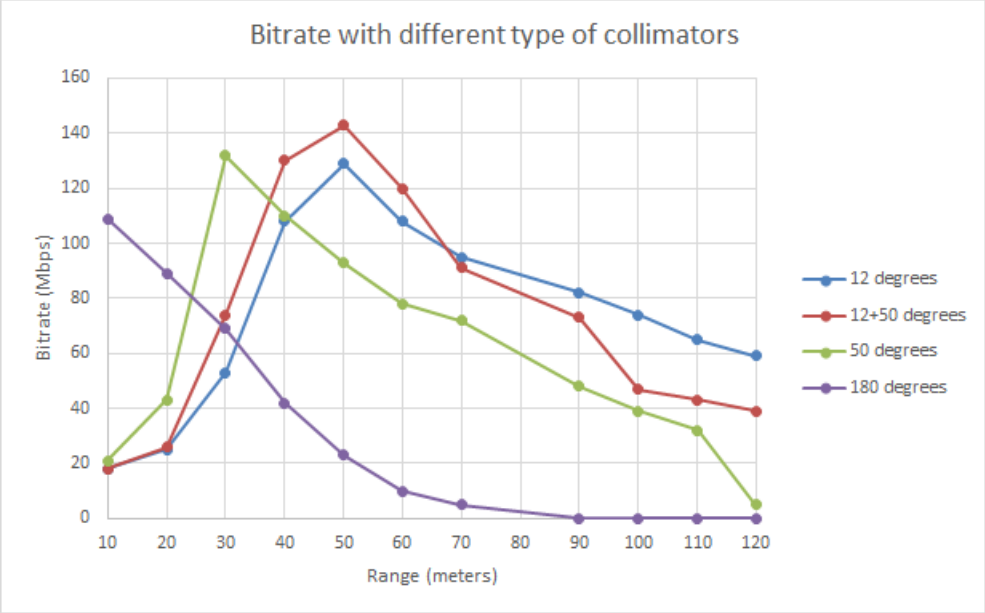

Figure 4.12: OWC in a tunnel

Multiple outdoor tests (Figure 4.6) showed that this OWC system can replace IEEE 802.11a/b/g/n/ac radios with multiple advantages, like a versatile scalability that allows reaching 1 Km of range just by installing another 24 LED IOWCC module. These experiments proved that range scalability of OWC systems are far superior than standard RF, because emitter directivity in OWC can be achieved using compact optics, while in RF, directivity is often associated with the installation of a bulky antenna.

Penguin ASI OWC teleoperated demolition robot (Figure 4.20) required long range (over 100 metres) operation and short range (0 to 10 meters), a project requirement that was achieved wit the use of programmable LED power (Figure 4.13).

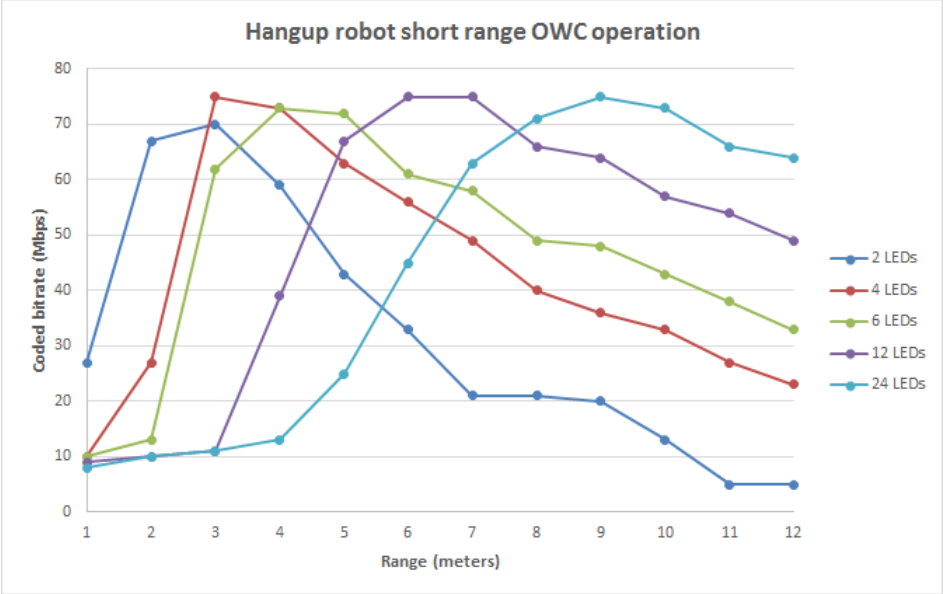

Figure 4.13: Penguin ASI hangup robot short range LED panels

Experiments and simulation demonstrated that the WLS spiral receiver responsivity require one LED (910 mW) as the minimal power resolution (Figure 4.14).

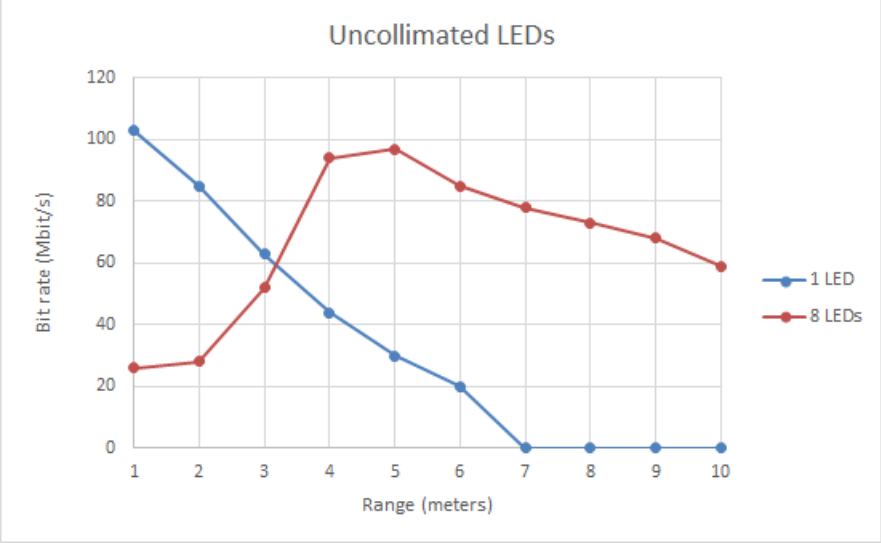

Figure 4.14: Short range bit rate

4.4.2 Underwater experiments

Figure 4.15: OWC experiments at LU Olympic pool

OWC networks in atmospheric environments offer high availability, long ranges and high bitrates in the absence of dense fog, snow or rainfall, and underwater OWC systems have the same medium limitation. Underwater OWC performance is highly compromised by turbid environments [39], where acoustic or magnetic induction communications can be a more effective solution. The developed link budget models, and experiments confirm that it is not feasible to increase the OWC range just by increasing the LED emitting power, e.g. doubling the LED power can result in an insignificant range gain because of the exponential (Figure 4.16) decay of photons in absorptive mediums.

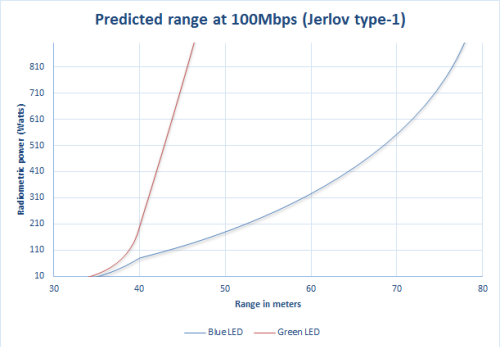

Figure 4.16: Underwater OWC exponential decay

During underwater OWC experiments (Figure 4.15), it was verified that tests executed in depths above 2 meters suffer from reflection from the air-water interface (Figure 4.17) that contributes with more photons arriving to the receiver, contribution that fades away when testing at bigger depths, or when using tight collimating optics in the developed underwater OWC modems (Figure 4.19).

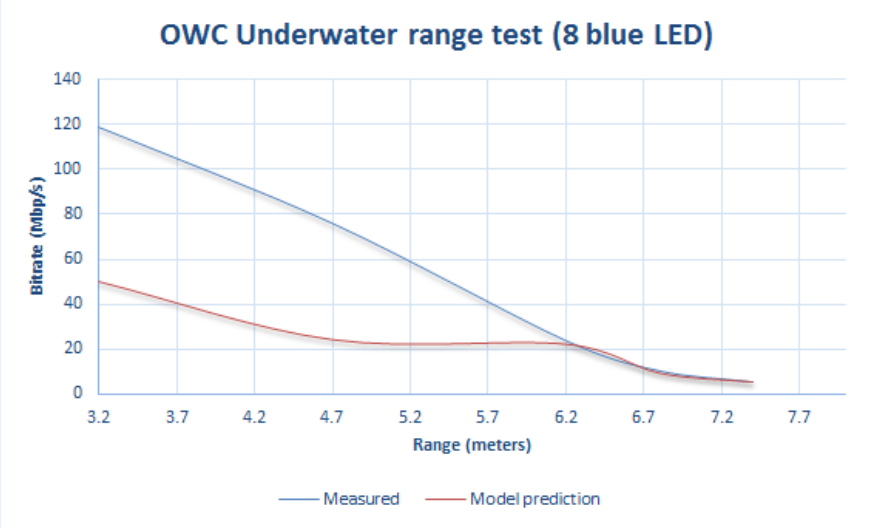

Figure 4.17: OWC Water-Air interface reflections

OWC experiments executed in the deepest zone of Long Lake (Ontario, Canada) demonstrated that the waters of this lake are Jerlov type-7, giving a poor transmission for light in the blue region. In a test using 4 radiometric Watts of uncollimated LED light in Long Lake waters, it was verified a maximum range below 2 meters when using 450nm blue LEDs, and below 9 meters when using 630nm red LEDs.

Experiments executed in coastal water in the Florida Keys demonstrated that long ranges can be obtained in turbid waters, using the green to red light spectrum range (Figure 4.18) and implementing a mesh structure with a distance between nodes specified for the required bitrate.

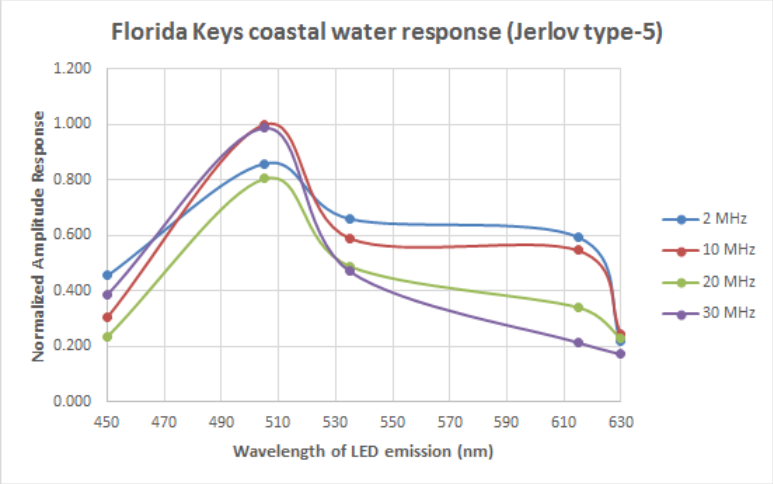

Figure 4.18: Florida Keys coastal water color response

A statistical link sensing handshake in the OFDM-OOK modulator was tested during these experiments, with the objective of implementing underwater OWC mesh networks. It was verified that the point-to-pint OWC link adapted to different (environmental illumination noise, water localized turbidity, system thermal de-rating, etc.) signal-to-noise ratio (SNR) at both receivers, with the collected bitrate statistics showing asymmetric values for the up-link and down-link connections.

Figure 4.19: Underwater OWC modems

4.4.3 OWC Teleoperated demolition robot

Figure 4.20: Penguin ASI OWC teleoperated demolition robot

Industrial operations frequently require the use of teleoperated robots in zones that are too dangerous to permit human presence. The Fukushima-Daiichi accident [23], the Deep-water Horizon oil spill [25], Coal mine fires [47], and ore passing hang-up [16] are examples of situations with a high level of risk that require the use of teleoperated equipment.

In some operational scenarios, the use of standard radios is unpractical [12] or have usage restrictions [19] [13]. To address this problem, Penguin ASI developed the world first OWC teleoperated robot able to install demolition explosive charges in high risk work environments.

This robot (Figure 4.20) integrates multiple owl-eye FSO receivers with an inertial controlled LED phased array and an amphibious design enabling it to place demolition charges in underwater environments [15]. Experimental evaluation of this WLS spiral receiver demonstrated its low sensitivity to indoor halogen or fluorescent illumination (Figure 4.21).

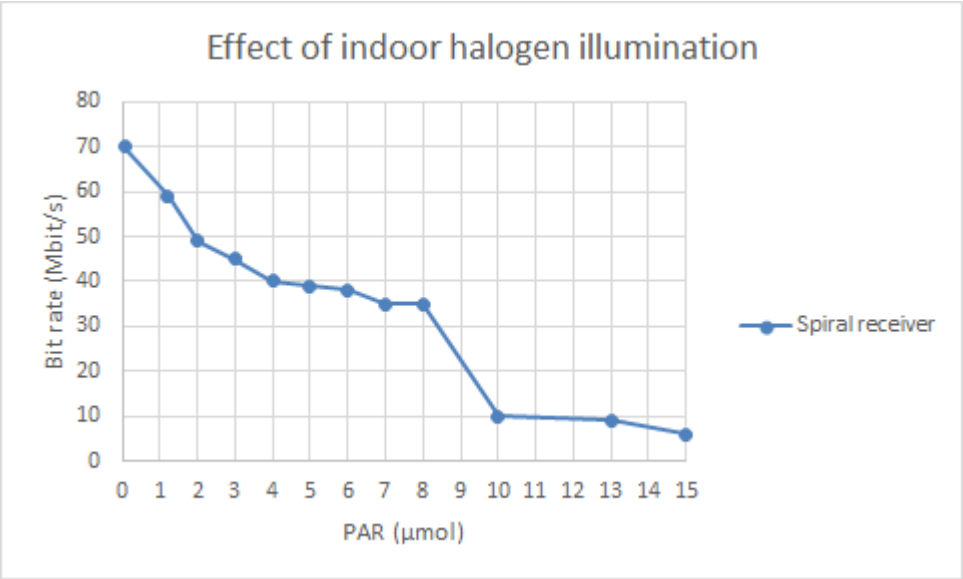

Figure 4.21: Interference experiment with halogen illumination

The use of optical wireless communications allows one to teleoperate the robot using high definition video in environments (underwater and tunnels) where standard RF perform with an inferior warranty of service.

4.5 Conclusions

An Optical Wireless Communications system for remote operation of mobile mining equipment has been implemented.

Experimentation showed advantages of the IOWCC over the conventional bias tee LED modulation, and it was proved that WLS fibers can be used to design high gain omnidirectional FSO receivers replicating the FOV of diverse biological eyes.

Tests and simulations indicated that the owl eye shape is more appropriated to be integrated in teleoperated vehicles with quadrant optical reception, and that pigeon eye shaped receivers can maximize hemispherical photon reception.

References

[1] Akyildiz, I. F., Sun, Z., and Vuran, M. C. Signal propagation techniques for wireless underground communication networks. *Physical Communication 2*, 3 (2009), 167 – 183.

[2] Armstrong, J. Optical domain digital-to-analog converter for visible light communications using LED arrays [invited]. *Photonics Research 1*, 2 (2013), 92–95.

[3] Arnon, S., Barry, J., Karagiannidis, G., Schober, R., and Uysal, M. *Advanced optical wireless communication systems*. Cambridge University Press, 2012.

[4] Bergh, A., and Copeland, J. A. Optical sources for fiber transmission systems. *Proceedings of the IEEE 68*, 10 (Oct 1980), 1240–1247.

[5] Campbell, M. D., King, J. D., Wise, H. M., Handley, B., Conca, J. L., and Campbell, M. D. Nuclear power and associated environmental issues in the transition of exploration and mining on earth to the development of off-world natural resources in the 21st century.

[6] Canada, I. Canadian table of frequency allocations, January 2015. http://www.ic.gc.ca/eic/site/smt-gst.nsf/eng/h_sf01678.html.

[7] Chehri, A., and Mouftah, H. Radio channel characterization through leaky feeder for different frequency bands. In *Personal Indoor and Mobile Radio Communications (PIMRC), 2010 IEEE 21st International Symposium on* (Sept 2010), pp. 347–351.

[8] Chen, T., Liu, L., Tu, B., Zheng, Z., and Hu, W. High-spatial-diversity imaging receiver using fisheye lens for indoor MIMO VLCs.

[9] Cox, W., and Muth, J. Simulating channel losses in an underwater optical communication system. *JOSA A 31*, 5 (2014), 920–934.

[10] Elgala, H., Mesleh, R., and Haas, H. A study of LED nonlinearity effects on optical wireless transmission using OFDM. In *Wireless and Optical Communications Networks, 2009. WOCN'09. IFIP International Conference on* (2009), IEEE, pp. 1–5.

[11] Fair, N., Chave, A., Freitag, L., Preisig, J., White, S., Yoerger, D., and Sonnichsen, F. Optical modem technology for seafloor observatories. In *OCEANS 2006* (2006), IEEE, pp. 1–6.

[12] Frater, M. R., Ryan, M. J., and Dunbar, R. M. Electromagnetic communications within swarms of autonomous underwater vehicles. In *Proceedings of the 1st ACM international workshop on Underwater networks* (2006), ACM, pp. 64–70.

[13] Galuga, J., and Bray, J. R. Induced currents on electric detonators for improvised explosive device pre-detonation. In *Electromagnetic Compatibility (EMC), 2011 IEEE International Symposium on* (2011), IEEE, pp. 758–762.

[14] Giles, J. W., and Bankman, I. N. Underwater optical communications systems. Part 2: basic design considerations. In *Military Communications Conference, 2005. MILCOM 2005. IEEE* (2005), IEEE, pp. 1700–1705.

[15] Glasby, G. Deep seabed mining: past failures and future prospects. *Marine Georesources and Geotechnology 20*, 2 (2002), 161–176.

[16] Hadjigeorgiou, J., and Lessard, J. Numerical investigations of ore pass hang-up phenomena. *International Journal of Rock Mechanics and Mining Sciences 44*, 6 (2007), 820–834.

[17] Haemisch, Y., Frach, T., Degenhardt, C., and Thon, A. Fully digital arrays of silicon photomultipliers (dSiPM)–a scalable alternative to vacuum photomultiplier tubes (pmt). *Physics Procedia 37* (2012), 1546–1560.

[18] Hakem, N., Delisle, G., and Coulibaly, Y. Radio-wave propagation into an underground mine environment at 2.4 GHz, 5.8 GHz and 60 GHz. In *Antennas and Propagation (EuCAP), 2014 8th European Conference on* (April 2014), pp. 3592–3595.

[19] Heard, N. A., Strachan, D. C., and Maddocks, A. Measurements of the field strengths on offshore oil platforms for assessing radio-frequency hazards with electroexplosive devices. *Electromagnetic Compatibility, IEEE Transactions on*, 3 (1985), 162–167.

[20] Inan, B., Jeffrey Lee, S., Randel, S., Neokosmidis, I., Koonen, A. M., and Walewski, J. W. Impact of LED nonlinearity on discrete multitone modulation. *Journal of Optical Communications and Networking 1*, 5 (2009), 439–451.

[21] Jiang, S., and Georgakopoulos, S. Electromagnetic wave propagation into fresh water. *Journal of Electromagnetic Analysis and Applications 3*, 07 (2011), 261.

[22] Kahn, J. M., and Barry, J. R. Wireless infrared communications. *Proceedings of the IEEE 85*, 2 (1997), 265–298.

[23] Kawatsuma, S., Fukushima, M., and Okada, T. Emergency response by robots to Fukushima-Daiichi accident: summary and lessons learned. *Industrial Robot: An International Journal 39*, 5 (2012), 428–435.

[24] Khan, A. R., Gulhane, S. M., and Kaushik, P. G. Performance comparison of ultra wide band IEEE channel and underground mine channel. In *Wireless Communications, Networking and Mobile Computing (WiCOM), 2012 8th International Conference on* (2012), IEEE, pp. 1–6.

[25] Kinsey, J. C., Yoerger, D. R., Jakuba, M. V., Camilli, R., Fisher, C. R., and German, C. R. Assessing the deepwater horizon oil spill with the sentry autonomous underwater vehicle. In *Intelligent Robots and Systems (IROS), 2011 IEEE/RSJ International Conference on* (2011), IEEE, pp. 261–267.

[26] Komine, T., Lee, J. H., Haruyama, S., and Nakagawa, M. Adaptive equalization system for visible light wireless communication utilizing multiple white LED lighting equipment. *Wireless Communications, IEEE Transactions on 8*, 6 (2009), 2892–2900.

[27] Le Minh, H., O'Brien, D., Faulkner, G., Zeng, L., Lee, K., Jung, D., and Oh, Y. High-speed visible light communications using multiple-resonant equalization. *Photonics Technology Letters, IEEE 20*, 14 (2008), 1243–1245.

[28] Lee, L. P., and Szema, R. Inspirations from biological optics for advanced photonic systems. *Science 310*, 5751 (2005), 1148–1150.

[29] Liu, C., Zheng, L.-G., and Li, Y.-P. Study of ELF electromagnetic fields from a submerged horizontal electric dipole positioned in a sea of finite depth. In *Microwave, Antenna, Propagation and EMC Technologies for Wireless Communications, 2009 3rd IEEE International Symposium on* (Oct 2009), pp. 152–157.

[30] Liu, Y.-F., Chang, Y. C., Chow, C.-W., and Yeh, C.-H. Equalization and pre-distorted schemes for increasing data rate in in-door visible light communication system. In *Optical Fiber Communication Conference* (2011), Optical Society of America, p. JWA083.

[31] Loft, M. P. Pigeon eye and colors, May 2016. http://mumtazticloft.com/pigeongenetics7.asp.

[32] Logics, E. Underwater acoustic modems, March 2015. http://www.evologics.de/en/products/acoustics/index.html.

[33] Lundin, M., Contin, A., Dellacasa, G., DeSalvo, R., Gallio, M., Gorodetzky, P., Helleboid, J., Johnson, K., Juillot, P., Lazic, D., et al. On the electromagnetic energy resolution of Cherenkov-fiber calorimeters. *Nuclear Instruments and Methods in Physics Research Section A: Accelerators, Spectrometers, Detectors and Associated Equipment 372*, 3 (1996), 359–367.

[34] Monteiro, E., and Hranilovic, S. Design and implementation of color-shift keying for visible light communications. *Journal of Lightwave Technology 32*, 10 (2014), 2053–2060.

[35] Muhammad, S. S., Kohldorfer, P., and Leitgeb, E. Channel modeling for terrestrial free space optical links. In *Transparent Optical Networks, 2005, Proceedings of 2005 7th International Conference* (2005), vol. 1, IEEE, pp. 407–410.

[36] Penguin. Automation Systems inc., March 2015. http://www.penguinasi.com.

[37] Photonics, S. Neptune underwater communications, March 2015. http://www.saphotonics.com/high-bandwidth-optical-communications/underwater/.

[38] Robinson, B., Boroson, D., Burianek, D., and Murphy, D. The lunar laser communications demonstration. In *Space Optical Systems and Applications (ICSOS), 2011 International Conference on* (May 2011), pp. 54–57.

[39] Smart, J. Underwater optical communications systems part 1: variability of water optical parameters. In *Military Communications Conference, 2005. MILCOM 2005. IEEE* (2005), IEEE, pp. 1140–1146.

[40] Sonardyne. Bluecomm underwater optical modem, March 2015. http://www.sonardyne.com/products/all-products/instruments/1148-bluecomm-underwater-optical-modem.html.

[41] Stefan, I., Elgala, H., Mesleh, R., O'Brien, D., and Haas, H. Optical wireless OFDM system on FPGA: Study of LED nonlinearity effects. In *Vehicular Technology Conference (VTC Spring), 2011 IEEE 73rd* (2011), IEEE, pp. 1–5.

[42] Sterckx, K., Elmirghani, J., and Cryan, R. Sensitivity assessment of a three-segment pyramidal fly-eye detector in a semidisperse optical wireless communication link. In *Optoelectronics, IEE Proceedings-* (2000), vol. 147, IET, pp. 286–294.

[43] Trisno, S., Ho, T.-H., Milner, S. D., and Davis, C. C. Theoretical and experimental characterization of omnidirectional optical links for free space optical communications. In *Military Communications Conference, 2004. MILCOM 2004. 2004 IEEE* (2004), vol. 3, IEEE, pp. 1151–1157.

[44] WARP. Wireless open access research platform, March 2015. http://warpproject.org.

[45] WFS. Seatooth subsea modems, March 2015. http://www.wfs-tech.com/index.php/products/seatooth/.

[46] YOUTUBE. Penguin ASI - Testing innovative optical communications in the Florida Keys, March 2015. https://www.youtube.com/watch?v=pKAzErzFp7k.

[47] ZHOU, F.-B., WANG, D.-M., ZHANG, Y.-J., ZHANG, Y.-L., AND XIANG, L. Practice of fighting fire and suppressing explosion for a super-large and highly gassy mine. *Journal of China University of Mining and Technology 17*, 4 (2007), 459–463.

Chapter 5

Conclusions

The experimental studies show that the use of WLS fiber is an effective optical component in the design of omnidirectional OWC systems. Experiments proved that a WLS filled balloon shape gives less gain than a toroidal omnidirectional receiver, and that a hemispherical flat WLS receiver is the less intrusive structure to integrate OWC systems in vehicles.

5.1 Contributions of this study

Broadband emission and omnidirectional reception are key characteristics of RF wireless systems, that current OWC equipment do not have. The simulation, analysis and practical design of broadband photon emission and omnidirectional reception technology are presented in this thesis.

Through theoretical and experimental research, this study gave contributions to theory and practice, delivering novel technology that allows the design of compact omnidirectional OWC receivers.

5.2 Future work

This dissertation was pioneer in the use of WLS fibers to build OWC omnidirectional receivers, exposing the potential of the creation of an OWC leaky feeder to be used in tunnels, and other cylindrical shaped structures (airplanes, trains, boat corridors, etc.). A triaxial WLS fiber is suggested to be manufactured, using a transparent inner core with a refractive index superior to the WLS sleeve to allow total internal reflection and photon capture. It is also suggested to pump the triaxial transparent core to amplify the fluorescence converted optical signal using stimulated Raman scattering.

WLS fibers also have the potential to be used to build orbital angular momentum OWC receivers, receiving twisted photons emitted by orbital angular momentum microlasers.

For underwater OWC systems using WLS receivers, photon emission using sonoluminescence have the potential to be an alternative for LED or laser photon emission.

Appendices

Appendix A

Matlab code

A.1 VNA data acquisition

```
instrchoice = menu('Please choose your instrument','S5048','S7530','Planar804',
'Planar304','S8081 (Planar808/1)','R54','R140','TR1300','TR5048','TR7530');
switch instrchoice
case 1
instrument = 'S2VNA'; % S5048
case 2
instrument = 'S2VNA'; % S7530
case 3
instrument = 'S2VNA'; % Planar804
case 4
instrument = 'S2VNA'; % Planar304
case 5
instrument = 'S4VNA'; % S8081
case 6
instrument = 'RVNA';  % R54
```

```
case 7
instrument = 'RVNA';  % R140
case 8
instrument = 'TRVNA'; % TR1300
case 9
instrument = 'TRVNA'; % TR5048
case 10
instrument = 'TRVNA'; % TR7530
otherwise
instrument = 'S2VNA'; % Planar804
end
% ask user to choose user span type.
freqtype = menu('use_center_and_span','Start and stop frequency',
'Center and span frequency');
if(freqtype == 1)
use_center_and_span = false;
else
use_center_and_span = true;
end
%prompt for freq, num of points and power level
temp1 = inputdlg({'Enter the start/center frequency (Hz)',
'Enter the stop/center frequency (Hz)','Enter the number of points',
'Enter Power level (dbm)'},'Input',4,{'3e6','6e9','201','0'});
f1_hz = str2num(temp1{1});
f2_hz = str2num(temp1{2});
num_points = str2num(temp1{3});
```

```
power_level_dbm = str2num(temp1{4});
% prompt for measurement parameter
% default to S11
parchoice = menu('Please choose the parameter',
'S11','S21','S22','S12','A','B','R1','R2');
switch parchoice
case 1
parameter = 'S11';
case 2
parameter = 'S21';
case 3
parameter = 'S22';
case 4
parameter = 'S12';
case 5
parameter = 'A';
case 6
parameter = 'B';
case 7
parameter = 'R1';
case 8
parameter = 'R2';
otherwise
parameter = 'S11';
end
% prompt for format
```

```
% default to Log magnitude
formatchoice = menu('Please format type','Logarithmic magnitude'
,'Phase','Smith chart format (R + jX)','Group delay time','Polar format (Real/Imag)');
switch formatchoice
case 1
format = 'MLOGarithmic';
case 2
format = 'PHASe';
case 3
format = 'SMITh';
case 4
format = 'GDELay';
case 5
format = 'POLar';
otherwise
format = 'MLOGarithmic';
end
%prompt for time per iteration, number of iteration
and number of iteration to store
temp2 = inputdlg({'Enter time per iteration (sec)',
'Enter number of iteration','Enter number of iteration to store'},
'Input',3,{'1','10','0'});
time_per_iter_sec = str2num(temp2{1});
num_iter = str2num(temp2{2});
num_iter_to_store = str2num(temp2{3});
%%%%%%%%%%%%%%%%%%%%%%%%%%%%%%%%%%%%%%%%
```

```
%Instantiate COM client
try
app=actxserver([instrument,'.application']);
catch ME
disp('Error establishing COM server connection.');
disp('Check that the VNA application COM server was registered');
disp('at the time of software installation.');
disp('This is described in the VNA programming manual.');
return
end
%Wait up to 20 seconds for instrument to be ready
ready = 0;
count = 0;
while ~ready
ready = app.ready;
if count>20,
disp('Error, instrument not ready.');
disp('Check that VNA is powered on and connected to PC.');
disp('The status Ready should appear in the lower right');
disp('corner of the VNA application window.');
return
end;
%Check every so often whether the instrument is ready yet
pause(1)
count = count + 1;
end
```

```
%Get and echo the instrument name, serial number, etc.
disp(sprintf(app.name));
%Set the instrument to a Preset state
app.scpi.system.invoke('preset');
%Configure the stimulus
if use_center_and_span
app.scpi.get('sense',1).frequency.set('center',f1_hz);
app.scpi.get('sense',1).frequency.set('span',f2_hz);
else
app.scpi.get('sense',1).frequency.set('start',f1_hz);
app.scpi.get('sense',1).frequency.set('stop',f2_hz);
end
app.scpi.get('sense',1).sweep.set('points',num_points);
if(instrument(1) ~= 'R')
app.SCPI.get('SOURce',1).POWer.LEVel.IMMediate.set('AMPLitude',power_level_dbm);
end
%Configure the measurement type
app.scpi.get('calculate',1).get('parameter',1).set('define',parameter);
app.scpi.get('calculate',1).selected.set('format',format);
app.scpi.trigger.sequence.set('source','bus');
tic;
for iter = 1:num_iter
%Execute the measurement
app.scpi.trigger.sequence.invoke('single');
Y = app.scpi.get('calculate',1).selecte.data.fdata;
Y = Y(1:2:end);
```

```
F = app.scpi.get('sense',1).frequency.data;
figure(1);
plot(F,Y);
if iter<=num_iter_to_store
app.scpi.mmemory.store.set('image',[num2str(iter),'.png']);
app.scpi.mmemory.store.set('fdata',[num2str(iter),'.csv']);
end
while(toc<iter*time_per_iter_sec)
pause(0.01);
end
end
```

A.2 WLS fiber model identification

```
measured_data = read(rfdata.data,'01baresensor.s2p');
measured_data2 = read(rfdata.data,'02BCF91A.s2p');
input_pad =
 rfckt.cascade('Ckts',{rfckt.seriesrlc('L',1e-9),rfckt.shuntrlc('C',100e-15)});
output_pad =
 rfckt.cascade('Ckts',{rfckt.shuntrlc('C',100e-15),rfckt.seriesrlc('L',1e-9)});
freq = measured_data.freq;
analyze(measured_data,freq);
analyze(input_pad,freq);
analyze(output_pad,freq);
z0 = measured_data.Z0;
input_pad_sparams = sparameters(measured_data,freq);
output_pad_sparams = extract(output_pad.AnalyzedResult,'S_Parameters',z0);
```

```
de_embedded_sparams =
 deembedsparams(measured_data2.S_Parameters, input_pad_sparams, output_pad_sparams);
de_embedded_data =
 rfdata.data('Z0',z0,'S_Parameters',de_embedded_sparams,'Freq',freq);
figure
hold off;
h = plot(measured_data2,'S21', 'db');
set(h, 'Color', [1 0 0]);
hold on
i = plot(de_embedded_data,'S21','db');
set(i,'Color', [0 0 1],'LineStyle',':');
l = legend;
legend('Measured S_{21}', 'De-embedded S_{21}');
legend show;
hold off;
%
measured_data1 = read(rfdata.data,'BARE.s2p');
measured_data2 = read(rfdata.data,'01.s2p');
freq = measured_data1.freq;
[S_Params1, freq] = extract(measured_data1,'S_Parameters');
[S_Params2, freq] = extract(measured_data2,'S_Parameters');
TrFunc1 = s2tf(S_Params1);
TrFunc2 = s2tf(S_Params2);
tira = TrFunc2./TrFunc1;
RationalFunc = rationalfit(freq,tira,'NPoles',2);
[fresp,freqa]=freqresp(RationalFunc,freq);
```

```
figure

plot(freqa/1e6,db(fresp),freqa/1e6,db(tira));

xlabel('Frequency, MHz')

ylabel('Amplitude, dB')

legend('Fitted Model Data','Experimental Data')
```